



**UNIVERSITY of LIMERICK**

OLLS COIL LUIMNIGH

**Motion Artefact Minimisation from a  
Photoplethysmography based Non-invasive Sensor**

**Hongwei Yuan**

A thesis submitted in requirement for

Doctor of Philosophy

in the

Optical Fibre Sensors Research Centre

Department of Electronic and Computer Engineering

Supervisor: Assoc. Prof. **Elfed Lewis**, Dr. **Gabriel Leen** & Dr. **Thomas Newe**

Submitted to

University of Limerick

December, 2017



# **Declaration of Authorship**

I, Hongwei Yuan, declare that this thesis titled, ‘Motion Artefact Minimisation from a Photoplethysmography based Non-invasive Sensor’ and the work presented in it are my own. I confirm that:

- This work was done wholly or mainly while in candidature for a research degree at this University.
- Where any part of this thesis has previously been submitted for a degree or any other qualification at this University or any other institution, this has been clearly stated.
- Where I have consulted the published work of others, this is always clearly attributed.
- Where I have quoted from the work of others, the source is always given. With the exception of such quotations, this thesis is entirely my own work.
- I have acknowledged all main sources of help.
- Where the thesis is based on work done by myself jointly with others, I have made clear exactly what was done by others and what I have contributed myself.

Signed: \_\_\_\_\_

Date: \_\_\_\_\_



# **Motion Artefact Minimisation from a Photoplethysmography based Non-invasive Sensor**

Hongwei Yuan

## **Abstract**

The collection of photoplethysmography (PPG) signals from optical based sensor probes has been used extensively for the monitoring of heart rate (HR), respiration rate, blood pressure, oxygen saturation ( $\text{SpO}_2$ ), haemoglobin concentration (Hb). One of the drawbacks of PPG based measurement is that the signal is strongly degraded by motion artefact. Much research has been undertaken relating to the removal of motion artefact noise resulting from the wearer's movement. Research reports show that the autonomic nervous system (ANS) of the human body, as part of the peripheral nervous system, can be disturbed by body motion events, leading to unconsciously varying vital physiological parameters including body temperature, blood pressure, respiration rate, eye pupils, and heartbeat. The PPG signal, as a recordable biosignal, can also be affected by ANS when accompanied by variations in physiological events e.g., exercise, breathing and motion, in general.

An accelerometer and a wearable chest respiration monitor are introduced into the PPG sensor device to remove/minimise the low frequency noise induced by such physiological events. The results have shown that the baseline of PPG signal is affected by acceleration, particularly in the vertical direction as opposed to acceleration in the horizontal plane for the system under test. Experimental results from a total of 23 subjects demonstrated that PPG signals during motion events are influenced by the variation of local blood pressure at the point of measurement which is in turn induced from: (1) the vertical height difference between the measuring site and the reference level (the heart level); and (2) the ANS variation.

Furthermore, a novel proposed filtering method based on envelope algorithm (not previously reported work) has been proposed with the analysis and comparison of existing artefact removal techniques. All data have been brought together to enable measurement of vital physiological parameters without corruption by noises including motion artefact, blood pressure and respiration variations.



# Acknowledgements

I would like to give my sincere thanks to my supervisors, Prof. Elfed Lewis, Dr. Gabriel Leen and Dr. Thomas Newe for the immense amount of guidance, help and the unstinting support they have provided for research.

Special thanks to Dr. John Clifford, Dr. Eoin O'Connell, and Jimmy O'Sullivan for their help, advice and guidance in the laboratory.

I also wish to thank Dr Máirtín Ó'Droma for our friendship.

I want to thank Dr Gerard Dooly, Dr Sinead O'Keefe, and Dr Thomas Newe for the many ways in which they provided assistance whenever necessary.

I also want to give my thanks to Stefan Zenger who has contributed technical support in this research.

Sincere thanks must go to the members of the Optical Fibre Sensors Research Centre and the administrative staff of the Department of Electronic and Computer Engineering at the University of Limerick who were very supportive in so many ways. In this context, I would like to acknowledge Sven Poeggel, Daniele Tosi, Dinesh Duraibabu, Mohd Anwar Zawawi, Tim Lam, Muzaffar Rao, Lingxia Chen, Damien Meere, and Dr Urich Timm. They have always been there to give advice and support.

The authors would like to acknowledge the clinical observation and practice provided by Registered General Nurse Ann Lewis during the clinical testing.

I wish to thank the Science Foundation Ireland (grant number: 11/RFP/ECE3335) for funding this work.

My family also deserves special thanks, for all the support they have given me over the years.

I would finally like to extend my thanks to all my friends outside of the university who have been a constant support.



# **Ethics Approval by the University of Limerick**

All subjects gave their informed consent for inclusion before they participated in the study. The study was conducted in accordance with the Declaration of Helsinki, and the protocol was approved by the University of Limerick Ethics Committee (**2016\_11\_04\_S&E** and **2016\_12\_09\_S&E**).



# Table & Contents

Declaration of Authorship .....	I
Abstract .....	III
Acknowledgements .....	V
Ethics Approval by the University of Limerick .....	VII
Table & Contents.....	IX
List of Figures .....	XIII
List of Tables .....	XIX
Abbreviations .....	XXI
CHAPTER 1. INTRODUCTION .....	1
1.1 Research Motivation.....	3
1.2 Contributions of the Thesis .....	4
1.3 List of Publications.....	6
1.4 Outline of the Thesis .....	7
CHAPTER 2. PHOTOPLETHYSMOGRAPHY .....	9
2.1 Bio-Photonics .....	9
2.1.1 Human Skin .....	9
2.1.2 Haemoglobin.....	12
2.1.3 Optical Properties.....	13
2.2 Autonomic Nervous System (ANS) .....	17
2.3 Photoplethysmography (PPG) based Concept .....	19
2.3.1 What is PPG .....	19
2.3.2 Theory and Method of Non-Invasive SpO <sub>2</sub> and Hb Monitoring.....	21
2.4 PPG Device Design based on an Embedded System .....	24
2.4.1 An Embedded System.....	24

2.4.2	Microcontroller.....	24
2.4.3	Digital Accelerometer.....	25
2.4.4	PPG-Based Device .....	28
2.5	Blood Pressure Monitor.....	30
2.6	Summary .....	31
<b>CHAPTER 3.</b>	<b>DEVELOPMENT OF MONITORING AND COMPENSATION TECHNIQUES</b> .....	<b>33</b>
3.1	Review of Development of Non-Invasive Monitoring Techniques .....	33
3.1.1	Haemoglobin from Invasive Monitoring to Non-invasive Monitoring .....	34
3.1.2	From Non-invasive SpO <sub>2</sub> Monitoring to Non-invasive SpHb Monitoring.....	36
3.2	Review of Existing Methods for Compensation of Motion Artefact .....	38
3.2.1	Adaptive Noise Cancellation (ANC).....	40
3.2.2	Empirical Mode Decomposition (EMD) .....	42
3.3	The Proposed Envelope-Based Filtering Method .....	44
3.4	Summary .....	45
<b>CHAPTER 4.</b>	<b>MULTI-SENSOR SYSTEM</b> .....	<b>47</b>
4.1	PPG Sensor Device Layout .....	48
4.1.1	Main Sensor Board.....	49
4.1.2	Development of the Finger Sensor Probe.....	53
4.1.3	Accelerometer Data Optimization .....	56
4.2	Experimental Setup .....	57
4.2.1	Typical Medical Devices for Reference Data Capture .....	57
4.2.2	Schematic of the PPG-Based Sensor System .....	59
4.3	IAR System (Code on the MCU) and LabVIEW .....	61
4.4	Summary .....	64
<b>CHAPTER 5.</b>	<b>ANALYSIS OF PPG SIGNALS IN THE CONTEXT OF EXTERNAL PHYSIOLOGICAL PARAMETERS</b> .....	<b>65</b>

5.1	Introduction .....	65
5.2	BL and Local BP .....	66
5.2.1	The BL of the PPG Signal.....	66
5.2.2	BP Response to VHD .....	70
5.3	Factors which can Affect PPG Signals .....	71
5.3.1	VHD Variation .....	71
5.3.2	Analysis of ANS Variation.....	75
5.3.3	External Pressure at the Measuring Site.....	83
5.3.4	PPG Signal Response to Wrist Rotation .....	84
5.4	Severe Motion Tests .....	85
5.5	Summary .....	88
CHAPTER 6. ANS EFFECT ON HUMAN VITALS.....		91
6.1	Introduction .....	91
6.2	SpO <sub>2</sub> , HR and Hb Affected by ANS .....	92
6.2.1	SpO <sub>2</sub> Analysis .....	92
6.2.2	HR and Hb Analysis.....	93
6.3	Summary .....	94
CHAPTER 7. MOTION ARTEFACT REMOVAL IN HB MONITORING .....		97
7.1	Filtering Methods Used on PPG Data .....	97
7.1.1	Low Pass/High Pass Filtering on Raw PPG Signal .....	97
7.1.2	Empirical Mode Decomposition Method.....	99
7.1.3	The Proposed Method Based on an Envelope Algorithm .....	102
7.1.4	Comparison of Filtering Methods .....	103
7.2	Hb coefficients in Stationary and Non- Stationary States .....	104
7.2.1	Hb Coefficient Development in a Stationary State .....	104
7.2.2	Hb Coefficient Development in Non-Stationary States .....	108
7.3	Hb Coefficient with Respect to VHD Variation .....	110

7.4	The Test of Proposed Method in a Series of Distortions.....	113
7.5	Summary .....	115
CHAPTER 8.	CONCLUSIONS AND FUTURE WORK .....	117
Bibliography.....		121
Appendix A: Publications Arising from This Work .....	App-A-1	
Appendix B: MCU Code.....	App-B-1	
Appendix C: Parts List.....	App-C-1	

# List of Figures

Figure 1.1: Health Care Cost (1970-2015) [7] .....	2
Figure 1.2: Illustration of the change in health spending over the period 2010–2013 [8]	2
Figure 1.3: (a) Raw Hb coefficients, (b) raw PPG signals, (c) acceleration signals, and (d) respiration intensity .....	4
Figure 1.4: Factors which can affect PPG signals.....	5
Figure 2.1: The human skin structure [24] .....	10
Figure 2.2: Different absorption spectra of haemoglobin derivatives according to wavelength [39].....	16
Figure 2.3: The principle of PPG describe by the schematic diagrams of light attenuation [68] .....	20
Figure 2.4: Diagram block of an embedded system.....	24
Figure 2.5: Pin designation for MSP430F1611 [80] .....	25
Figure 2.6: (a) 3-Wire SPI Connection Diagram and (b) 4-Wire SPI Connection Diagram [81] .....	26
Figure 2.7: ADXL345 general pin connection [81] .....	27
Figure 2.8: The PPG sensor system block diagram .....	28
Figure 2.9: The embedded system for PPG signal monitoring [93] .....	30
Figure 2.10: Influence of the contact pressure in pulse oximetry [94] .....	30
Figure 2.11: Philips arm BP Monitor [96] .....	31
Figure 3.1: Radiometer ABL-820 CO-Oximeter, from Radiometer Company [97] .....	34
Figure 3.2: HemoCue®201, from HemoCue Company [98].....	35
Figure 3.3: Radical-7™ Pulse CO-Oximeter [86] .....	35
Figure 3.4: ChoiceMMed, one of commercial pulse Oximeters .....	37
Figure 3.5: TouchHb and the data transmitted to Cell Phone wirelessly [91] .....	37

Figure 3.6: Removal of motion artefact by adaptive filter.....	41
Figure 3.7: (a) motion artefact and (b) removal of motion artefact by adaptive filter [118].....	41
Figure 4.1: The custom designed multi-sensor system .....	48
Figure 4.2: Schematic of the probe board .....	49
Figure 4.3: Top view of Optical Bio-Sensor Device _Main Board.....	50
Figure 4.4: Bottom view of Optical Bio-Sensor Device _Main Board.....	50
Figure 4.5: MSP430 MCU clock system .....	51
Figure 4.6: Schematic of the main sensor board.....	52
Figure 4.7: First generation of a finger clip with an embedded ADXL345 .....	53
Figure 4.8: The second generation of a finger clip with an embedded ADXL345 .....	54
Figure 4.9: Top view of the probe board.....	55
Figure 4.10: Bottom view of the probe board.....	55
Figure 4.11: Three-dimensional coordinate system: (a) ADXL345EB (REV.1 by Intempco) and (b) PPG finger sensor probe.....	56
Figure 4.12: A HemoCue®201 used as Hb monitoring reference .....	57
Figure 4.13: OXYGEN SATURATION PULSOX-8 used as oxygen saturation and HR monitoring reference .....	58
Figure 4.14: Electronic Blood Pressure Monitor used as HR and BP monitoring reference.....	58
Figure 4.15: The PPG sensor system block diagram and the main steps for Hb estimation .....	59
Figure 4.16: Experimental setup of the custom sensor system .....	60
Figure 4.17: The block diagram of the overall process of the motion artefact minimisation algorithm .....	60
Figure 4.18: The code flow on the MCU .....	62

Figure 4.19: the code for Raw Labview readings required calibration.....	63
Figure 4.20: ACC and motion detection interface .....	64
Figure 5.1: (a) PPG and (b-d) AAC signals measurement with main motion acceleration in x-axis.....	68
Figure 5.2: (a) PPG and (b-d) AAC signals measurement with main motion acceleration in y-axis.....	68
Figure 5.3: (a) PPG and (b-d) AAC signals measurement with main motion acceleration in z-axis .....	69
Figure 5.4: Enlarged portion of Figure 5.3 in the interval 990–1110 s .....	70
Figure 5.5: PPG baseline intensities and standard deviations when the subjects were in the sitting position and the finger sensor probe set at three different vertical levels .....	73
Figure 5.6: PPG baseline amplitudes and standard deviations when the subjects were in the standing position and the finger sensor probe set at three different vertical levels... <td>73</td>	73
Figure 5.7: PPG baseline amplitudes and standard deviations when the subjects were in the lying position and the finger sensor probe set at three different vertical levels .....	74
Figure 5.8: PPG baseline amplitudes for 18 subjects whilst in the sitting position and the finger sensor probe set at three different vertical levels.....	75
Figure 5.9: (a) ACC; (b) respiration and (c) PPG signals recorded from changing body positions .....	77
Figure 5.10: (a) PPG and (b) ACC signals for which the subject maintained the finger sensor probe at the same height above the floor and varied the VHD by changing body positions .....	79
Figure 5.11: Enlarged portion of the PPG (a) and the ACC signals (b) in the interval 1110–1280 s in Figure 5.10 .....	80
Figure 5.12: (a) PPG signal and (b) ACC signals with a deep yawn event.....	82
Figure 5.13: (a) Respiration including deep breathing and talking events and (b) PPG signal .....	83

Figure 5.14: The PPG signal affected by local BP variations at the measuring site due to (a) external pressure applied on finger probe and (b) external pressure applied on wrist by processing the inflatable-cuff type blood pressure monitor .....	84
Figure 5.15: Illustration of (a) PPG and (b) ACC signals recorded from rotating wrist.	85
Figure 5.16: (a) PPG and (b) X-axis ACC signals captured in the process of swinging the arm up and down with long resting time intervals .....	87
Figure 5.17: (a) PPG and (b) ACC signals captured in the process of swinging the arm up and down with short resting time intervals .....	87
Figure 5.18: Factors which can affect PPG signals.....	88
Figure 6.1: (a) PPG intensity, (b) SpO <sub>2</sub> and (c) ACC signals. Dotted line a1 indicates the wearer standing up; dotted lines b1 and c1 indicates a deep yawn and a cough, respectively .....	93
Figure 6.2: (a) HR and (b) Hb readings .....	94
Figure 7.1: <b>(a)</b> Respiration; <b>(b)</b> raw PPG signal at 810 nm; <b>(c)</b> FFT of PPG at 810 nm during 620–730 s; <b>(d)</b> FFT of PPG at 810 nm during 870–950 s and <b>(e)</b> low/high pass filtered PPG at 810 nm (cutoff frequency at 0.5 Hz) .....	99
Figure 7.2: (a) Raw PPG signal, subsequent and 1 <sup>st</sup> IMF, and <b>(b)</b> FFT of 1 <sup>st</sup> IMF component.....	100
Figure 7.3: <b>(a)</b> Raw PPG signal, subsequent and 2 <sup>nd</sup> IMF, and <b>(b)</b> FFT of 2 <sup>nd</sup> IMF component.....	100
Figure 7.4: <b>(a)</b> Raw PPG signal, subsequent and 3 <sup>rd</sup> IMF, and <b>(b)</b> FFT of 3 <sup>rd</sup> IMF component.....	101
Figure 7.5: (a) Raw PPG signal, subsequent and 4th IMF, and (b) FFT of 4 <sup>th</sup> IMF component.....	101
Figure 7.6: <b>(a)</b> Raw PPG signal, subsequent and 5th IMF, and <b>(b)</b> FFT of 5 <sup>th</sup> IMF component.....	101
Figure 7.7: (a) Raw PPG signal, subsequent and 6th IMF, and (b) FFT of 6 <sup>th</sup> IMF component.....	102

Figure 7.8: <b>(a)</b> Respiration; <b>(b)</b> raw PPG signal at 810 nm with both upper and lower envelopes; <b>(c)</b> envelope filtered PPG at 810 nm by the proposed method; <b>(d)</b> FFT of PPG at 810 nm during 620–950 s and <b>(e)</b> enlarged portion of raw and envelope filtered PPG signals (in the intervals 680–710 s and 900–930 s) .....	103
Figure 7.9: Raw PPG signal, 0.7–3 Hz bandpass filtered PPG, EMD filtered PPG ( $1^{\text{st}}$ IMF component $c1(t)$ ), and AC part of proposed method filtered PPG .....	104
Figure 7.10: <b>(a)</b> Acceleration; <b>(b)</b> respiration; <b>(c)</b> raw PPG at 810 nm and 1300 nm with no filtering enabled; <b>(d)</b> Hb coefficient from raw PPG; <b>(e)</b> 0.8–3.9 Hz band pass filtered PPG signals at 810 nm and 1300 nm; <b>(f)</b> Hb coefficient during 0.8–3.9 Hz band pass filtered PPG; <b>(g)</b> proposed method filtered PPG signals at 810 nm and 1300 nm; and <b>(h)</b> Hb coefficient from proposed method filtered PPG .....	106
Figure 7.11: <b>(a)</b> EMD filtered PPG ( $XDC$ , low + XAC, EMD); <b>(b)</b> EMD filtered PPG ( $XDC$ , constant + XAC, EMD); <b>(c)</b> EMD filtered Hb ( $XDC$ , low + XAC, EMD); <b>(d)</b> EMD filtered Hb ( $XDC$ , constant + XAC, EMD) .....	107
Figure 7.12: <b>(a)</b> Acceleration; <b>(b)</b> respiration; <b>(c)</b> raw PPG at 810 nm and 1300 nm with no filtering enabled; <b>(d)</b> Hb coefficient from raw PPG; <b>(e)</b> 0.8–3.9 Hz band pass filtered PPG signals at 810 nm and 1300 nm; <b>(f)</b> Hb coefficient during 0.8–3.9 Hz band pass filtered PPG; <b>(g)</b> proposed method filtered PPG signals at 810 nm and 1300 nm; and <b>(h)</b> Hb coefficient from proposed method filtered PPG .....	109
Figure 7.13: <b>(a)</b> EMD filtered PPG ( $XDC$ , low + XAC, EMD); <b>(b)</b> EMD filtered PPG ( $XDC$ , constant + XAC, EMD); <b>(c)</b> EMD filtered Hb ( $XDC$ , low + XAC, EMD); <b>(d)</b> EMD filtered Hb ( $XDC$ , constant + XAC, EMD) .....	110
Figure 7.14: <b>(a)</b> Acceleration; <b>(b)</b> respiration; <b>(c)</b> raw and proposed method filtered PPG signals at 810 nm; <b>(d)</b> raw and proposed method filtered PPG signals at 1300 nm; and <b>(e)</b> raw Hb coefficient (black square point) and proposed method filtered Hb coefficient (red circle point) .....	112
Figure 7.15: Histograms of <b>(a)</b> raw Hb coefficients (standard deviations) with no filtering enabled and <b>(b)</b> Hb coefficients by proposed filtered method (standard deviations) for which the subjects were in the sitting position and the hands with the sensor probe on were set at three different vertical levels .....	113

Figure 7.16: **(a)** Raw Hb coefficients (black square points) and filtered Hb coefficients (red circle points), **(b)** raw PPG and envelope filtered PPG signals by the proposed method, **(c)** ACC signals, and **(d)** respiration intensity..... 115

# List of Tables

Table 2.1: The electromagnetic spectrum wavelength and visible light spectrum wavelength.....	14
Table 3.1: Comparison of three haemoglobin devices: Standard Laboratory Co-Oximeter (e.g., Radiometer ABL-820 CO-Oximeter (tHb)), point-of-care device (e.g., HemoCue ® 201), and SpHb monitoring (e.g., Radical-7®; Masimo Corp., Irvine, CA) .....	36
Table 4.1: The bus pin configuration .....	49
Table 5.1: Systolic, Diastolic And HR at Different Height Level.....	71
Table 5.2: Mean BLs and AMs at Different VHD Values for 18 individual subjects were in the sitting position and the finger sensor probe set at three different vertical levels ..	73
Table 5.3: Mean, Median, Standard Deviation, and Interquartile Range of Baseline from 18 sets of PPG signals at Different VHD Deviation .....	75
Table 5.4: Mean, Median, Standard Deviation, and Interquartile Range of AM from 18 sets of PPG signal at Different VHD Deviation.....	75
Table 5.5: Main parameters of body variation from a standing position to a sitting position.....	77
Table 5.6: Primary Parameters of Body Variation from Sitting Position to Standing Position.....	78
Table 5.7: Mean, Median, Standard Deviation, and Interquartile Range of Primary Parameters of Body Variation from Sitting to Standing.....	78
Table 7.1: Hb coefficients deduced from raw and proposed method filtered PPG signals for which the five individual subjects were in the sitting position and the finger sensor probe set at three different vertical levels.....	113



# Abbreviations

a	Acceleration
$a_t$	Angular Acceleration
$A_t$	Total Absorbance
AC	Alternating Current
ACC	Acceleration
ACC_X	X-axis Acceleration
ADC	Analogue-to-Digital Converter
A&E	Accident and Emergency
AM	Amplitude Modulation
ANC	Adaptive Noise Cancellation
ANS	Autonomic Nervous System
Arb	Arbitrary Analog Unit
BL	Baseline
BP	Blood Pressure
BPM	Beats Per Minute
$c$	The Speed of Light (approximately $3.0 \times 10^8$ m/s)

$c_1$	The First IMF Component of the Data $s(t)$
$c_n$	The $n^{\text{th}}$ IMF Component of the Data $s(t)$
$c_A$	Concentration of the Absorber
$c_{\text{Hb}}$	Haemoglobin Concentration
$\text{CO}_2$	Carbon dioxide
$\text{COHb}$	Carboxy-Haemoglobin
CPU	Central Processing Unit
CS	Chip Select
CSO	Central Statistics Office
$d$	Distance of Optical Path
D	Duty Cycle
DC	Direct Current
DSP	Digital Signal Processing
DST	Discrete Saturation Transform
DAC	Digital-to-Analogue Converter
DCO	Digitally Controlled Oscillator
DMA	Direct Memory Access

$E$	Light Extinction
EMD	Empirical Mode Decomposition
EU	European Union
$F$	Force
FBC	Full Blood Count
FFT	Fast Fourier Transform
FIR	Finite Impulse Response
$\varepsilon$	Extinction Coefficient/ Attenuation Coefficient
$g$	Anisotropy factor
GDP	Gross Domestic Product
GNI	Gross National Income
$\lambda$	Wavelength
$f_s$	Sampling Frequency
$h$	Planck's Constant
$h_1$	The Difference between the Data $s(t)$ and the Mean of the Upper and Lower Envelopes $m_1$
$h_{11}$	The Difference of $h_1$ and $m_{11}$

$h_{1k}$	The Difference of $h_{1(k-1)}$ and $m_{1k}$
H <sub>2</sub> O	Water
Hb	Haemoglobin concentration
HbCO	Carboxyhaemoglobin concentration
HbO <sub>2</sub>	Oxyhaemoglobin/Oxygenated Haemoglobin concentration
HHb	Deoxyhaemoglobin Haemoglobin concentration
HR	Heart Rate
HRV	Heart Rate Variability
$I_0$	Original Intensity
$I$	Measured Intensity
IC	Integrated Circuit
IMF	Intrinsic Mode Functions
I <sup>2</sup> C	Inter Integrated Circuit Communications
InGaAs	Indium Gallium Arsenide
iMEMS	Integrated Micro Electro Mechanical Systems
$k$	Spring Stiffness Constant
LCD	Liquid Crystal Display

LED	Light Emitting Diode
LMS	Least Mean Square
$m$	Mass
$m_1$	The Mean of the Upper and Lower Envelopes of $s(t)$
$m_{11}$	The Mean of the Upper and Lower Envelopes of $h_1$
$m_{1k}$	The Mean of the Upper and Lower Envelopes of $h_{1k}$
MC DST	Minimum Correlation Discrete Saturation Transform
MDF	Multidelay Block Frequency Domain Adaptive Filter
MetHb	Methaemoglobin
$M_{\text{Hb}}$	The Haemoglobin Molecular Weight 64,500 g/mol
Mid-IR	Mid-wave Infrared
MSE	Mean Square Error
NLMS	Normalized Least Mean Square
NIR	Near-Infrared
OECD	Organisation for Economic Co-operation and Development
OF SRC	Optical Fiber Sensor Research Centre
SpOC	Oxygen Content

$P$	Total Period of the Signal
PPG	Photoplethysmography
PI	Perfusion Index
PR	Pulse Rate
PPG	Photoplethysmography
PVI	Pleth Variability Index
$r$	Radius of an Arc
$r_1$	The First Residue Defined as the Difference between the Data $s(t)$ and the Subtracted $c_1$
$r_n$	The $n^{\text{th}}$ Residue Stated as the Difference between the $(n-1)^{\text{th}}$ Residue $r_{n-1}$ and the $n^{\text{th}}$ IMF Component $c_n$
RAM	Random Access Memory
$R_{\text{diff}}$	Diffuse Reflection
RF	Radio Frequency
RHb	Reduced Haemoglobin
RISC	Reduced Instruction Set Computing
RLS	Recursive Least Squares
$s(t)$	Source Data

SCLK	Clock for SPI
SD	Standard Deviation
SDA	Serial Data Input
SDO	Serial Data Output
SMI	Self Mixing Interferometry
SpCO	Carboxyhaemoglobin
SpO <sub>2</sub>	Saturation of Peripheral Oxygen
SpHb	Total Haemoglobin
SPI	Serial Peripheral Interface
SpMet	Methaemoglobin
SQI	Signal Quality Index
SNR	Singal-to-Noise Ratio
<i>T</i>	Time of the Active Signal
tHb	Total Haemoglobin Concentration
$\mu_a$	Absorption Coefficient
$\mu_s$	Scattering Coefficient
UART	Universal Asynchronous Receiver/Transmitter

UL	University of Limerick
UV	Ultraviolet
USART	Universal Synchronous/Asynchronous Receiver/Transmitter
$v$	Velocity
VHD	Vertical Height Difference
VI	Virtual Instrument
VLF	Very Low Frequency
$\omega$	Angular Frequency
$x_{\text{dis}}$	Distance the Spring Stretched from its Equilibrium Position
$X_{i,\text{raw}}(t)$	The Raw Signal
$X_{i,\text{upper}}(t)$	The Upper Envelope of the Raw Signal
$X_{i,\text{lower}}(t)$	The Lower Envelope of the Raw Signal
$X_{i,\text{AC}}(t)$	The AC (Time Varying) Component of the Raw Signal
$X_{i,\text{DC}}(t)$	The DC (Non-Time Varying) Component of the Raw Signal

# CHAPTER 1.

## INTRODUCTION

---

The current population of the world is about 7.5 billion [1], and this figure is estimated to reach 9.7 billion in 2050 [2]. In addition to the increasing number of people, the average life span around the world is also rising. Worldwide, the average life expectancy at birth was 71.0 years (68 years and 6 months for males and 73 years and 6 months for females) over the period 2010–2013 according to United Nations World Population Prospects 2012 Revision [3], or 70.7 years (68.2 years for males and 73.2 years for females) for 2009 according to the World Factbook [4]. Ireland is ranked 19<sup>th</sup> on the List of Healthcare by the World Health Organization (2015) [5]. Life expectancy at birth is now 76.8 years for men and 81.6 years for women (Central Statistics Office, CSO, 2013) [6].

This ageing of the older will intensify the rise in the number of the people living with all kinds of elderly diseases including cardiovascular diseases, arthritis, cancer, osteoporosis, diabetes, vision/hearing change/loss, sleep disorders and respiratory diseases. Health care cost of OECD (Organisation for Economic Co-operation and Development) countries is charted in Figure 1.1 [7]. The average spending in OECD countries in 2013 was 9 % of GDP (Gross Domestic Product, compared with 12.4 % of GNI (Gross National Income) in Ireland). Public spending in Ireland was 8.8 % of GNI in 2013. Health spending in Ireland appears to be relatively high by international standards. This is particularly so given consideration of our relatively a young demographic. OECD data shows that 12.7% of the population in Ireland was over 65 compared to an European Union (EU) average of 18%. Figure 1.2 illustrates the change in the health spending from 2000 to 2013. The public spending has increased by 164 percent over the period (€8.1 billion) whilst private spending 269 % (€3.9 billion) [8].

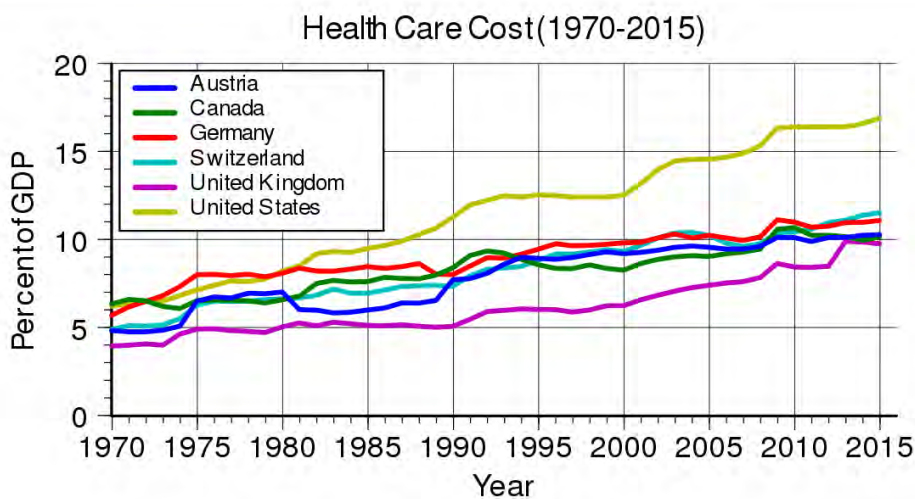


Figure 1.1: Health Care Cost (1970-2015) [7]

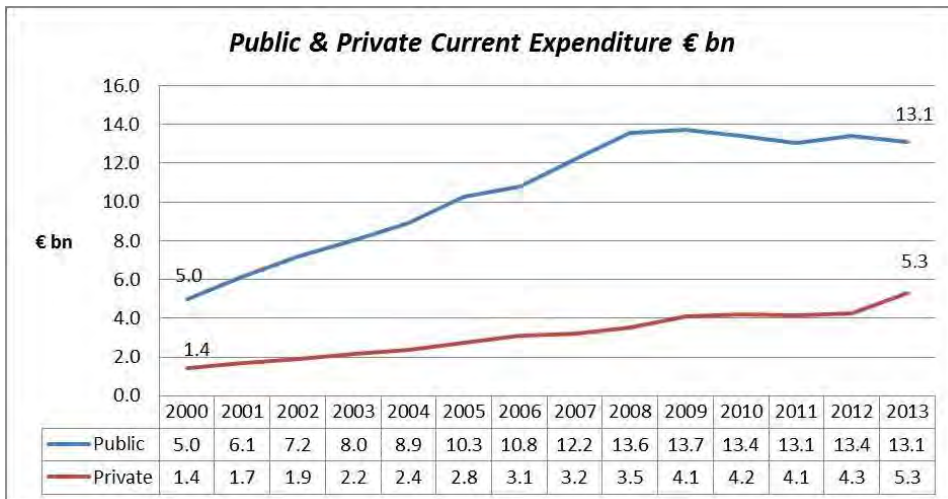


Figure 1.2: Illustration of the change in health spending over the period 2010–2013 [8]

However, Ireland's healthcare spending in 2016 ranked below that of lower-income countries, Macedonia and Slovenia, despite a relative increase in spending than last past several years. The waiting time of A&E (Accident and Emergency) service in Ireland continued to be the worst among the OECD countries, ranked 21<sup>st</sup> out of 35 countries according to the Euro Health Consumer Index and followed by Poland, Greece and the UK [9].

Rapidly growing population and long A&E waiting time raise the demand for human vital signs monitoring devices. Novel, compact and non-invasive operated monitoring devices hence have been promoted for being used by the subjects who are wearing it.

Such an optical photoplethysmography (PPG) sensor has been developed to measure anaemia, Blood Pressure (BP), blood oxygen saturation, Heart Rate (HR), vasomotor function and thermoregulation [10]. Monitoring human vital signs out of the hospital environment could greatly improve the quality of daily life.

However, despite the benefit of convenient and mostly real time monitoring, the drawback does exist such as the undesired artefacts/noises induced into the useful physiological signals. Motion artefact (that occurs with voluntary or involuntary human body motion during monitoring) is currently one of the toughest problems in the design of many commercial devices such as pulse oximeters.

### 1.1 Research Motivation

During recording of the various vital physiological signals, both in the hospital environment and daily care, contamination of the original signals due to noise is a limitation in the application of the wearable sensor devices. A drawback of the photoplethysmography (PPG) technology has been that the PPG signal is easily affected by any activities relating to hemodynamic pressure variation near the PPG sensor. These factors include movement of the subject (e.g., walking and swinging arm) accompanied with that of the measurement apparatus [11-17] and autonomic nervous system (ANS, e.g., changes in respiration) variations [18]. To avoid the errors induced by these factors, traditionally, measurements of human vitals are collected in the conditions that the subject is motionless and in a lying or sitting position.

For example, Figure 1.3 (one experimental study by the author) shows one case study of a series of distortion test in haemoglobin (Hb) monitoring. Region (A<sub>1</sub>) and Region (A<sub>2</sub>) in Figure 1.3d mark deep breathing and cough events, and accordingly PPG-fluctuations occurred with the ANS variation as shown in Figure 1.3b. Figure 1.3c depicts acceleration signals versus time, and region (B) indicates the vertical height difference (VHD, the vertical distance from the attached PPG probe to heart level) of the finger sensor position, and the raw PPG signal was mainly affected from the local BP variation near the finger sensor position. Region (C) in Figure 1.3c represents the movement of body position with no VHD between the finger sensor probe and the heart level. The PPG-fluctuation in Figure 1.3b indicates that a change of body position can stimulate

ANS variation to influence the raw PPG signal as well as raw Hb coefficients readings in Figure 1.3a. Region (D) in Figure 1.3c indicates the swing of an arm with the finger sensor probe on between 25 cm above heart level and 25 cm below heart level. Region (E) in Figure 1.3c shows the acceleration signal during a walking event while the subject tried to breath at an even speed (Figure 1.3d). The measurements of raw Hb coefficients and raw PPG signals are illustrated in Figure 1.3a and Figure 1.3b. The walking event disturbs the raw Hb coefficient readings more dramatically observable than other events in the series of the distortion test. Therefore, there is a demonstrable need for algorithms capable of detecting and removing these artefacts from the desired signals.

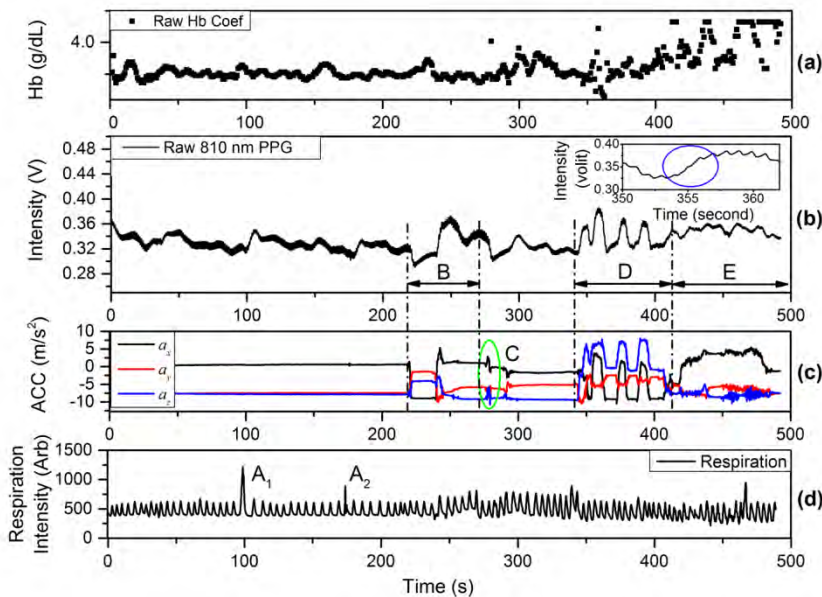


Figure 1.3: (a) Raw Hb coefficients, (b) raw PPG signals, (c) acceleration signals, and (d) respiration intensity

## 1.2 Contributions of the Thesis

A novel development of a filtering method based on an envelope algorithm has been proposed, building on, but improving the analysis and comparison of existing artefact removal techniques. The thesis focuses on signal artefact removal comparison between different filtering methods and validates the accuracy of Hb monitoring in a large group subjects through preliminary statistical analysis. A multi-sensor approach combining the optical probe, an accelerometer and a wearable chest respiration monitor has been adopted in our sensor device. The study of motion artefact removal in non-invasive

hemoglobin monitoring is based on the research of PPG signals in the context of external physiological parameters, not only motion artefact noise but also ANS (e.g., deep breathing, cough and talking events) and BP on the measuring location (e.g., VHD) have been brought into consideration for the first time, to the best of the knowledge of the author. Data from the multi-sensor system is combined to enable measurement of vital physiological parameters and furthermore used to minimise signal noise including motion artefact, BP and respiration variations. In its entirety, this thesis has produced a number of contributions which are described below.

- 1. Novel design of PPG sensor finger probe with an accelerometer embedded.**

The finger sensor probe was attached to the subject using Velcro tape in order to make the finger band size adjustable for different finger sizes.

- 2. Factors which can affect PPG signals.** Accompanied with motion artefact, BP near the measuring site is introduced with the motion events. To study of the effect of motion on human vital physiological information, the properties of the PPG signal have been investigated in detail and factors which can affect PPG signals are shown in Figure 1.4. Results demonstrate that a PPG signal is highly affected by BP at the measuring site from VHD, ANS and pressure variations.

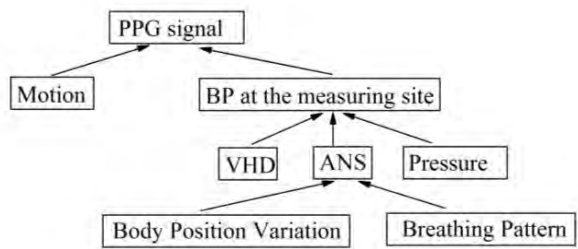


Figure 1.4: Factors which can affect PPG signals

3. Further research on the removal of the motion artefacts in human vitals monitoring is conducted and executed based on the experimental analysis of the PPG signals. Traditionally, a band-pass filter would be adopted in the removal of the noises in the corrupted PPG signals. However, some noise frequencies fall into that of the PPG signals, e.g., motion, so methods such as adaptive filtering and empirical mode decomposition (EMD) are used in the removal of these artefacts. In the thesis, the author has proposed a novel efficient envelope-based

filtering method. The result of Hb measurement between three methods (the band pass, the EMD, and the proposed methods) are compared in detail and tested on five subjects in both the stationary and the non-stationary states.

4. In Figure 1.4, body position variation (standing up) and a change in breathing pattern (a deep yawn and a cough) are two factors which tend to influence SpO<sub>2</sub>, HR, and Hb reading. These results are reported through the study of ANS during motion events.
5. The thesis mainly focuses on the research relating to the effects of motion on the quality of non-invasive blood diagnosis by PPG-based sensor system, with a particular emphasis on the VHD at the measuring site.

### 1.3 List of Publications

Journals:

- Yuan, H., Poeggel, S., Newe, T., Lewis, E., Viphavakit, C., & Leen, G. "An Experimental Study of the Effects of External Physiological Parameters on the Photoplethysmography Signals in the Context of Local Blood Pressure (Hydrostatic Pressure Changes)." *Sensors*, 17(3), pp. 556–576, 2017.
- Yuan, H., Memon, S.F., Newe, T., Lewis, E. G. "Motion Artefact Minimization from Photoplethysmography based Non-invasive Hemoglobin Sensor Based on an Envelope Filtering Algorithm." *Measurement*, 115, pp 288–298, 2018.

Conference papers:

- Yuan, H.; Leen, G.; Lewis, E. "Effects of autonomic nervous system on the quality of non-invasive blood diagnosis by PPG-based sensor system." In Proceedings of the 2015 11th Conference on Ph.D. Research in Microelectronics and Electronics (PRIME), Glasgow, UK, 29 June–2 July 2015; pp. 373–376.
- Yuan, H., et al. "A wireless, body-worn non-invasive device for measuring biometric parameters such as total haemoglobin concentration." University Hospital Limerick (UHL) Research Symposium, 2013.

- Duraibabu, Dineshbabu, Niall Kelly, Sven Poeggel, Hugh Flood, Hongwei Yuan, Gerard Dooly, Deirdre McGrath, Daniele Tosi, Elfed Lewis, and Gabriel Leen. "Optical fibre pressure and temperature sensor system designed for urodynamic applications." In Sixth European Workshop on Optical Fibre Sensors (EWOFS'2016), pp. 991617-991617. International Society for Optics and Photonics, 2016.
- Newe, T., O'Connell, E., Meere, D., Yuan, H., Leen, G., O'Keeffe, S., & Lewis, E. (2016, May). Optical fibre multi-parameter sensing with secure cloud based signal capture and processing. In Sixth European Workshop on Optical Fibre Sensors (EWOFS'2016) (pp. 99162V-99162V). International Society for Optics and Photonics.

## 1.4 Outline of the Thesis

The rest of this thesis is organized as follows:

Chapter 2 lays out the background of the topic, mainly from the aspects: 1) the introduction of human skin and its optical properties; 2) basic conception of ANS; 3) PPG based technique and sensor device; 4) a brief description of the electronic microcontroller hardware used in the investigation of the integrated circuit and 5) BP monitor.

Chapter 3 includes a literature review on the development of non-invasive monitoring technique and the methods for compensation of motion artefact in bio sensor systems.

In Chapter 4, the proposed optical sensor system is described from the view of the experimental setup and the schematic of the biomedical application flow diagram with particular emphasis on the proposed envelope-based filtering method.

Chapter 5 reports on the research relating to the effects of local BP variation in the quality of PPG signals. A corrupted PPG signal during the motion process tends to be varied by local BP, and factors that would or would not affect the PPG signal during a movement event of the probe are discussed in detail. To deal with this problem, firstly

method is proposed by using accelerometers to measure the acceleration and movement for PPG analysis and feature extraction. External pressure on/near measuring point, ANS, and VHD between the measuring site and heart level in the vertical direction are also all factors that can potentially affect local BP at the measuring site. A more severe test of motion by swinging an arm is included at the end of this chapter.

Chapter 6 describes the effects of ANS on the quality of the PPG based measurements, including HR, SpO<sub>2</sub> and Hb. Human vitals monitoring results presented here illustrate that a baseline (being the difference between 0 and the maximum value of this waveform during the interval) in PPG signal is highly affected by ANS induced both from a) movement of body position and b) physiological variation, such as yawning and coughing. A synthetic noise generation and moving average filtering method are used in a clean and enhanced signal.

Chapter 7 begins by comparison of existing artefact removal techniques with the novel development filtering method based on the envelope algorithm. The chapter focuses on the artefact removal comparison between different filtering methods and validates the accuracy of Hb monitoring in a large group subjects through a preliminary statistical analysis.

Chapter 8 concludes the thesis that PPG signals related measurements tends to be easily contaminated by BP variation at the measuring site caused from motion artefact. Suggestions for further work are also presented in this chapter.

# CHAPTER 2.

## PHOTOPILETHYSMOGRAPHY

---

### 2.1 Bio-Photonics

The real-time evaluation of a patient's physiological condition is essential not only during or after surgery, but also for on-going daily patient care. The current standard for the Hb determination requires invasive methods, involving the handling of blood and needles, and the subsequent *in-vitro* analysis of samples [19-21]. Analysis of different kinds of human tissues has been widely studied in biomedical research. Some biosensors are designed for monitoring human vitals from direct contact with human skin using optical non-invasive method. Hence, the constitution of the skin, its optical properties and the interaction of light with it are firstly described.

#### 2.1.1 Human Skin

The human skin is the outer covering of the body and it is the largest organ of the human body (15–20 % of the total body weight) [22]. The skin can be divided into several layers of ectodermal tissue and it protects the underlying muscles, bones, ligaments and internal organs from external influences, manages heat regulation, and assumes a part of the metabolism and immunology [23]. The complex structured skin can be described by three layers, which are epidermis, dermis, and fat layer (hypodermis). A 2-D view of the human skin structure is shown in Figure 2.1 [24]. Skin pigmentation depends on the melanin concentration: the darker of the skin the higher the melanin concentration in the epidermis [22].

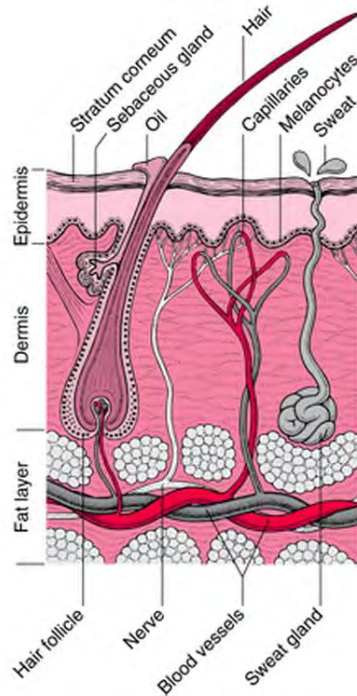


Figure 2.1: The human skin structure [24]

## **Epidermis**

The epidermis is the outer layer of the human skin tissue, and normally referred as the tough, strong and thin ‘coat’ for the human body. Its thickness can vary from  $40 \mu\text{m}$  near the forehead or the hand surface to  $1.5 \text{ mm}$  in the sole of the foot region. The stratum corneum is the outermost and most important section of the epidermis as it separates the human body from its surrounding environment and is relatively waterproof preventing most substances especially bacteria and viruses from entering the body [22]. The stratum corneum is generally the compositions of stratified squamous epithelium without blood vessels in it. On the other hand the epidermis also tends to fight against trauma to protect the internal tissues of the human body, e.g., muscles, blood vessels, organs, nerves, etc. Thicker skin can be seen in certain areas of the human body and gives higher strength protection by an enhanced stratum corneum. These locations typically can be found at hands between the palms or the bottom of the feet.

Keratinocytes (main part as outer keratin layer), Melanocytes (pigment melanin), Langerhans (part of the skin's immune system, against skin allergies) and Merkel cells are the main type of cells within the epidermis [25]. Melanin is the representation of the

tan of the skin, produced by melanocytes from absorption of sunshine. The cells in the epidermis layer are mainly nourished by a diffusion process: nutrients and air are transported by capillaries, part of the oxygen is diffused from the outside of human body that is surrounded by air [26]. In the areas as the end of the tips, like the ears, toes, fingertips and nose, the network is passed by the arterial shunt vessels around the cells. The mitosis takes the responsibility as the carrier for formation for cells through and between the basal layers. The replacement of cells in the epidermis takes place as the daughter cells increase, covering the cells that tend to decay from their isolation to the nutrients. The apoptosis and metabolism ultimately leads cells in the epidermis to death and are replaced in the stratum corneum by new and young cells [26].

## Dermis

The dermis normally can be divided into hair follicles, apocrine glands (sweat glands), sebaceous (oil) glands, lymphatic vessels, nerves endings, and blood vessels (capillaries); all these contained are located underneath the epidermis. The thickness of the dermis falls into the range of 1  $\mu\text{m}$  to 4  $\mu\text{m}$ . It has the function of cushion protecting the human body against external pressure and strain [22]. The dermis and the epidermis are tightly connected by a basement type membrane between them. It can be seen as a very thick layer of organic film made up from fibrous (elastin) and elastic (collagen) tissue that provides flexible strength for the daily care of skin protection. The details of the components of the dermis are described as following [27]:

***The hair follicles*** support the human body with different types of hair all over the body. Hair supports in the personal appearance also plays the important role in physics, e.g., adjusting skin temperature, acting as a cushion and buffer from outside forces, and providing extra sensation.

***The apocrine glands*** generate sweat stimulated from extra or inner heat. Stress and emotion are other factors can result in the production of sweat. In the aspect of chemical components, sweat is mainly made of water, salt, waste (excreta), and other chemicals. Sweat often evaporates away from the skin surface of the body. Through this process, the body temperature can be controlled (cooling).

**The sebaceous glands**, also named the oil glands, secrete sebum by nature of moisturizing hair follicles. Sebum is a kind of oil, which has the same function as a moisturizer, keeping the skin as moist and smooth, and as barriers, stopping harmful substances entering from outside.

**The nerve endings** transmit electrical signals which initiate the sensation, e.g., pain from hurting, touch scratching, pressure from an external force, and heat from the environment. Some portions of the human skin include more nerve endings than others. In general, the fingertips and toes have more nerve cells and hence they are much more sensitive to touch than other sections of the human body.

**The blood vessels** are widely distributed throughout the human body. Some of these are extended to the dermis. Both nutrients and oxygen are provided to the skin through the blood vessels. On the other hand, they play a key role in regulating body temperature and balance the temperature according to the environment. In detail, heat tends to broaden the blood vessels, allowing large volumes of blood to flow inside the vessels of the skin. This heat is released to cool down the body temperature. Similarly, when the environment is cold, the vessels in the skin tend to shrink, helping to maintain heat within the human body. As mentioned before, the blood vessels, nails, hair follicles, apocrine glands, and other components are classified belonging into the dermis.

## **The Fat Layer**

The fat layer, also called the hypodermis, contains largely loose connective tissue and elastin tissue with fat cells among them, responsible for a connecting link of the underlying tissue (e.g., bones and muscles) and the skin as the insulation layer [28]. It also provides a supply of a nervous network and blood vessels for the muscle. The fat in the hypodermis is up to 50% of the total body fat. Fibroblasts and adipocytes serve as the insulation and padding for the body.

### **2.1.2 Haemoglobin**

Oxygen is an essential requirement to support an individual's life. Brain damage, organ failure, or even death, can result from an inadequate supply of oxygen to vital organs and tissues. The cardiovascular system (responsible for transporting oxygen, nutrients,

and cellular waste products throughout the body) and respiratory system (transporting air into the lungs and facilitating the diffusion of Oxygen into the blood stream while receiving waste Carbon Dioxide from the blood and exhaling it) are two of the circulatory systems in the human body; they are working together, responsible for many body functions. Within the blood, Hb plays the role of transporting oxygen from the lungs to the rest of the human body. It is the iron-containing respiratory protein in red blood cells. Hb level/concentration, measured in grams per decilitre (g/dL), reflects the blood's ability for carrying oxygen and iron [29-31]. Normal haemoglobin levels of women are ranging from 12–16 g/dL and those of men are in the range of 13–18 g/dL.

### 2.1.3 Optical Properties

Further work in this thesis involves spectroscopic measurements in tissues, where the optical properties of the measured skin must be taken into account. The optical properties (e.g., scattering and absorption) of the skin have shown the details of the hypodermis structure by analysing Mie-scattering and Rayleigh reflected signals [32]. To describe the wave nature of the electromagnetic radiation, the terms wavelength  $\lambda$ , or frequency  $f$  are used. In detail, it includes: 1) amplitude, defined as the brightness of the light signal; 2) wavelength  $\lambda$  or frequency  $f$ , which is described by  $c = \lambda f$ , where  $c$  stands for the speed of light (approximately  $3.0 \times 10^8$  m/s) [33-35]. This was the classical interpretation of electromagnetic fields and waves, crystallized in Maxwell Equations, which dominated until in the late 19th century at which point Planck, Einstein and others came along with new-born quantum theory. In terms of the modern quantum theory, electromagnetic radiation consists of photons. From the particle description of the electromagnetic radiation, they are discrete particles carrying energy as  $E = hc/\lambda$ , where  $h$  denotes Planck's constant moving at the speed of light [34].

From the particle view of light, the number of photons decides the brightness of the light, and the energy contained in each photon determines the colour of the light. Different effects have been shown when several parts of the electromagnetic spectrum interacting with all kinds of matter, e.g., Microwave through far infrared: Plasma oscillation, molecular rotation; Near infrared: Molecular vibration, plasma oscillation (in metals only); Ultraviolet (UV): Excitation of molecular and atomic valence

electrons, including ejection of the electrons (photoelectric effect); X-rays: Excitation and ejection of core atomic electrons, Compton scattering (for low atomic numbers), etc. Therefore, the human body could act differently according to wavelength from 400 nm to 2000 nm [33]. The electromagnetic spectrum wavelength and visible light spectrum wavelength are shown in Table 2.1. The pigment melanin is the main and highly effective absorber of light in skin tissue, particularly in the UV light and the visible light ranges.

Table 2.1: The electromagnetic spectrum wavelength and visible light spectrum wavelength

Electromagnetic Wave	Wavelength (cm)
Radio waves	$>10$
Microwaves	$10 - 0.1$
Infrared rays	$0.1 - 7 \times 10^{-5}$
Visible	$7 \times 10^{-5} - 4 \times 10^{-5}$
Ultraviolet rays	$4 \times 10^{-5} - 10^{-7}$
X rays	$10^{-7} - 10^{-9}$
Gamma rays	$<10^{-9}$

Visible Light	Wavelength (nm)
Violet	$400 - 420$
Indigo	$420 - 440$
Blue	$440 - 490$
Green	$490 - 570$
Yellow	$570 - 585$
Orange	$585 - 620$
Red	$620 - 780$

Optical properties of light interaction events with human body can be divided into reflection/refraction, absorption, and scattering [36, 37]. These three optical properties are the main processes for investigation of human tissue by non-invasive optical methods. As the PPG sensor device is based on light transport through human skin and light propagation in biological tissues requires knowledge about the light interaction within the medium, light transport in biological tissue and turbid media is introduced. The haemoglobin measurement, based on the development of an optical sensor system, strongly depends on an understanding of the optical properties when light propagating through and interacting within the biological tissue.

**Reflection** is the variation of a wave front in direction when it meets the interface from one medium to another different medium. In the case of reflection the wave front tends to return towards the first medium. The law of reflection makes the thing clear that the incident and the reflection wave are on the same side of one medium and specular reflection makes the angles between the normal and the two waves the same.

**Refraction:** When a beam of light propagates from one medium into another transmission medium, the change in direction of light propagation is named as refraction.

**Absorption** of light is attributable to the absorption of electromagnetic energy within a molecule. In the case of absorption, the energy of a photon is imparted to an atom or molecule in that medium when a wave light transmits through it. The energy absorbed from the photon tends to transform into the absorber in the form of internal energy, often stored as thermal energy.

The medium discussed in this thesis is the human skin. Absorption of photons can cause damage of tissue if the incident light into the tissue results in heating leading to thermal effects. If sufficient energy is absorbed from photons, there will be energy transfer from the light into energy stored in the tissue so the tissue is highly affected. This can occur at any wavelength but is most efficient at shorter ones e.g. UV light and X-ray.

Molecules with the capability of efficiently absorbing photons are named chromophores. These chromophores can be divided into two types depending on how photons are absorbed in the tissue: vibrational transition absorption and electric transition absorption [38]. Water (via vibrational transitions) dominates as it comprises more than 90% of human tissue. In the case of electronic transition absorption, it is caused by porphyrins which are highly effective as chromophores in absorbing photons. The mechanical vibrational frequencies correspond with excitation wavelengths which are longer being well matched to microwave and Mid-wave Infrared (Mid-IR, in the wavelength range from  $2.5 \mu\text{m}$  to  $8 \mu\text{m}$ ). Hence UV, visible, and near infrared light normally fall in the range of electronic transition absorption as they are associated with relatively energetic (higher frequency) absorption. Since the absorption could provide information on the concentration of various chromophores and due to the low absorption of light near the visible and near infrared range, light between 500 nm and 1500 nm is often used as light source for non-invasive human vitals measurements. UV light wavelengths are generally considered unsuitable for direct exposure to tissue.

**Scattering** happens when a photon interacts with a particle. The variations in refractive index of the medium where the irregular changes tend to force the photon to deviate

from a straight trajectory to many possible angular directions. Light interaction through scattering occurs when the photon passes through media, such as cellular content, collagen fibres, ultrastructure of the chromophores, nuclei, and cells. In the scattering event, the photon changes direction or polarisation state when it bounces off a microscopic obstacle as described above. Scattering can be divided into Mie scattering and Rayleigh scattering according to the size of particles compared with the wavelength of the light [32]. Mie scattering occurs in the case when particles have similar scale as the wavelength of light; while Rayleigh scattering occurs when the particle sizes are much smaller than the incident photon wavelength. The concentration of the scattering components is derived from the scattering properties. For example, scattering signals are affected by the size, form, discrete particles, and continuous variations in the medium. The refractive index, which greatly affects the scattering and absorption properties of tissue, is given special care in the design of bio sensor monitoring device.

Different absorption coefficients of haemoglobin derivatives, according to wavelength are shown in Figure 2.2, such as Oxy-haemoglobin ( $\text{HbO}_2$  or  $\text{O}_2\text{Hb}$ ), Reduced haemoglobin (RHb) or Deoxyhaemoglobin haemoglobin (HHb), carboxy-haemoglobin (COHb) and methaemoglobin (MetHb). The concentration of these haemoglobin derivatives and water comprise the main absorption medium in blood, leading to specific attenuations to light signals with different wavelengths [39].

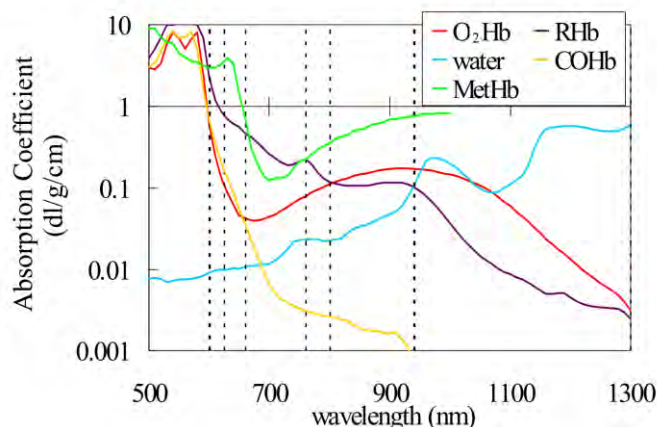


Figure 2.2: Different absorption spectra of haemoglobin derivatives according to wavelength [39]

## 2.2 Autonomic Nervous System (ANS)

The ANS, referred to the bundle of motor neurons and the axonal connections [40], is part of the peripheral nervous system that regulates involuntary body functions subconsciously, such as BP [18, 41-44], heart and breathing rates [45-49], digestion [43, 49, 50], body temperature [51-53] and other processes [40, 53-57]. An ANS contains two sets of nerve cells, brain stem and spinal cord. They are connected to the other cells called autonomic ganglia by nerve fibres. Nerve fibres from these ganglia in general have the function of connecting internal organs within.

The sympathetic and parasympathetic nervous systems, two divisions of the ANS, usually function in opposition to one another and have a complementary relationship, creating a balance within the human body [58-60]. In general, the sympathetic nervous system speeds up heart and respiration rates, boosts BP; the parasympathetic nervous system, in contrast, counters the sympathetic one by mediating the body's relaxing functions, slowing down HR and breathing speed, releasing BP [59-61]. ANS variations induced by physiological events include changes in the breathing pattern, e.g., yawning, coughing, gasping, and are activated by activities such as exercise and eating. ANS activity can affect BP and breathing rate and reduce the quality of PPG signals.

The sympathetic nervous division of the ANS regulation can be described as the flight-or-fight responses [62]. The sympathetic nervous division of the ANS, speeding up HR, plays the role to make the body to engage with and function under different kinds of stress. In standard physiology, the sympathetic nervous division tends to govern arousal, has the fight or fight reaction, and is activated by any stimulus signals if over an individual's threshold (this threshold can vary enormously). The stimulus signals include feelings, noise, light, drugs and chemicals (e.g., caffeine). An immediate anticipatory state tends to be generated by the release of adrenaline in response to the stimulus signal, which would cause the heart to beat more strongly and quickly, increasing blood supply to the muscles and raising BP.

Meanwhile, the parasympathetic nervous division of the ANS, slowing down HR, tends to be constantly opposing the sympathetic system [63]. It helps maintain normal body functions, calms down moods, and conserves physical resources. Many organs are

controlled by both the sympathetic nervous division and the parasympathetic nervous division. Most of the time, the two divisions have opposite functions of the same organ. The parasympathetic nervous division of the ANS also performs such tasks as relaxing the bladder, speeding up the HR and dilating eye pupils. One of the examples could be that when the heart receives a neural signal stimulated from the neurons of the sympathetic nervous division, the heart will speed up and on the other hand, the heart tends to slow down when it receives a neural stimulation generated from the parasympathetic nervous division.

The parasympathetic division comes into operation when the stimulus being responded to initiates. It acts in a way opposite to the sympathetic division, and allows the human body to cool down and rebuild a balance within the body [18, 56, 58]. In detail, the parasympathetic nervous division activates encouragement to relax muscles, and specially would slow the HR and lower the BP. It also tends to assist the breathing system to get back to its normal rate. The parasympathetic division supports rest and sleep modes. The standard for ANS analysis is that the two divisions keep each other in check, e.g., the sympathetic division goes up while the parasympathetic division goes down.

A good example of optimal balance between sympathetic nervous system and parasympathetic nervous system can be seen in animals (e.g., cats) that could respond to certain environmental alerting sounds and motions switching quickly from a relaxed state, and then as soon as the situation is considered safe, they return quickly to the relaxed state. Normally, when the ANS receives stimulation information from around the human body and externally, it tends to respond by adjusting the processes between the body and the environment, usually through the sympathetic nervous division to oppose the original stimulus and through the parasympathetic nervous division to tolerate them. The parasympathetic nervous division and sympathetic nervous division usually work together in opposition to each other, creating a new balance which is the same as existed within the body before the stimulus event.

The Heart Rate variability (HRV) consists of low and high frequency mediation which are fluctuated by the sympathetic and the parasympathetic nervous systems [64]. Very

low frequency (VLF) fluctuation and low frequency mediations are known to be influenced by the sympathetic nervous system while high frequency fluctuation tends to be affected from parasympathetic nervous systems [65]. On the other hand, the variation in sympathetic and parasympathetic activities has been reported due to the induced respiratory changes [66]. The PPG signal at the fingertip has been used for the assessment of the limb BP change induced by pulse volume variation. The sympathetic nervous system tends to innervate the systolic blood volume in the peripheral arteries and arterioles to which PPG signal is highly proportional [67].

## 2.3 Photoplethysmography (PPG) based Concept

### 2.3.1 What is PPG

Photoplethysmography (PPG) is an optics based technique monitoring blood volume variations in the microvascular vessels at the site of measurement. It is often used at the skin surface to make measurements of blood volumetric variation in organs [10]. A PPG signal is often collected from the absorption changes measured by a photodiode, e.g., in a pulse oximeter, when light illuminates the skin surface. During optical illumination process, part of the transmitted light (travelling through biological tissue) is used to be absorbed by the skin and tissue, the light absorbent properties of tissue within skin surface, e.g., muscle, are constant while the blood volumetric variation shows up as a pulsatile signal broadly corresponding to each heartbeat. The principle of monitoring human vitals using a PPG technique is based on the fact that haemoglobin derivatives, mainly  $\text{HbO}_2$  and HHb, compared with the rest of the blood plasma (mainly water in optical property), have different light absorption in the visible red and near infrared regions. Thus, based on this principle, it is possible to separate the non-pulsatile (Direct Current, DC part) component from the pulsatile (Alternating Current, AC part) component in the arterial blood using a multi-wavelength based Light Emitting Diode (LED, a semiconductor device that converts an electrical current into light) system.

In detail, the principle of PPG as the schematic diagrams of light attenuation by tissue shown in Figure 2.3, peripheral blood volume tends to rise during cardiac contraction, resulting in the decrease of light absorption (attenuation) in photodetector; the diastole process will decrease the blood volume, leading to the increase of the signal. The PPG

signal variation in the photodiode (a semiconductor device that converts light into an electrical current) is strongly related to changes in the blood flow process and the blood volume variation in the underlying-skin tissue. The AC component shows changes in the blood volume that occurs between the systolic and diastolic phases of the cardiac cycle; the fundamental frequency of the AC component depends on the heart rate and is superimposed onto the DC component [68]. The DC (steady part) and AC (pulsatile part) components can be separated in the PPG signal providing a pulsatile wave.

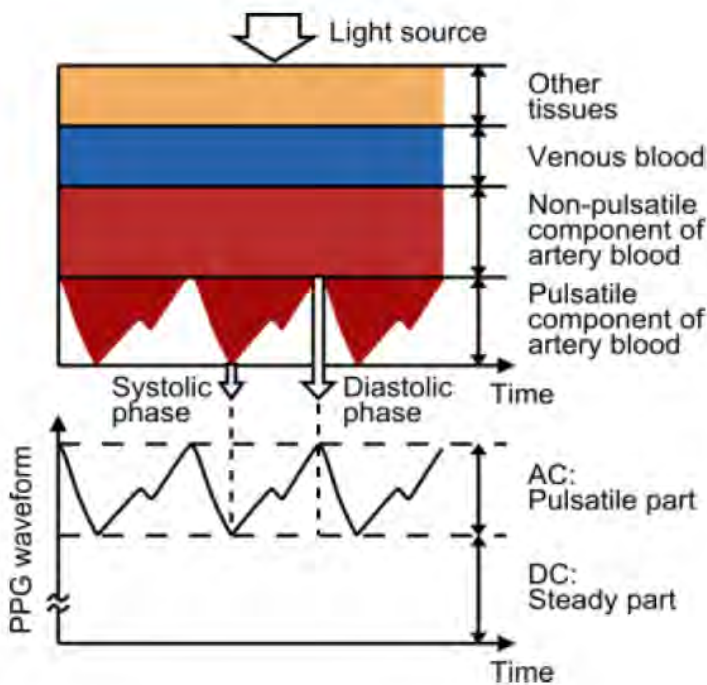


Figure 2.3: The principle of PPG describe by the schematic diagrams of light attenuation [68]

With each cardiac cycle, the heart functions as a pump sending arterial blood out to the periphery. The arterial blood and the venous blood tend to perfuse to the dermis and the fat layer of the skin as mentioned in section 2.1.1. The pressure at the end tip of the skin can be weak, but still be sufficient to allow important information to be captured from the pulse [69]. A common property is that one large initial peak is followed by another small secondary peak and this pattern is found in each cardiac cycle. The volume variation of blood is detected by a photodiode measuring the transmitted or reflected intensity of the incidental light, and the source light is provided normally by multiple wavelength LEDs. The PPG based sensor device can be used for the monitoring

physiological parameters such as respiration, BP, HR, hypo- and hypervolemia as well as other circulatory conditions. The PPG signal can vary widely from one person to another and from the location that the finger clip is placed but with the common property as mentioned above used for human vital monitoring.

### 2.3.2 Theory and Method of Non-Invasive SpO<sub>2</sub> and Hb Monitoring

When light is transported in biological tissue, the overall effect of absorption causes a reduction in the intensity of the light beam traversing the medium [70, 71]. A relationship between the absorption of light in a purely absorbing medium and the thickness of the medium is fundamentally described by the Beer-Lambert law [72, 73],

$$I = I_0 e^{-\mu_a d} \quad (2.1)$$

where  $I_0$  and  $I$  are the incident (original, the intensity entering the sample at  $z = 0$ ) and transmitted light respectively,  $\mu_a$  ( $\text{mm}^{-1}$ ) is the molar absorption coefficient, and  $d$  (mm) is the optical path length along the medium. The absorbance  $A$  is defined as the negative natural logarithm of the transmittance (ratio  $I$  to  $I_0$ ) of light,

$$A = -\ln \frac{I}{I_0} = \mu_a d = \varepsilon d c_A \quad (2.2)$$

where  $\varepsilon$  ( $M^{-1}\text{mm}^{-m}$ ) is molar attenuation coefficient of the absorbing substance at a specific wavelength, also known as the molar extinction coefficient, and  $c_A$  is the concentration of the absorbing substance.

The Beer-Lambert law is also valid if more than one absorbing substance is present. Each absorber contributes in part to the total absorbance. The resulting total absorbance  $A_t$  of a medium with  $n$  absorbing substances for a given light is written as:

$$A_t = \sum_{i=1}^n \varepsilon_i(\lambda) d_i c_{A,i} \quad (2.3)$$

The Beer-Lambert law is only valid under certain limited conditions: the light entering the medium must be monochromatic and perfectly collimated, and the medium itself must be purely and uniformly absorbing [72, 73]. Therefore, the Beer-Lambert law allows the concentrations of  $n$  different substances to be determined if the absorbance of

light is measured at  $n$  different wavelengths and the extinction coefficients of the substances are known [74].

The measuring principle of pulse oximetry is based on the different absorbance properties of oxygenated and deoxygenated haemoglobin and the pulsatile intensity variation. The volume and pressure fluctuations are generated in the systolic phase of the heart.  $\text{HbO}_2$  and  $\text{HHb}$  are the main light absorbers in human blood. A further distinction is drawn between functional and dysfunctional haemoglobin. Functional Haemoglobin is able to bind reversible oxygen, dysfunctional is not. Most of the haemoglobin in healthy blood is functional haemoglobin whose extinction coefficient is greater than that of dysfunctional haemoglobin. In pulsoximetry the oxygen saturation is defined as [75, 76]

$$\text{SpO}_2 = \frac{c_{\text{HbO}_2}}{c_{\text{HbO}_2} + c_{\text{HHb}}} \quad (2.4)$$

The  $\text{SpO}_2$  is an indirect/non-invasive measurement of the oxygen content of blood (pulse oximetry) where  $\text{SaO}_2$  is a direct/invasive measurement of the oxygen content of the blood (arterial blood analysis).

$$\text{SaO}_2 = \frac{c_{\text{HbO}_2}}{c_{\text{HbO}_2} + c_{\text{HHb}} + c_{\text{COHb}} + c_{\text{MetHb}}} \quad (2.5)$$

Pulse oximeters normally work in the wavelength range from 600 nm to 1000 nm. The  $\text{SpO}_2$  reading in blood is to be measured at wavelengths where the differences in the extinction coefficients of  $\text{HHb}$  and  $\text{HbO}_2$  are high. The absorption spectra of haemoglobin derivatives in Figure 2.2 shows the significant absorption differences of  $\text{HHb}$  and  $\text{HbO}_2$  are at the selected wavelengths (660 nm and 905 nm) [77].

To determine non-invasive Hb concentration, suitable wavelengths of light need to be selected based on the absorption properties of tissue components. Research has shown that blood has a stronger absorption at short wavelengths and water ( $\text{H}_2\text{O}$ ) at long wavelengths. The near-infrared window (also known as the optical window) falls into the range of wavelengths from 650 nm to 1350 nm where light has its maximum depth

of penetration in tissue [78]. The light absorption in the near-infrared window dominates attenuation over light scattering. Assumptions are made for which (1) the absorption of plasma and water is similar, and (2) red blood cells are mainly filled with Hb and water. Blood basically consists of two different types of haemoglobin: deoxyhaemoglobin (HHb) and oxygenated haemoglobin ( $\text{HbO}_2$ ). These two different types of haemoglobin exhibit different absorption spectra that are normally represented in terms of molar extinction coefficients. During the measurement of Hb, the absorption should not be dependent on the oxygen saturation. That means the measurement is only practicable at so called isosbestic points where the molar extinction coefficient spectra of HHb and  $\text{HbO}_2$  intersect. One such point is known to exist around 810 nm [23]. Also at the wavelength of 810 nm the absorption coefficient of water is insignificantly small in comparison to the Hb concentration. According to the assumption that red blood cells are mainly filled with water, another wavelength of 1300 nm is selected as the absorption spectra of HHb and  $\text{HbO}_2$  above 1200 nm is identical and the absorption is indistinguishable to the absorption of water [23].

Finally the determination of Hb concentration measurement is performed at the wavelengths  $\lambda_1 = 810 \text{ nm}$  and  $\lambda_2 = 1300 \text{ nm}$ . The ratio of the ratio of both wavelengths leads to the quotient  $H$ , also known as Hb coefficient [72],

$$H = \frac{A_{t,810 \text{ nm}}}{A_{t,1300 \text{ nm}}} = \frac{\ln\left(\frac{I_{\text{AC+DC},810 \text{ nm}}}{I_{\text{DC},810 \text{ nm}}}\right)}{\ln\left(\frac{I_{\text{AC+DC},1300 \text{ nm}}}{I_{\text{DC},1300 \text{ nm}}}\right)} = \ln(10) \frac{\varepsilon_{\text{Hb}}(\lambda_{810 \text{ nm}}) c_{\text{Hb}}}{\mu_{\text{H}_2\text{O}}(\lambda_{1300 \text{ nm}}) M_{\text{Hb}}} \quad (2.6)$$

where the approximate haemoglobin molecular weight  $M_{\text{Hb}}$  is 64,500 g/mol.

Finally the haemoglobin concentration can be determined as follows:

$$c_{\text{Hb}} = 0.434 \frac{H \cdot \mu_{\text{H}_2\text{O}}(\lambda_{1300 \text{ nm}}) \cdot 64,500 \text{ g/mol}}{\varepsilon_{\text{Hb}}(\lambda_{810 \text{ nm}})} \quad (2.7)$$

## 2.4 PPG Device Design based on an Embedded System

### 2.4.1 An Embedded System

An Embedded system is as a computer system in a combination of hardware and software for a larger machine. Daily accessible electronic devices, except for personal computers, are generally based on an embedded systems with the properties of small size, low power consumption, and without human intervention. There are large areas of applications but not limited to these including medical sensor systems, transportation, banking and office equipment [79]. In general, the hardware included in an embedded system is based on the microcontroller, power source, clock oscillator, Real Time Clock (RTC), reset circuit, power-up reset and watchdog timer reset, memory, I/O (Input/Output), I/O buses, interrupt handler, Digital-to-Analogue Converter (DAC) and Analogue-to-Digital Converter (ADC), Liquid Crystal Display (LCD) and LED display, keypad/keyboard, sensors, actuators, etc. A simple diagram block of an embedded system is shown in Figure 2.4.

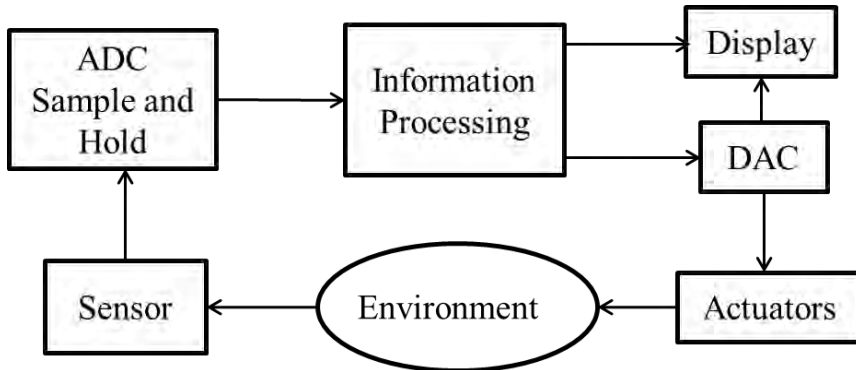


Figure 2.4: Diagram block of an embedded system

### 2.4.2 Microcontroller

The microcontroller is a small computer, generally on a single Integrated Circuit (IC), containing a processor core, memory, and programmable input/output peripherals. For example, the ultra-low power microcontrollers from the Texas Instruments MSP430 family consist of devices featuring different sets of peripherals and targeting of different applications. The architecture combines five low power modes and has been optimized to achieve extra battery life in a wearable measurement application. The

microcontrollers feature a powerful 16-bit Reduced Instruction Set Computing (RISC) CPU (Central Processing Unit), 16-bit registers, and constant generators. The internal digitally controlled oscillator (DCO), as one of the clock sources, allows wake-up from low power mode to active mode in less than 6  $\mu$ s. Figure 2.5 shows the pin designation for MSP430F1611, which is one of MSP430X161X series. In detail, the MSP430F1611 is a microcontroller configured with two Universal Synchronous/Asynchronous Receiver/Transmitter (USART), two built-in 16-bit timers (Timer A and Timer B), double 12-bit DAC, a 12-bit ADC, Inter Integrated Circuit Communications ( $I^2C$ ), Serial Peripheral Interface (SPI), Direct Memory Access (DMA), and 48 I/O pins. Moreover, the MSP430X161X series also have extended Random Access Memory (RAM) address for stack and memory applications [80].

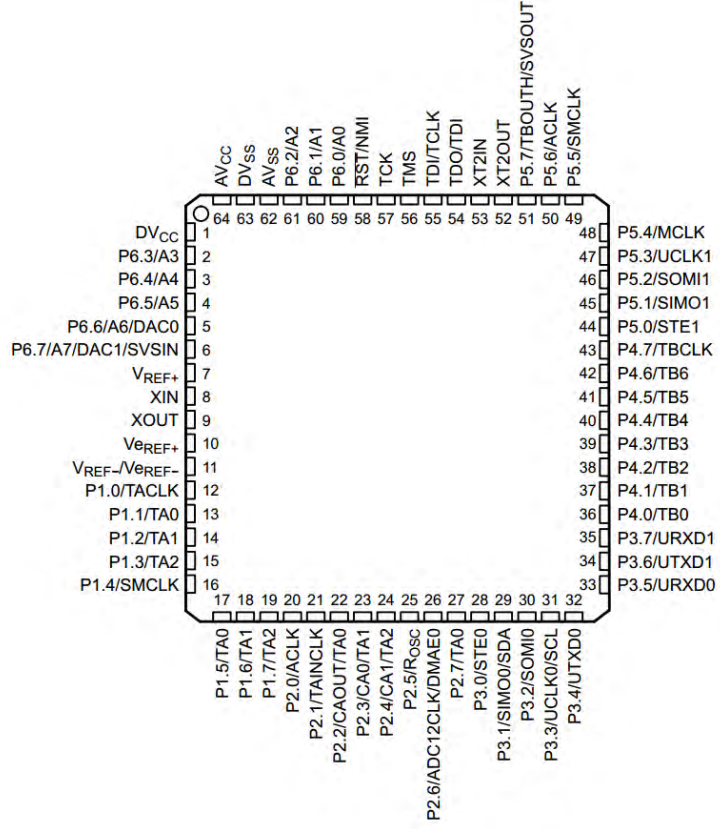


Figure 2.5: Pin designation for MSP430F1611 [80]

#### 2.4.3 Digital Accelerometer

Processing of physical data starts with capturing this data. Sensors can be designed for virtually every physical and chemical quantity including weight, velocity, acceleration,

electrical current, voltage, temperatures etc. chemical compounds. Many physical effects used for constructing sensors.

Digital accelerometer is a IC device that measures both static gravity and dynamic acceleration (e.g., vibration or falling movement). The custom built PPG finger clip device used in the project incorporates an ADXL345 accelerometer. Since it is a small, ultra-low power needed, triple-axis accessible, the MEMS accelerometer is well suited for wearable sensor device applications. Both SPI (3-wire and 4-wire SPI connection diagram shown in Figure 2.6) and I<sup>2</sup>C connection interface can be used for communication in master input and slave output mode.

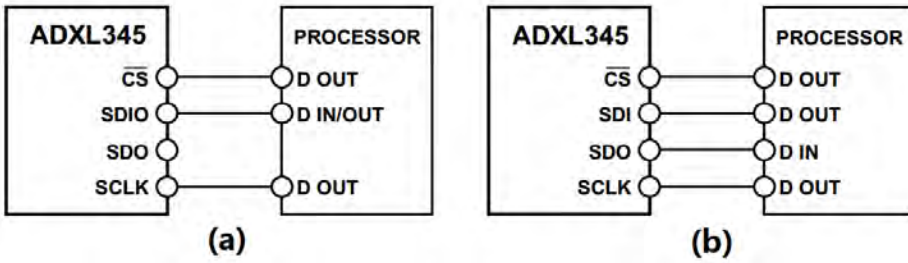


Figure 2.6: (a) 3-Wire SPI Connection Diagram and (b) 4-Wire SPI Connection Diagram [81]

The ADXL345 (resolution being 3.9 mg/LSB and sensor access range  $\pm 16$  g) is based on capacitance-sensing. The accelerometer contains capacitive plates internally. Some plates have fixed positions and others movable with minuscule springs. The acceleration detected from that causes the internal capacitances between all the plates to change as the acceleration forces applied to the sensor. The amplitude of the capacitance variation is proportional to the strength of acceleration while the polarity and magnitude are determined by an internal phase-sensitive demodulator.

The general pin connection of ADXL345 is portrayed in Figure 2.7. C1 and C3 are two 100 nF capacitors used as bypass capacitors to reduce analog supply noise C2, located between VS and GND, is provided to reduce digital I/O clocking noise. SDA, SDO, CS, INT1, and SCLK are connected to the main sensor board by FH12-12S-0.5SH, a 12-pin cable. Sensing functions such as tap sensing and freefall sensing are provided [81].

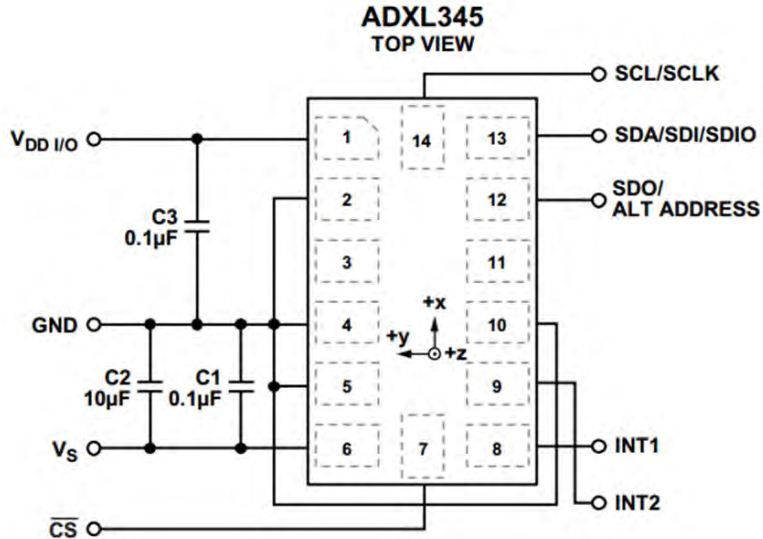


Figure 2.7: ADXL345 general pin connection [81]

The calculation of forces  $\mathbf{F}$  and moments in biomechanics relies on the accurate measurement of the kinematics of the body segments. The motion of the skin and the underlying soft tissue with respect to the bone is the source of the skin-motion artefact. In order to measure the kinematics different sensors can be used, passive markers, optical devices or inertial sensors, but all of them are placed on the skin. Two useful kinematic sensors for the measurement of human movement include the accelerometer and rate gyroscope. An accelerometer is a device that measures acceleration  $\mathbf{a}$ , based on variation of the mass-spring system.  $\mathbf{F} = \mathbf{kx}_{\text{dis}} = m\mathbf{a}$  (Hooke's law and Newton's second law of motion), so  $\mathbf{a}$  is proportional to the length of extension or contraction, where  $\mathbf{k}$  is a spring constant,  $x_{\text{dis}}$  is the distance the spring stretched from its equilibrium position and  $m$  is the mass of the object [82].

From the acceleration signal it is relatively easy to compute the natural frequency of the finger sensor clip. It must be noted that the impacts normally occurring during biomechanical measurements, e.g. the foot contact during gait, will cause a vibration of the attachment. If the natural frequency is very close to or below the frequencies of interest (the natural frequency of the internal organs is in the range from 4 Hz to 12 Hz), a measurement distortion will occur. The accelerometer is located inside the finger clip of the sensor and the sensor uses the output signals of these to actively compensate for rapid or rhythmic movement during ambulation. The frequency behaviour of the soft

tissue between the bone and a skin-mounted accelerometer (to decide if the sensor device is appropriate for the application) is given in the reference [83].

#### 2.4.4 PPG-Based Device

The PPG technique has been widely used as a bio sensor device for monitoring of human vitals in clinical and home based applications. The PPG-based system block diagram is shown in Figure 2.8. The design of a non-invasive PPG sensor system usually including these several modules: a processor, light sources (LEDs with different wavelengths), sensor devices, such as, a light detector (photodiode), pressure sensor, temperature sensor; memory unit, for the storage of data; user interfaces, including an LCD screen and buttons; a pre-processing filtering and amplifier circuit; an input and output programming interface for coding, testing and debugging; a communication component, wireless or cable used for data transition; power supply unit, from a battery or USB plug cable. The fingertip, earlobe or forehead is often selected as the preferred locations for locating a PPG sensor probe. The PPG sensor probe can be designed to be such that the detector and the LEDs are on the same side or on the opposite sides (i.e., reflective or transmissive). Hence, a PPG sensor device tends to be classified as a reflective PPG sensor or transmissive PPG sensor according to the structure of the probe. Additionally, the PPG signal collected from the sensor probe tends to be optimized by a filtering and amplifying function to maximize the quality of information.

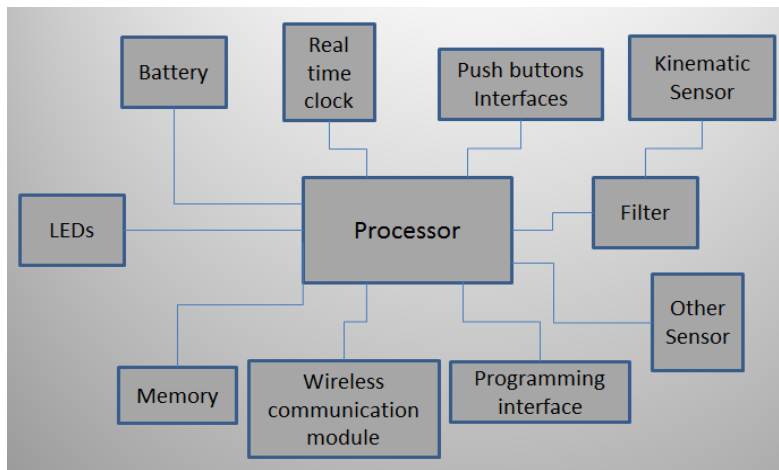


Figure 2.8: The PPG sensor system block diagram

The PPG sensor device is deployed for blood volume monitoring by an optical method [10]. A typical application is the pulse oximeter. It uses one or multiple LEDs and photodetectors to spectrally resolve the transmitted signal and obtain the oxygen concentration ( $\text{SpO}_2$ ) and pulse rate (HR) continuously and noninvasively. Furthermore, the PPG technique is used for the design of more functional bio sensor devices. Masimo rainbow® Pulse CO-Oximetry makes the measurement of Total Haemoglobin (SpHb), Oxygen Content (SpOC), Carboxyhaemoglobin (SpCO), and Methaemoglobin (SpMet) [84-88]. The NBM 200 product range from OrSense (the NBM 200 system, OrSense, Ness Ziona, Israel), another medical device company, focus mainly on the blood parameter monitoring of perfusion index (PI), pleth variability index (PVI),  $\text{SpO}_2$ , and arterial blood haemoglobin [89-91]. The region of the sensor probe applied on the human body is important and specially selected based on the signal quality and the wearable condition limitation. In general, the sensor probe is a clip type and normally clipped to the earlobe, foot toe or fingertip. For example, the cell walls of the dermis are rich with vessels and therefore greatly affects the intensity of the signals, and the finger compared with the earlobe is therefore more sensitive to variations in the ANS system [92]. More details about PPG-based monitors are described in Chapter 3 of this thesis, the literature review.

One example of an embedded system for PPG application [93] is show in Figure 2.9. The sensor is a reflective mode, with the actuators (in this case, IR LED) and Si photodiode. The microprocessor is programmed at a 100 Hz sampling frequency rate for the 10-bit DAC converter (PPG signal and 2-axes acceleration data) and to drive a bluetooth communication. Filters, amplifiers and step-up DC/DC converters (electronic circuits or electromechanical devices that convert a source of DC between different voltage levels) are also shown in the block diagram.

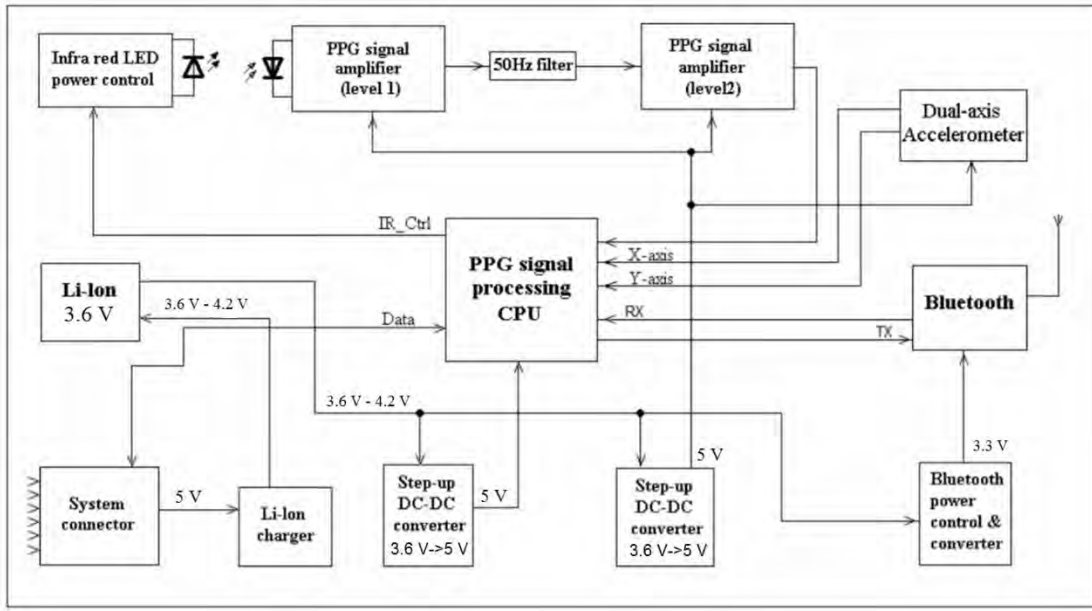


Figure 2.9: The embedded system for PPG signal monitoring [93]

## 2.5 Blood Pressure Monitor

When the finger clip was put on the finger, the subject changed the locations of the finger clip from the thumb to the little finger (the normal blood flow patterns were altered by the externally applied clip pressure in a different manner) and the haemoglobin and oxygen concentration readings were observed to slightly increase. This was explained by Timm in his thesis in Chapter 8 [77]. The influence of the contact pressure which will finally lead to the local limb BP change is shown in Figure 2.10 [94].

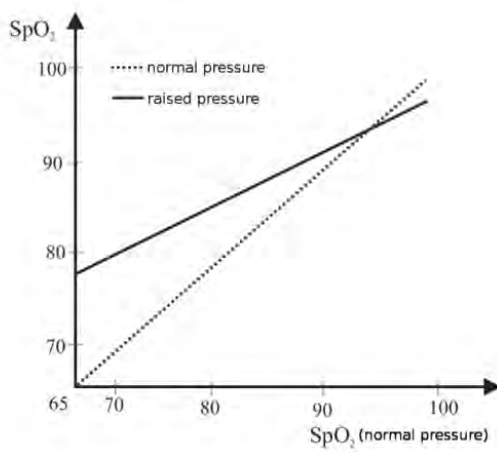


Figure 2.10: Influence of the contact pressure in pulse oximetry [94]

It is assumed that the application of the external pressure from a clip will have an influence on the local BP. Therefore, the pressure in blood should be taken into consideration as an important parameter in designing the haemoglobin sensor device. The easiest way to adjust the configuration of the finger clip is by making its diameter adjustable. Hence the finger should be just in contact with the finger clip (e.g., as an adjustable wrench to correctly suit a screw nut), so that the finger clip will not affect blood flow in the tissue.

Another solution is by using an internally mounted electrical pressure sensor (BP monitor) that continuously measures finger arterial pressure to calculate BP change ( $\Delta P$ ) and the pressure-haemoglobin coefficient so as to compensate for any pressure applied on fingers accordingly, e.g., the Finapres® NOVA [95] and Philips arm BP monitor (Figure 2.11) [96].



Figure 2.11: Philips arm BP Monitor [96]

## 2.6 Summary

Some biosensors are designed for monitoring human vitals from direct contact with human skin using optical non-invasive method. Hence, the constitution of the skin, its optical properties and the interaction of light with it are firstly described. PPG signal contents the information for human vitals measurement and the related theory and method of non-invasive Hb monitoring are introduced in this chapter. Also a brief introduction to integrated circuit is necessary for further design of the bio sensor device

in the development of motion artefact minimisation from photoplethysmography based non-invasive haemoglobin sensor.

# CHAPTER 3.

## DEVELOPMENT OF MONITORING AND COMPENSATION TECHNIQUES

---

The development of non-invasive monitoring technique based on PPG method is studied in this chapter. It concentrates mainly on the difference of invasive and non-invasive monitoring of SpO<sub>2</sub> and Hb readings in Section 3.1. Then, Section 3.2 describes the literature review relating to motion artefact removal methods, mainly focusing on methods for compensation of motion artefact and the associated algorithms.

### 3.1 Review of Development of Non-Invasive Monitoring Techniques

The most common method for monitoring the Hb in the blood is by drawing blood from individuals and testing it at the location or removed to a laboratory. Arterial blood samples are analysed using a laboratory CO-oximeter (a blood gas analyser) [87]. The GEM Premier 3000 Oximeter is one of solutions used for point-of-care measurement. The patient's vitals can be provided from comprehensive oxygenation analysis. However, it requires several steps, and often a considerable time delay to receive the results. Another measurement result by invasive measurements from hospital is the so called full blood count (FBC) method which is also used for monitoring haemoglobin.

The ability to measure haemoglobin noninvasively and continuously using the PPG technique is a breakthrough measurement that guarantees a more rapid assessment of an individual's condition. Non-invasive monitoring promises no need of handling blood and needles and no need for the risk of biohazard waste disposal.

### 3.1.1 Haemoglobin from Invasive Monitoring to Non-invasive Monitoring

Haemoglobin Monitoring is becoming more important as it is widely adopted both in hospital care and home care. The traditional method used for monitoring Hb is invasive and uncomfortable as blood samples are extracted from patients to analyse for haemoglobin concentration. There are mainly two types: Standard Laboratory CO-Oximeter (arterial blood samples are analysed in laboratory, e.g., Radiometer ABL-820 CO-Oximeter (total Haemoglobin, tHb) [97], shown in Figure 3.1), and point-of-care device (e.g., HemoCue®201 [98], shown in Figure 3.2). The former method is base on chemical electrolyte electrodes. The latter one is using the method of spectrophotometry which measures the intensity of light substance absorbs or transmits light through sample solution over a certain range of wavelength. The latter has several advantages over the former; a major one being the whole measurement procedure itself to get the Hb takes less than one minute, the other being the cost. The point-of-care device is based on the Azide methaemoglobin method which relies on the use of dry reagents [99]. The instrument of Figure 3.1 is much more accurate than the HemoCue device, but is confined to being used in the pathology laboratory.



Figure 3.1: Radiometer ABL-820 CO-Oximeter, from Radiometer Company [97]



Figure 3.2: HemoCue®201, from HemoCue Company [98]

Then non-invasive (prick-less) techniques (Acoustic Methods [100], Conductance Methods [101] and Optical Methods [102, 103]) are being increasingly used in medical devices to detect Hb without extracting blood samples from human body. Although they were firstly used as auxiliary parameters, they are showing great advantages over invasive methods. Specifically, PPG based haemoglobin monitoring technology (e.g., Radical-7®; Masimo Corp., Irvine, CA [86], as shown in Figure 3.3), which can provide non-invasive, continuous online Hb measurements [72, 102, 104]. It uses a similar operation principle to that established by Timm and et al and which forms the basis for the device in this investigation. The comparisons of these three haemoglobin monitoring methods are described in Table 3.1



Figure 3.3: Radical-7™ Pulse CO-Oximeter [86]

Table 3.1: Comparison of three haemoglobin devices: Standard Laboratory Co-Oximeter (e.g., Radiometer ABL-820 CO-Oximeter (tHb)), point-of-care device (e.g., HemoCue® 201), and SpHb monitoring (e.g., Radical-7®; Masimo Corp., Irvine, CA)

Device	Standard Laboratory CO-Oximeter (e.g., Radiometer ABL-820 CO-Oximeter)	Hematology Analyzer, Point-of-Care Device (e.g., HemoCue 201)	Non-invasive Monitoring Device (e.g., Radical-7)
Method	Chemical Electrolyte electrodes	Spectrophotometry	Multiple wavelengths of light
Characteristics	Invasive, Delayed, Intermittent	Invasive, Delayed, Intermittent	Noninvasive, Immediate, Continuous
Substrate for Analysis	Blood	Blood	Blood
Sample Chamber	Test Tube	Cuvette	Finger
Needle Stick Hazard	Yes	Yes	No
Biohazard Waste Disposal	Yes	Yes	No
Special Training /Quality Control	Yes	Yes	No
Calibration	Yes	Yes	Internal
Patient Apprehension	Moderate to High	Moderate to High	Low
Accuracy Class	High	Moderate to High	Moderate

The clinical definition of anemia in adults is defined as having a Hb in blood which is less than 12–13 mg/L [105], usually manifested as a lack of red blood cells. Lionel Lamhaut et al performed a survey in order to compare the accuracy of non-invasive haemoglobin monitoring and HemoCue®201 with automated laboratory haemoglobin measurement [106]. The study shows that SpHb monitoring with the Radical-7® gives lower reading accuracy than the HemoCue®201 for the assessment of Hb(finger clip samples may overestimate in haemoglobin measurements from 0.1 g/dl to 0.4 g/dl and ear clip may differ from the Hb in a range of 0.7 g/dl to 2.8 g/dl).

### 3.1.2 From Non-invasive SpO<sub>2</sub> Monitoring to Non-invasive SpHb Monitoring

Pulse Oximeter is widely used as a continuous, non-invasive technique that measures the oxygen saturation (SpO<sub>2</sub>) and the pulse rate of a patient. One called ChoiceMMed is shown in Figure 3.4. From non-invasive SpO<sub>2</sub> monitoring to non-invasive SpHb

Monitoring was considered a great breakthrough for PPG signal applications in the monitoring of human health [23, 107-109].



Figure 3.4: ChoiceMMed, one of commercial pulse Oximeters

One example of non-invasive SpHb monitoring device is NBM 200 (Lmb, Schwaig, Germany) [91], as seen in Figure 3.5. It includes a probe into which the finger is inserted. It consists of a reusable ring shaped sensor that is placed on the donor's finger using a pneumatic finger sensor cuff. When LEDs in the probe shine light through the finger, a photodiode on the opposite side interprets the absorption patterns to produce an instant reading of the Hb in the patient's blood in less than 60 seconds. The major difference in the instruments design between SpO<sub>2</sub> and SpHb monitoring lies in the former is employed with 660 nm and 905 nm wavelength LEDs while the latter with 805 nm and 1300 nm wavelength LEDs.



Figure 3.5: TouchHb and the data transmitted to Cell Phone wirelessly [91]

Other SpHb commercial monitoring devices include the one from Masimo Rainbow® SET® platform, e.g., Pronto-7™ Pulse CO-Oximeter, as shown previously in Figure

3.3. It allows a continuous non-invasive measurement of haemoglobin (SpHb), oxygen saturation ( $\text{SpO}_2$ ), pulse rate (PR) and perfusion index (PI), and also it has a good interactive interface. Human clinical studies have been undertaken successfully to prove the validity of this device, thus far [110-113]. However, neither the mode of operation, nor the number of wavelengths used, is publicly available.

The research team in Optical Fiber Sensor Research Centre (OFSRC) of University of Limerick (UL) and teamwork have previously conducted preliminary groundwork on optical sensor probes for monitoring Hb [73, 104, 108]. Their devices are also based on PPG signal, which is a technique using waveform to detect blood volume changes in the microvascular bed of tissue and also it can be used to assess the concentrations of blood components. With four suitable wavelength LEDs in the finger clip, this sensor system could simultaneously do a measurement of total haemoglobin concentration, oxygen saturation and pulse rate [23, 107-109] and the data could be transmitted to a PC and output through wireless sensor networks based on Bluetooth.

### **3.2 Review of Existing Methods for Compensation of Motion Artefact**

The digital accelerometer was introduced in section 2.4.2. The reliability of the PPG signal being strongly influenced by the motion of the wearer has been widely reported [14-16, 114], which will be described in detail below.

The movement of an individual wearing a PPG device can be classified into several different types. Yan et al proposed finger motion in five different positions, e.g., horizontal movement of finger and waving hand [11], and Peng et al studied four types of finger motion, such as bending and pressing of the finger [12].

The collection of PPG signals from optical based sensor probes has also been used extensively for the monitoring of HR, respiration rate and oxygen saturation [15, 73, 115]. One of the drawbacks of PPG based measurement is that the signal is strongly degraded by motion artefact [11]. Much research has been undertaken relating to the removal of motion artefact noise resulting from the wearer's movement.

The correction introduced using accelerometers, gyroscopes (relative and global sensors motion, angular velocity), laser diode, and motion-resistant algorithms are introduced to

remove the deviation of motion artefact. Methods used to minimise the impact of motion artefact include: adaptive noise cancellation algorithm (e.g., Normalized Least Mean Square, NLMS) to recover signals corrupted due to body motion using acceleration data [14], relative sensor motion via self-mixing interferometry in a laser diode [15], periodic moving average filter [16], and a method that uses synthetic noise reference signal without any extra hardware [17]. Most of the methods are effective on the condition that the corrupted signal is only affected by the factor of motion noise. However, other physiological interfering parameters, e.g., breathing pattern and BP variations, can also affect the original PPG signal quality during the motion events.

For the research study of reducing motion artefact in the Hb monitoring system, commercial pulse oximetry ( $\text{SpO}_2$ ) is a good place to start, since it is also based on the PPGs waveform theory and its motion artefact elimination techniques have been widely investigated. Some pulse oximeters include a motion-resistant algorithm and show good performance and improvement in rhythmic human movements (e.g., uniform walking pace) by software compensation [16]. But the breakthrough of such robust motion elimination pulse oximetry capable of measurement whilst in motion continuously and in real time is still in research and was not yet been achieved. Most pulse oximeters that are used in physical care in sports are not recommended to be used during the process of training. It has been reported that there is a strong need of special care in the elderly groups and in sports (health care in real-time), so the highest demand of reducing motion artefacts are pushing the research work on these PPGs sensor devices to improve the accuracy of those sensor devices.

A PPG signal obtained from a wearer in motion contains a motion artefact signal mixed with the desired physiological signal. The motion artefact tends to be induced through ambient lighting, a loose of skin contact between led and photodiode, inertial blood flow and tissue shaping (hydrostatic pressure changes). Kinematics is the description of the movement of the body segments, independent of the forces that cause movement. Kinematic variables include linear and angular displacements, velocities, and accelerations. Motion artefacts in PPGs as a result of finger bending and motion artefacts in forehead obtained PPGs as a result of walking are described in reference [83]. Voluntary and involuntary movements, such as movement during transport,

tapping, rubbing, scratching, waving, shivering, and seizures in adult and pediatric patients; and kicking, stretching, crying, flexing, and imposed motion in neonates, are some common sources of patient motion in the clinical setting [116].

### 3.2.1 Adaptive Noise Cancellation (ANC)

Over the past three decades, the adaptive filter as a linear filtering system involving the transfer function controlled by variable parameters to adapt to changing signal over time by the mathematical optimization. Most of the adaptive filters have the features of digital filtering due to the convenience of optimization algorithm and development of applications. The adaptive filtering technics are widely adopted in the situations where some applications possess the unknown or constantly changing environments whereas some parameters are uncorrelated with each other's [117].

The removal of motion artefact from a sensor signal using adaptive filtering method is shown schematically in Figure 3.6 for which the closed cycle in the adaptive filter works as a loop with the difference signal  $e(n)$  as the feedback.  $s(n)$  should be uncorrelated with the motion noise  $v(n)$  (which cannot be detected directly), and if both the motion artefact in bio-sensor clip  $v_1(n)$  and the motion received by accelerometer  $v_2(n)$  are extremely correlated with movement of wearer  $v(n)$ ,  $v_1(n)$  then can be assessed using the ANC process by regulating the coefficients of the filtering system. the system then can The elimination of the motion artefact finally realized by the filtering system with the decrease of the difference between output value  $y(n)$  and  $v_1(n)$ . The subtraction between  $y(n)$  and an expected value  $d(n)$  is defened as the error signal  $e(n)$  which is close to the desired signal  $s(n)$ . In general, the closed cycle in the adaptive filtering process (modification of the filtering transfer algorithm) consists of the iteration of a cost function by which the goal of minimisation the cost of the next iteration is achieved. One such is the mean square error (MSE) of the signal.

Filter consistency, filter performance, tools, and digital signal processing (DSP) requirements are the primary concern in selecting the adaptive filter that best suits the needs in real applications. As the power of DSP greatly improved nowadays, all kinds of adaptive filtering methods have been more and more commonly and routinely used in smart digital devices such as mobile cell phones, video cameras, and medical

monitoring machines [117]. Adaptive filtering can be divided into least mean squares (LMS), NLMS, recursive least squares (RLS), and multidelay block frequency domain adaptive filter (MDF) in terms of filtering implementations.

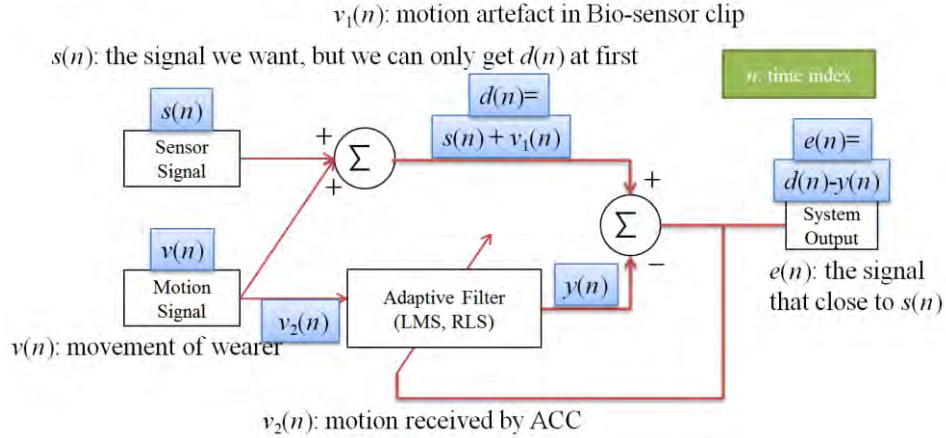


Figure 3.6: Removal of motion artefact by adaptive filter

The adaptive removal of motion artefact is highlighted in the reference [118] which stated that adaptive motion artefact reduction only induced into the PPG signal when the motion event occurred along the axis of the sensor probe. The acceleration data from the digital accelerometer is remodelled as an additional  $w(t)$  into the desired signal. Then this motion corrupted PPG signal can be compensated by the estimated motion artefact part. The schematic of the motion artefact minimisation process is plotted in Figure 3.7 [118].

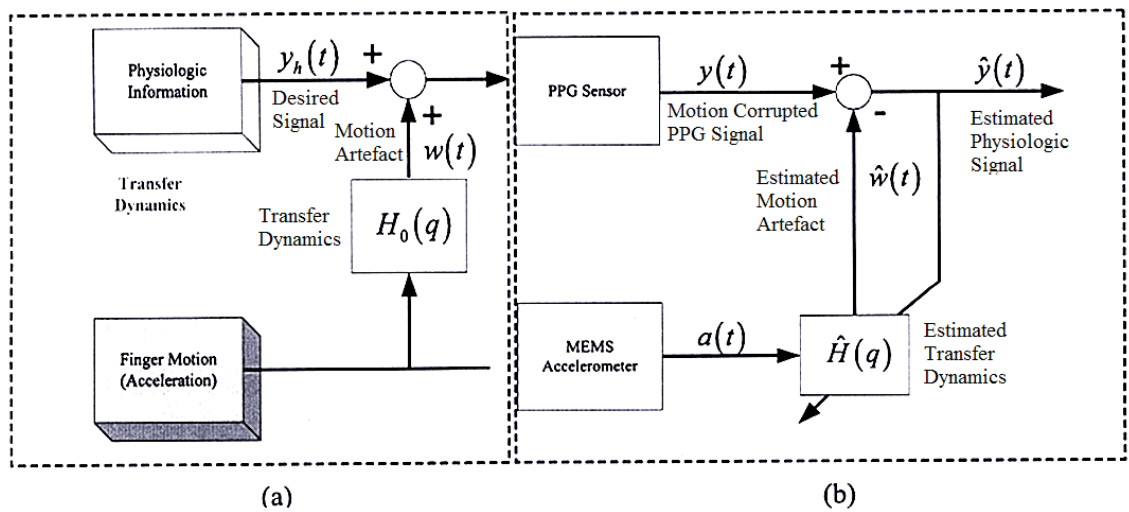


Figure 3.7: (a) motion artefact and (b) removal of motion artefact by adaptive filter [118]

The adaptive filtering methods adopted by wearable sensor devices to reduce the effect of the motion artefact are to guarantee devices such as pulse oximetry capable of being in full function in the motion events both short periods and long periods for the wearers. A newly developed motion-noise-removal algorithm named discrete saturation transform (DST), is developed by Masimo for monitoring SpO<sub>2</sub> non-invasively in motion and low peripheral perfusion situations by the proposed adaptive filter. The Masimo pulse oximetry is designed based on the Beer–Lambert law described in Chapter 2 of this thesis. Research reports have proved that the adaptive filter method adopted measurements are significantly improved and less alarm rate than without the method applied on. Minimum correlation discrete saturation transform (MCDST) demonstrates that the linear fitting method in DST can be used to replace the traditional adaptive filter, reducing the energy consumption whilst boosting the development of measurements [119].

### 3.2.2 Empirical Mode Decomposition (EMD)

Empirical mode decomposition (EMD) method is one essential step in Hilbert–Huang transform (HHT) (another being Hilbert spectral analysis). By decomposing the complicated original signal into several other partial components in specific rules, the EMD method can be as useful as other analysis methods in signal processing, e.g., Finite Impulse Response (FIR) and Kalman filters. The direct advantage of the EMD method is its application in clarify the analysis of a complicated signal by a small number of components, described as intrinsic mode functions (IMFs). The EMD algorithm turns out to be very useful in the study of seismic records series [120, 121]. Unlike the analysis of frequency domain of Fourier Transforms, EMD is simply but highly efficient for the nonlinear and non-stationary time series analysis in time domain [122].

IMF has in a more general features as a simple harmonic component with inconstant amplitude in the time domain. The procedure of extracting each unit of IMFs has to follow the rules that (1) Throughout the original signal in a continuous time domain, there is only one extreme between each set of zero crossings and (2) the mean value of the upper and lower envelopes of the signal is zero [123, 124].

In every ‘raw’ data set, ‘extreme’ values exist which are those points whose first-order derivatives are equal to zero in the data  $s(t)$ , the interpolated data can be determined by a cubic spline interpolation through these extreme values. A loop following the rules above for the procedure of each IMF was obtained from the upper  $X_{i,\text{upper}}(t)$  and lower  $X_{i,\text{lower}}(t)$  envelopes of the raw signal. The difference between the data  $s(t)$  and the mean of the upper and lower envelopes  $m_1$  is the first component  $h_1$ :

$$h_1 = s(t) - m_1 \quad (3.1)$$

$h_1$  has the potential to be the the first IMF if only it satisfies the rules. If  $h_1$  is not the first IMF, the subsequent shifting process will then be necessary. In another loop procedure,  $h_1$  is treated as input data similar to the position of  $s(t)$ , the mean of the upper and lower envelopes of  $h_1$  is defined as  $m_{11}$ , the difference of  $h_1$  and  $m_{11}$  is  $h_{11}$ :

$$h_{11} = h_1 - m_{11} \quad (3.2)$$

The loop can be up to  $k$  times until  $h_{1k}$  is found for being qualified as an IMF:

$$h_{1k} = h_{1(k-1)} - m_{1k} \quad (3.3)$$

For simplification purpose, the first IMF component of the data  $s(t)$  is described as  $c_1$  instead of  $h_{1k}$ :

$$c_1 = h_{1k} \quad (3.4)$$

the residue,  $r_1$ , is the rest of the data  $s(t)$  subtracted  $c_1$ , and treated as the new data similar to data  $s(t)$  as the input for deducing of the next IMF component of the data  $s(t)$ .

The  $n^{\text{th}}$  residue  $r_n$  is stated as the difference between the  $(n-1)^{\text{th}}$  residue  $r_{n-1}$  and the  $n^{\text{th}}$  IMF component  $c_n$ :

$$r_n = r_{n-1} - c_n \quad (3.5)$$

A decomposition of the data  $s(t)$  into  $n$ -empirical modes is realised by repeating the processure of the  $n^{\text{th}}$  IMF component  $c_n$  until the residue  $r_n$  becomes a monotonic function. So the data  $s(t)$  can be described as:

$$s(t) = \sum_{j=1}^n c_j + r_n \quad (3.6)$$

### 3.3 The Proposed Envelope-Based Filtering Method

A novel method for implementing the PPG filtering is described which is based on an existing standard envelope algorithm as opposed to traditional filtering methods. The envelope is a curve “enveloping” the source data. The envelope is formed as a tangent to every peak in the source dataset. Different methods have been proposed to compute an envelope, e.g., Hilbert-Huang transforms (HHT) [125], the cubic spline interpolation algorithm [126], and Akima interpolation algorithm [127]. Each envelope algorithm has their set of limitations: e.g., HHT is required to fit the envelope of a signal including the extreme points of the signal; the cubic spline interpolation algorithm might be not flexible enough and overshoot may occur; the Akima interpolation algorithm [126] may incur break points on the data and this may result in a lack of ‘smoothness’ in the signal.

In every ‘raw’ data set, ‘extreme’ values exist which are those points whose first-order derivatives are equal to zero in the raw signal,  $X_{i,\text{raw}}(t)$ , where  $i$  stands for a variable and  $t$  is the time (in second). The upper  $X_{i,\text{upper}}(t)$  and lower  $X_{i,\text{lower}}(t)$  envelopes of the source data were obtained from the adjacent-averaging smoothing of the interpolated data, which takes the average of a certain number of data points around each point in original data (in this case, five-point-smoothing was employed on the grounds that it provides sufficient noise suppression). The methodology for obtaining the upper and lower envelopes of a signal is based on a standard subroutine within the commercial package OriginPro (OriginLab Corporation, Northampton, Massachusetts, USA) and explained in greater detail in the reference related to envelope algorithm [128]. The raw PPG signal,  $X_{i,\text{raw}}(t)$ , can be optimized and expressed as the AC (time varying) component  $X_{i,\text{AC}}(t)$  and the DC (non-time varying) component  $X_{i,\text{DC}}(t)$ .

$$X_{i,\text{AC}}(t) = \frac{(x_{i,\text{raw}}(t) - x_{i,\text{lower}}(t)) \cdot (\frac{1}{n} \sum_{i=0}^n (x_{i,\text{upper}}(t) - x_{i,\text{lower}}(t)))}{(x_{i,\text{upper}}(t) - x_{i,\text{lower}}(t))} \quad (3.7)$$

$$X_{i,\text{DC}}(t) = \frac{1}{n} \sum_{i=0}^n (X_{i,\text{raw}}(t)) \quad (3.8)$$

where  $n$  stands for the size of the raw signal (positive integer). The combination of AC and DC components from a raw PPG signal can be considered as the original PPG signal from which an updated Hb coefficient is derived. Note that real PPG signals often contain a very slowly varying baseline but this can be distinguished from the targeted PPG signal as it is generally of much lower frequency ( $< 0.5$  Hz).

### 3.4 Summary

In this chapter, the development of non-invasive monitoring technique and the methods for compensation of motion artefact in bio sensor systems are presented. The ANC is newly applied in motion removal in bio sensor devices on the condition that the PPG signal only affected by the factor of motion noise. EMD is a method of breaking down a signal (in this case, the signal is PPG signal) into IMF and a monotonic function. The first IMF usually carries the most oscillating (high-frequency) components with limited motion noise. Finally, the proposed filtering method based on the envelope algorithm was proposed in the study of motion noise removal.



# CHAPTER 4.

## MULTI-SENSOR SYSTEM

---

The optical multi-sensor system includes a number of separate wavelengths of light, usually emitted from LEDs, towards specific area of a patient's skin. Similar to non-invasive SpO<sub>2</sub> monitoring, non-invasive Hb measuring is an example of a PPG derived signal, which is based on the absorption of light in the visible and near infrared range of haemoglobin derivatives and H<sub>2</sub>O in blood. Through the analysis of the level to which these wavelengths are absorbed whilst passing through the patient's skin, the patient's diagnostic parameters, such as SpO<sub>2</sub>, total Hb concentration and pulse rate can be discerned. In addition to the two wavelengths used in pulse oximetry, 660 nm and 905 nm, two additional wavelengths are employed within this platform, 805 nm and 1300 nm, which allow for the determination of Hb measurement.

The received optical signal at the photodiode is defined as the PPG signal and its intensity is represented by the PPG amplitude (volts versus time (s)). The detected signal at the output of the receiver amplifier (volts) corresponds to the optical attenuation in that channel which comprises all losses including absorption, scattering and losses due to geometrical transmission. The finger sensor probe in this investigation is attached to the subject using velcro tape in order to make the finger band size adjustable for different finger sizes. It has been widely reported that the local BP at the measuring point potentially introduces variability in measured PPG waveforms [129]. In all the following experiments, the PPG finger probe was placed on the right hand index finger in the same position in order to avoid potential error from external pressure variations between the finger and the probe caused by the need for over tightening or loosening the probe during operation.

## 4.1 PPG Sensor Device Layout

The custom designed multi-sensor system is displayed in Figure 4.1. It is mainly composed of a main sensor board and a finger sensor probe. The background of microcontrollers and digital accelerometers were presented in detail in section 2.4. The interface of the main sensor board contains a mini USB port, a 14 pin socket for microcontroller programming and program debugging for the MCU, extra LEDs intensity resistor group for adjustment of the LEDs' brightness, and a 12 pin sensor probe bus connected to the finger sensor probe. Specially, the 1300 nm wavelength LED is driven by an extra battery due to the high power (7 V) needed to active it. The main difficulty of this technique is to provide good contact between the skin and the detection units. The dimension of the finger sensor is adjustable as described in the previous section.

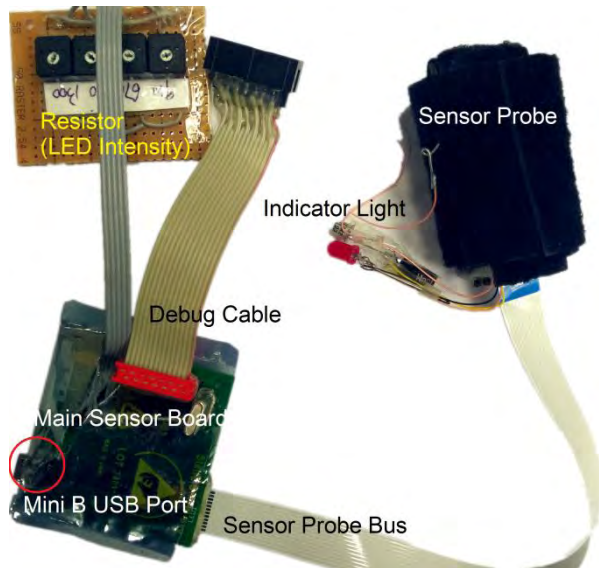


Figure 4.1: The custom designed multi-sensor system

The circuit design and schematic are described in Figure 4.2. The four LEDs are driven by 4 LEDs drivers on the main sensor board and the anodes are connected to the VCC (pin X1-1). LEDs are pulsed sequentially to provide multiplexing of the signal: for example, in first  $7.5 \mu\text{s}$  the state of LED1 is on and the other three LEDs are off; in the next  $2 \mu\text{s}$  all LEDs are off; and then the LED2 is on for another  $7.5 \mu\text{s}$  and the other three LEDs are off, etc. Transmitted signals are amplified and collected by a wide spectral range sensitive photodiode. The signal captured by the photodiode is pre-

amplified (current to voltage) by the operational amplifier circuit. C1 and C3 are two 100 nF capacitors used as capacitors to reduce analog supply noise C2, located between VS and GND, is provided to reduce digital I/O clocking noise. SDA, SDO, CS, INT1, and SCLK are connected to the main sensor board by FH12-12S-0.5SH, a 12-pin cable.

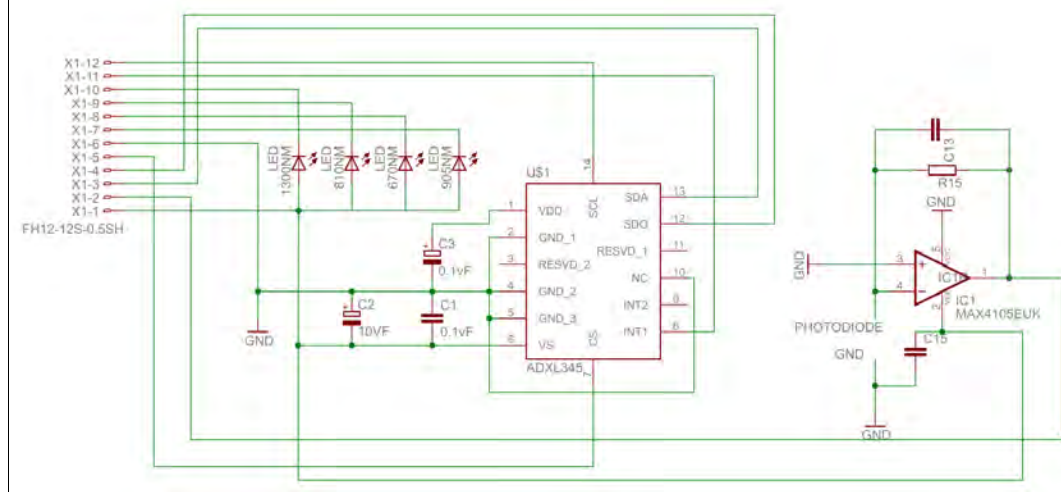


Figure 4.2: Schematic of the probe board

#### 4.1.1 Main Sensor Board

Figures 4.3 and 4.4 show a top view and bottom view of the main board from the multi-sensor system, respectively. The board was designed using the EAGLE PCB design package. A processor MSP430F1611 is configured to host the system signal processing and data transition. A digital accelerometer is also included in the sensor finger clip. A 12-pin cable is used for the connection between the main sensor board and the finger sensor probe. There are 5 extra pins defined as P4.3 for SDA (Serial Data Input), P5.0 for SDO (Serial Data Output), P5.4 for CS (Chip Select), P2.5 for INT1 (Interrupt 1 Output), and P3.2 for SCLK (the clock for SPI). More pin configurations are given in Table 4.1. The following provides detail regarding the design of the main sensor board in the aspect of analogue to digital converters (ADC), sampling rate, amplification, filtering and noise analysis.

Table 4.1: The bus pin configuration

From top to bottom	1	2	3	4	5	6	7	8	9	10	11	12
Description	VCC	PD	SDA	SDO	CS	GND	910	660	805	1300	INT1	SCLK
Pin to main board			P4.3	P5.0	P5.4		nm	nm	nm	nm	P2.5	P3.2

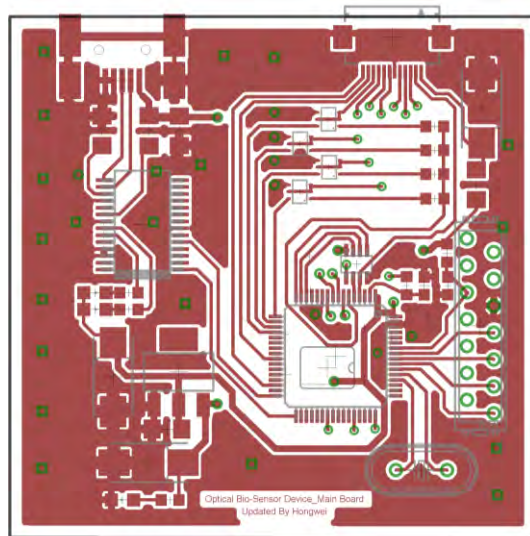


Figure 4.3: Top view of Optical Bio-Sensor Device\_Main Board

Auxiliary clock (ACLK), sourced from a 32.768 kHz watch crystal or a high frequency crystal (in this case, for watch crystal on pin XIN/XOUT), main clock (MCLK), the system clock used by the CPU, and sub-main clock (SMCLK), the sub-system clock used by the peripheral modules, are three basic clocks in a digital MCU system. In our digital system, MCLK and SMCLK are sourced from XT2, which is driven by an 8 MHz crystal while ACLK sourced from LFXT which is driven by a 32.600 kHz crystal. ACLK can be used as the clock signal for Timer A and Timer B. The MSP430 MCU clock system is shown in Figure 4.5.

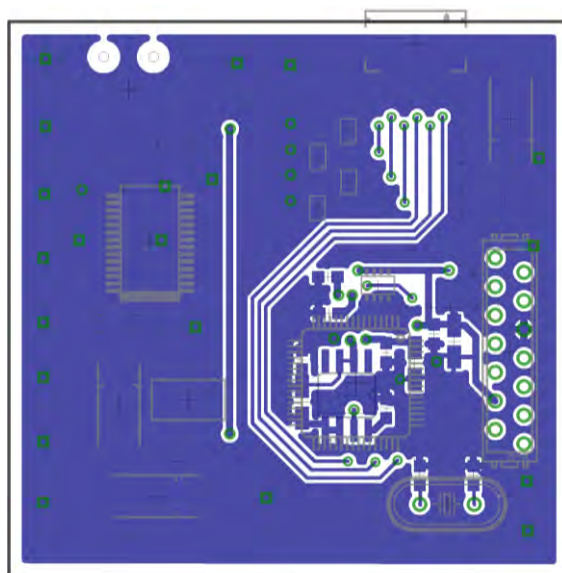


Figure 4.4: Bottom view of Optical Bio-Sensor Device\_Main Board

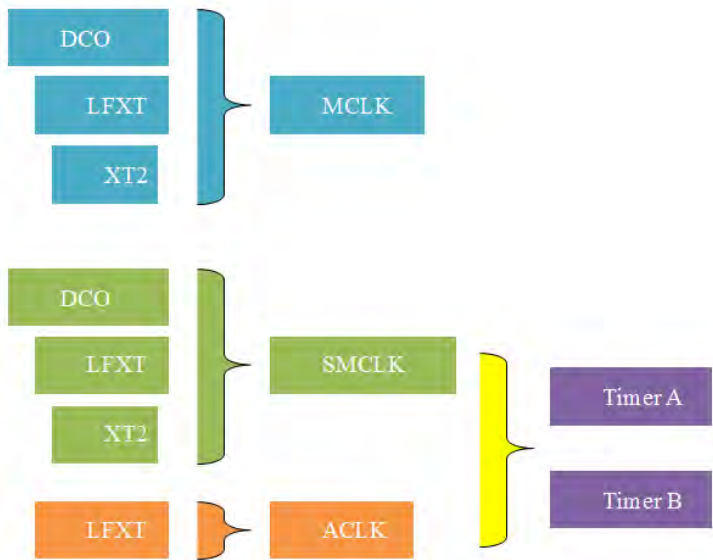


Figure 4.5: MSP430 MCU clock system

The schematic of the main sensor board is shown in Figure 4.6. FT232RL is an interface IC device for the USB UART (Universal Asynchronous Receiver/Transmitter) convertor. USBDM is short for USB Data Signal Minus as I/O port. USBDP stands for USB Data Signal Minus. VCC is a PWR (power) pin supplied by USB 2.0 to mini B from Laptop. RXD is the receive asynchronous data input and TXD is transmit asynchronous data output. CBUS0 is configurable CBUS I/O pin. The default function of this pin is TXLED# which is the LED drive for transmitting data (pulses low when transmitting data via USB). CBUS1 is also a configurable CBUS I/O pin. The default function of this pin is RXLED# which is the LED drive for receiving data (pulses low when receiving data via USB) [130]. In this case, the pins of CBUS0 and CBUS1 are driven by a low dropout regulator ADP3338 (input voltage 5 V) [131] which provides a stable 3.3 V. The same 3.3 V is also as input of AV<sub>CC</sub> and DV<sub>CC</sub> of the processor MSP430F1611. The REF02HCSA provides a stable 5 V output for the V<sub>eREF+</sub> as the DAC12 reference selected by DAC12SREF\_2 (2\*0x2000u) for LED output. AS1102 is chosen as the four LEDs Drivers with DAC function. It has three outputs with up to 40 mA per LED. LTC6910-1 is a digitally controlled programmable gain amplifiers with a ADC function. Its digital inputs (pins 5, 6 and 7) are programmable for gain value. P6DIR= 0xC0 sets P6.3 and P6.5 being the amplified input and raw input while P6.4, P6.6 and P6.7 being outputs.

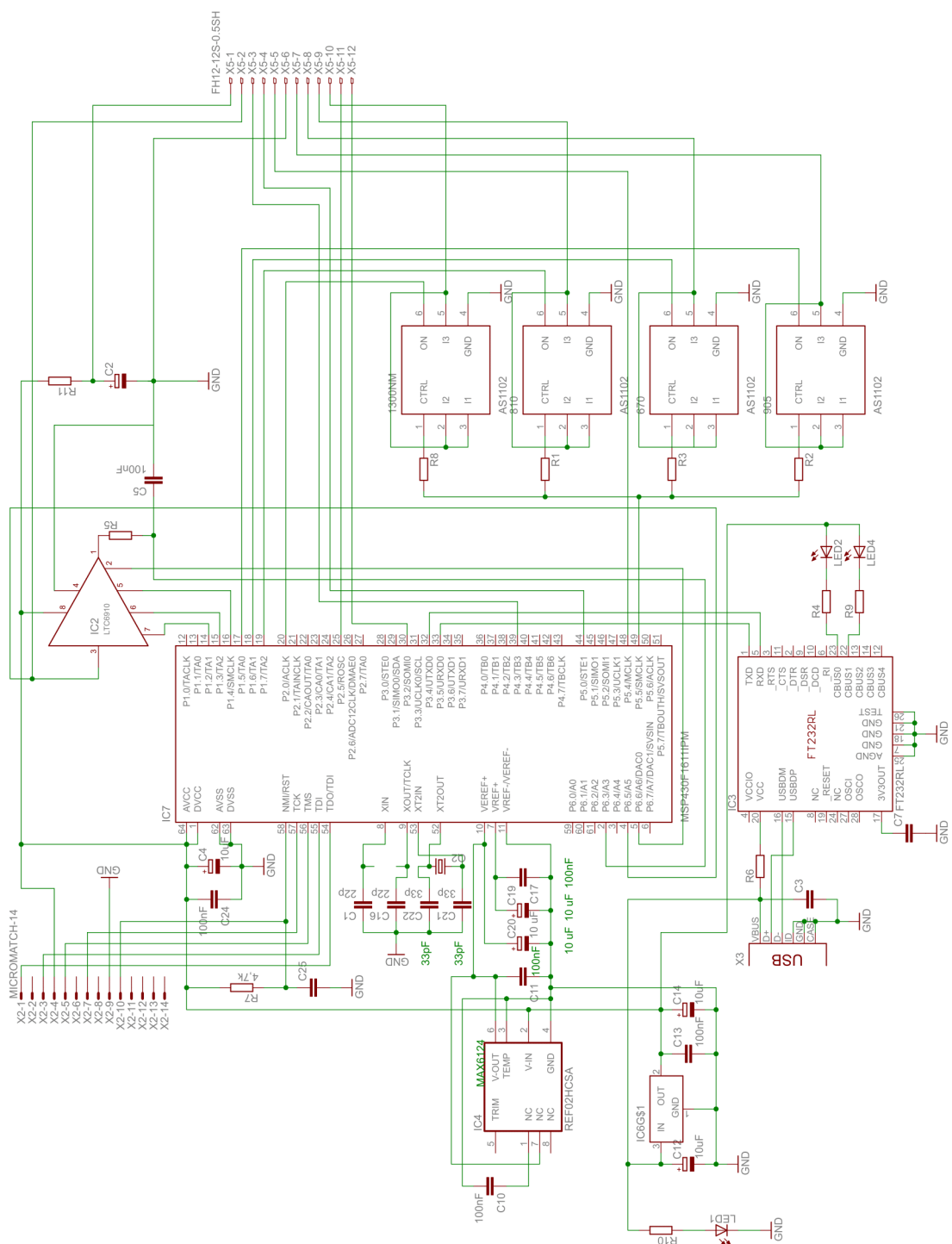


Figure 4.6: Schematic of the main sensor board

#### 4.1.2 Development of the Finger Sensor Probe

A LED has good performance in directionality and intensity. The newly developed optical sensor system uses four separate LEDs each with their unique wavelengths for the simultaneous measurement of HR, SpO<sub>2</sub> and Hb. An additional 3 axis accelerometer brings the possibility of detecting the motion of the sensor probe, providing values for the static (gravity) and dynamic acceleration. The combination of multi-wavelength signals and digital ACC signals makes the non-invasive measurement method of human vitals more robust provides the opportunity to correct for movement artefact.

The finger sensor probe consists of a custom designed four LED package, a photodiode, an ADXL345 circuit and amplifier/filter circuits. The finger clip is a custom design whereby the contact force between the sensor and the measurement site applied on the finger can be adjusted, as research results have been found that the level of pressure applied to the finger by the clip also influences the quality of the PPG signal. When the probe is too loose, the PPG signal tends to have low amplitude due to poor optical coupling. On the other hand, when the probe is too tight, apart from the subject not being comfortable, the local pressure at the measuring point tends to introduce variability in the PPG waveforms. Hence, the finger sensor probe is adjusted before each experiment in order to ensure a good baseline reference signal from the device.

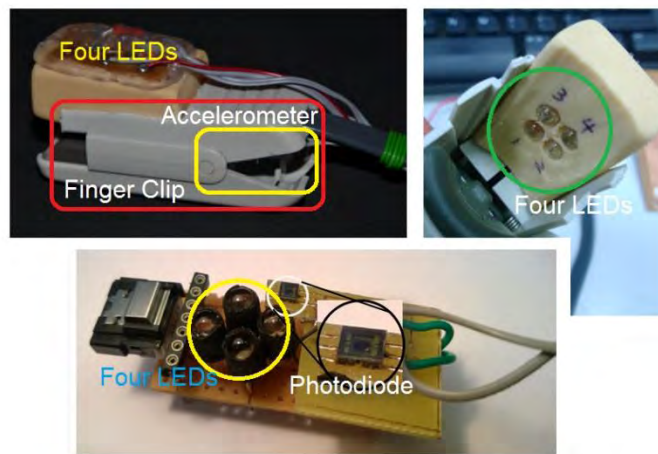


Figure 4.7: First generation of a finger clip with an embedded ADXL345

The first generation of finger clip is shown in Figure 4.7. It is designed with both a reflective PPG sensor probe (on the top) and a transmission type sensor probe (on the

bottom). For the transition type sensor probe, the accelerometer is embedded with the finger clip and the four LEDs are inserted into an eraser. Compared with the reflective sensor probe, the transmitted type finger clip shows higher amplitude PPG signals received by the photodiode.

The second generation of finger sensor probe is shown in Figure 4.8. An ADXL345 package is fully embedded into it and the custom designed four-wavelength LED package is much smaller than the first generation; all these improvements make the sensor probe wearable and potentially more resistant to motion having a better and fully integrated functionality. Figure 4.8a illustrates the finger sensor band using hook&loop (flexible and light proof). The ADXL345 package is fitted along the base with the same direction as the fingertip, as seen in Figure 4.8b. The top view and bottom views of the finger sensor probe are shown in Figure 4.8c and Figure 4.8d, respectively. The length between two bands can be adjusted to fit different sizes of finger.

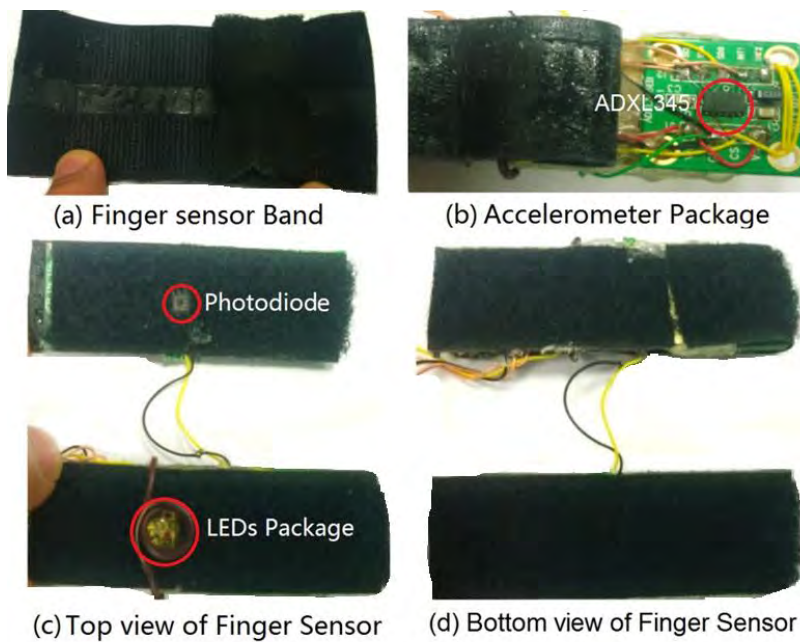


Figure 4.8: The second generation of a finger clip with an embedded ADXL345

The additional circuit is needed to be re-arranged to suit the base board. The acceleration package is required to be accommodated on the same board due to that the LEDs package used in the second generation of the finger sensor probe is factory

printed on the base board. The top and bottom views of the probe PCB board are shown in Figure 4.9 and Figure 4.10, respectively.

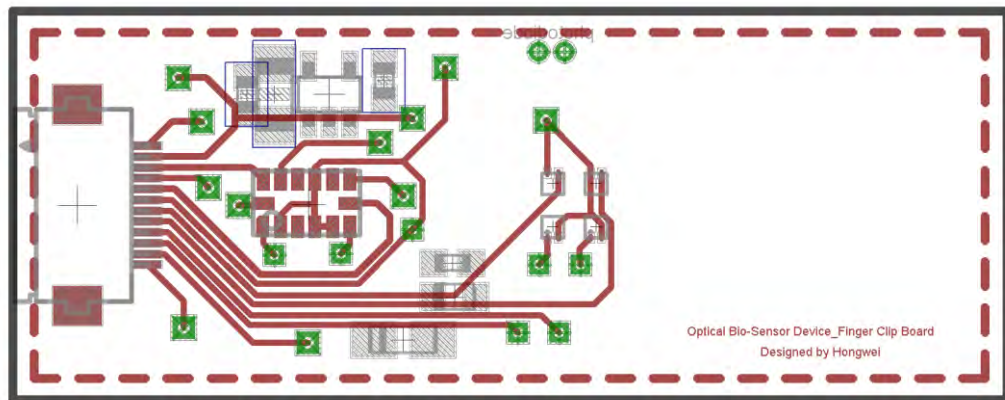


Figure 4.9: Top view of the probe board

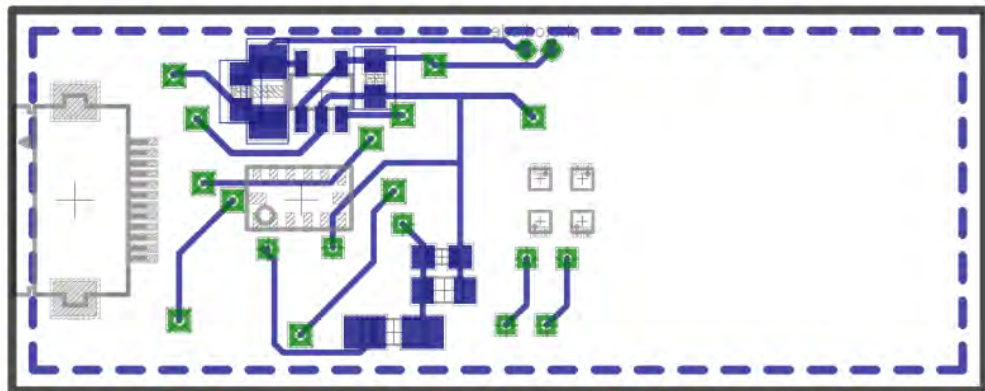


Figure 4.10: Bottom view of the probe board

Figure 4.11 shows three-dimensional coordinate system of the finger sensor probe with ADXL345EB (REV.1 by Intempco) embedded. The accelerometer measures the static acceleration of gravity and dynamic acceleration caused by motion or shock. It is defined that the normal position of the finger sensor probe to be such that the positive side of the accelerometer reference z-axis points in the upright direction against gravity, the x-axis points along the finger, and y-axis is orthogonal to the x-axis in the horizontal plane. Prior to the experiments described here, the wearer is at rest and relaxing quietly for 3 to 5 minutes in order to ensure that the PPG signal is stable and accurate. The hand on which the finger sensor probe is placed is kept straight and horizontal.

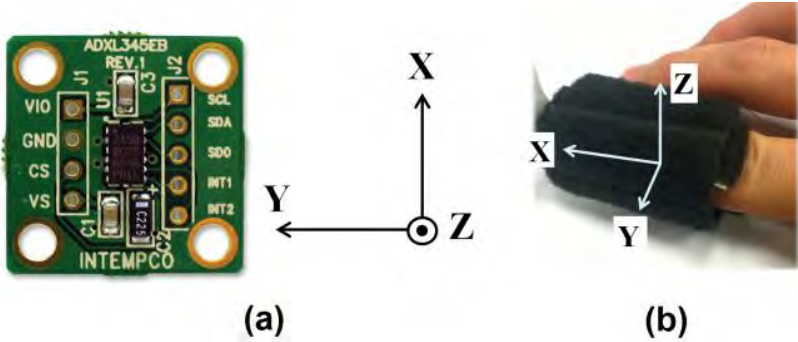


Figure 4.11: Three-dimensional coordinate system: (a) ADXL345EB (REV.1 by Intempco) and (b) PPG finger sensor probe

The PPG and ACC signals, captured using the hardware described in this section, have been validated through extensive experimentations to get a promising performance. The motion is captured by the embedded accelerometer and is used as the noise reference to the proposed PPG based sensor device. The experimental procedures and resulting measurements to determine the effect of motion on the PPG signal are described in more detail in the following chapters.

#### 4.1.3 Accelerometer Data Optimization

The special purpose transmission-type PPG finger probe used in the experiments of this work has been designed and fabricated in order to study PPG signals in conjunction with motion. For this reason, an ADXL345 digital 3-axis MEMS accelerometer has been embedded within the PPG finger probe. It measures the static acceleration of gravity in tilt-sensing applications (for standard gravity,  $1 \text{ g} \approx 9.81 \text{ m/s}^2$ ), as well as dynamic acceleration resulting from motion and shock. The PPG finger probe can be divided into four parts: an LED, a photodiode, an acceleration unit and a processing circuit. The ADXL345 accelerometer can measure the motion in the PPG finger probe in three orthogonal directions (corresponding to  $X$ ,  $Y$  and  $Z$  axes). The normal orientation of the PPG finger probe has been defined to be such that the positive side of the accelerometer reference  $Z$ -axis points in the upright direction (against gravity), the  $X$ -axis points along the finger (when held horizontal), and the  $Y$ -axis is orthogonal to the  $X$ -axis in the horizontal plane. Each experiment was conducted on the condition that the PPG finger probe was in the normal position and the subject had been sitting straight having been relaxed for at least 4 minutes prior to any testing.

## 4.2 Experimental Setup

### 4.2.1 Typical Medical Devices for Reference Data Capture

The sensor system designed in this project is compared to commercial medical devices. A HemoCue®201 was used as Hb reference for cross evaluation and comparison, and is shown photographically in Figure 4.12. Microcuvettes are used with lancets to collect blood samples in an invasive manner. The Hb readings are displayed after ten seconds.

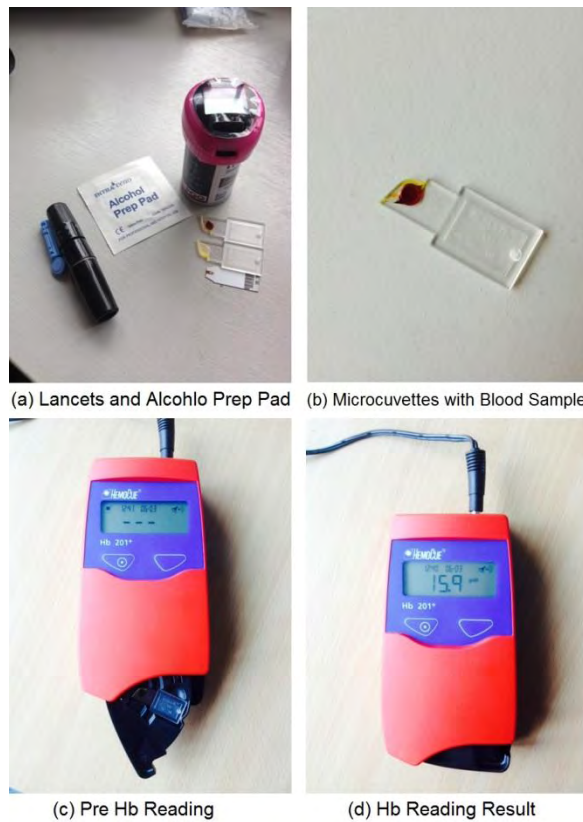


Figure 4.12: A HemoCue®201 used as Hb monitoring reference

In Figure 4.13, an OXYGEN SATURATION PULSOX-8 was used as the oxygen saturation and HR monitoring reference. It provides continuous non-invasive measuring of the oxygen saturation and pulse rate readings by optical methods.



Figure 4.13: OXYGEN SATURATION PULSOX-8 used as oxygen saturation and HR monitoring reference

An inflatable wrist-type cuff BP monitor (SBC 27-wrist blood pressure monitor, Sanitas, Kaunas, Lithuania), as shown in Figure 4.14, was used to record BP. It was used to simultaneously measure the local BP in close proximity to the point of measurement when the subject's hand was placed at different height levels. It was also used as an external force generator on the wrist for the research related to PPG signal analysis.



Figure 4.14: Electronic Blood Pressure Monitor used as HR and BP monitoring reference

A respiration monitor, (Neulog Respiration Monitor Belt logger NUL-236, Fisher Scientific, Pittsburgh, PA, USA) was also included for monitoring the subject's breathing in real time during testing. It is a piezoresistive device used to measure the deformation in a bellows diaphragm when an internal air cavity in the belt is compressed by stress due to abdominal expansion when breathing.

#### 4.2.2 Schematic of the PPG-Based Sensor System

The key requirements for designing an optical sensor system have been introduced in the last sections. The implementation of the measurement of HR, SpO<sub>2</sub>, and SpHb is shown schematically in Figure 4.15. The flow charts can be divided into seven main steps marked by the red blocks. The bio-signal first received by the finger sensor probe is communicated to the PC through a standard USB cable. LabVIEW (National Instruments, Austin, Texas, United States), a digital signal processing software package, is adopted as the data processing tool for the estimation of human vitals. The Data process is described in the diagram structure on the top right.

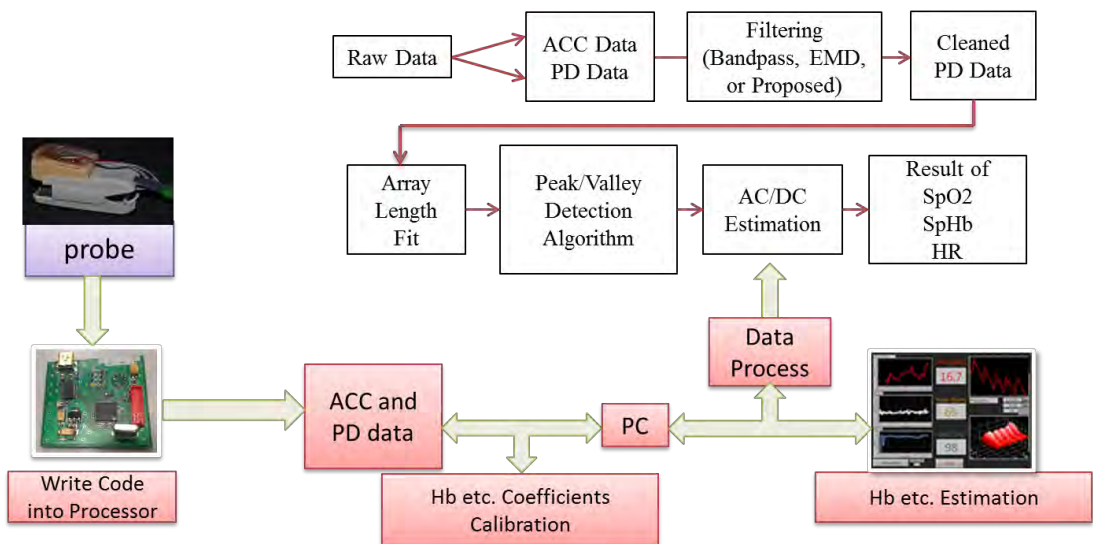


Figure 4.15: The PPG sensor system block diagram and the main steps for Hb estimation

Figure 4.16 portrays a schematic diagram of the current implementation of the bio-sensor monitoring in two main steps: human information collection state and PC signals processing and output state. The PPG and ACC signals collected from the finger sensor probe are in-real time data arrays. The sketch of blue blocks in Figure 4.16 shows the further analog signal processing. The blocks relating to signal processing represents processing of the bio parameters and optimization with data stored.

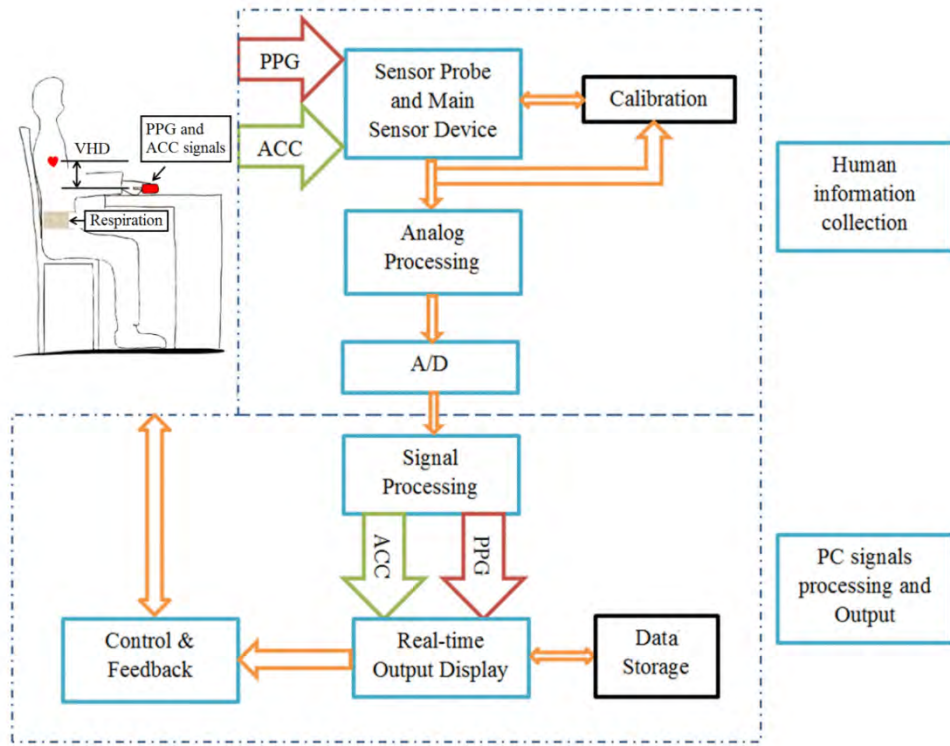


Figure 4.16: Experimental setup of the custom sensor system

The block diagram of the overall process of the motion artefact minimisation algorithm is shown in Figure 4.17. The DSP is running as a LabVIEW Virtual Instrument (VI) programme. The raw PPG signals were collected from the custom built PPG sensor device. During the motion event, PPG signals could be affected from motion artefact, VHD, ANS (respiration variations, reference mine). The proposed filtering method then was adopted to provide minimisation of the noise from motion events.

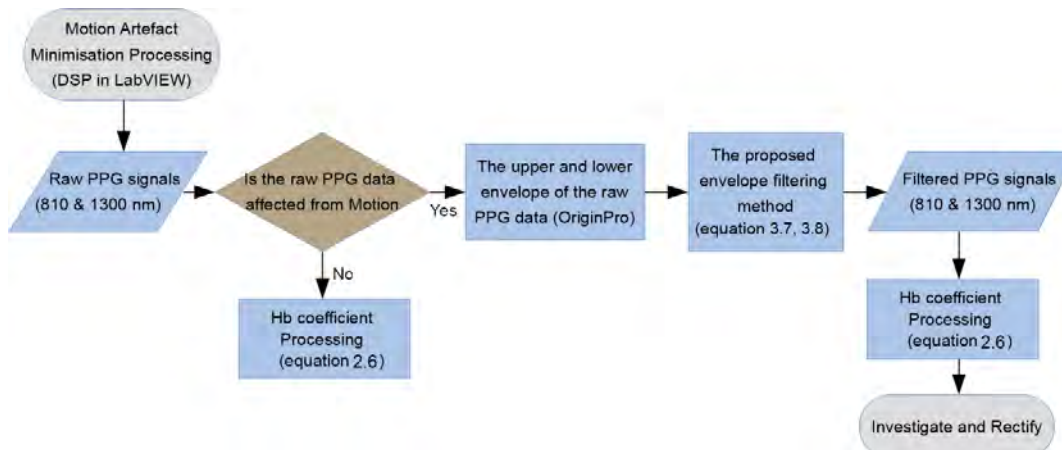


Figure 4.17: The block diagram of the overall process of the motion artefact minimisation algorithm

### 4.3 IAR System (Code on the MCU) and LabVIEW

The flow diagram of the code on the MCU is shown in Figure 4.18. Since an extra accelerometer is embedded in the finger probe, the sample rate of one cycle is increased by the ACC data processing. The debug tool of IAR system was used to write code into the MSP430 MCU. Timer A is the LEDs flashing intervals used in the sensor device. For timer A, in each cycle, TACCR0 = 0x4e stands for 420Hz sampling rate and 105Hz for each LED. Timer B is the sub-time array for ADC conversions and PPG and ACC signals are saved in a buffer. For timer B, TBCCR0 = 0x06 means 5 KHz sampling rate for data process. The ACC signal is collected during LEDs off period, as can be seen as follows. The C code for the MCU is attached in Appendix.

```
if(n_led == 1)
{
    810 nm LED on while the other three LEDs off; // P1.7 ADC data
process
}
if(n_led == 2)
{
    All LEDs off; //offset data process
    ADXL345_ReadXYZ( , , );
    count_acc++;
}
if(n_led == 3)
{
    670 nm LED on while the other three LEDs off; // P1.6 ADC data
process
}
if(n_led == 4)
{
    All LEDs off; //offset data process
    ADXL345_ReadXYZ( , , );
    count_acc++;
}
if(n_led == 5)
{
    905 nm LED on while the other three LEDs off; // P1.5 ADC data
process
}
if(n_led == 6)
{
    All LEDs off; // offset data process
    ADXL345_ReadXYZ( , , );
    count_acc++;
}
```

```

}

if(n_led == 7)
{
    1300 nm LED on while the other three LEDs off; // P2.0 ADC data
process
}

```

Parameter n\_led is used to select different statuses for the four LEDs on-and-off. For example, n\_led == 1 tends to set 810 nm wavelength LED on while the other three LEDs off for P1.7 ADC data process. n\_led == 2 supposed to set all LEDs off in the offset data process and also the ACC data can be collected and saved in buffer by ADXL345\_ReadXYZ (x,y,z) when the ACC\_flag is triggered. The value of n\_led increases from 1 to 7, and the four LEDs flash in interval sequence. Hence, it is expected to be an easier task to carry out the experiments based on PPG and ACC signals given that the signal strings transmitted to PC terminal synchronously.

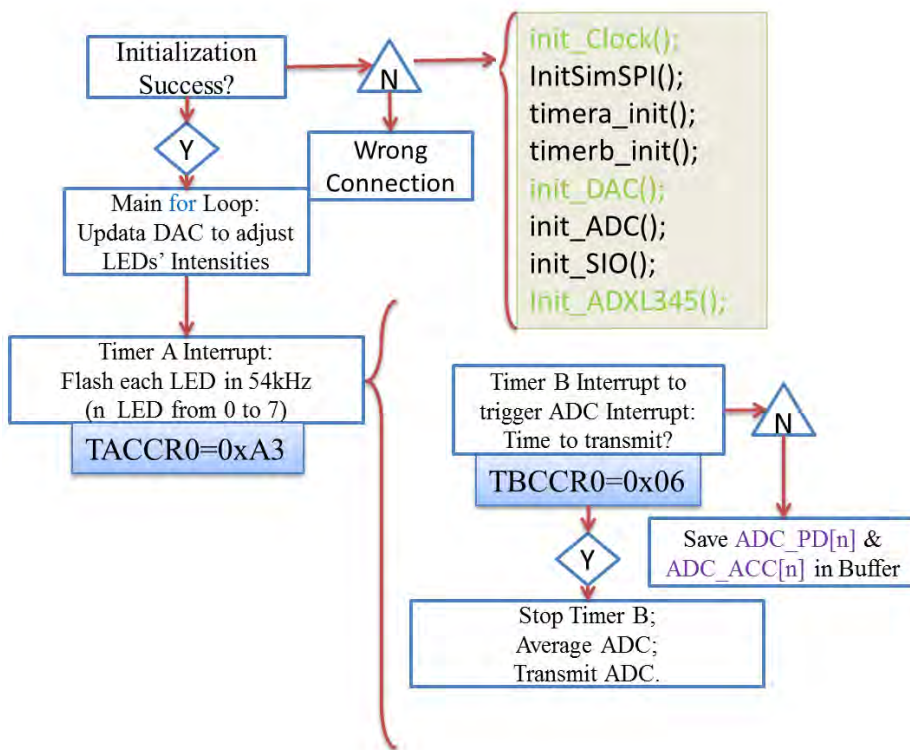


Figure 4.18: The code flow on the MCU

PPG and acceleration (ACC) signals are collected from the sensor device and later analysed for human vitals monitoring. LabVIEW was used to compute the various

optical absorption parameters, accelerometer coefficients and the derived coefficients (e.g., ( $\text{SpO}_2$ ), Hb and HR). A study of the effects of motion of the probe on the PPG signal shows that the PPG signal is potentially corrupted/degraded by movement, and strongly affected by height variation in vertical direction.

When the second generation of the finger sensor probe running for the first time, its code written on the chip was not suitable for the new sensor device, especially the time array and the bio reading calibration coefficients. As can be seen in Figure 4.19, the cHb reading is 19.3 g/dL in that moment while pulse and  $\text{SpO}_2$  readings are relatively in a correct range.

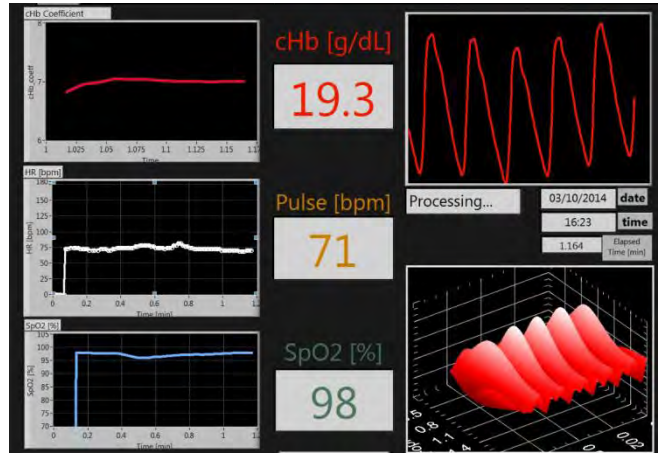


Figure 4.19: the code for Raw Labview readings required calibration

The new interface with peak of heart pulse marked by red circle, digital filters used to filter noise, and acceleration in 3-axis can be determined from the accelerometer. The value of cHb is 13.1 g/dL, as shown in Figure 4.20. ACC and motion detection code are added for further application. When there is relatively no distortion in motion corrupting the ACC signal, information about sensors in still is displayed. When distortion is present in any axis direction, information of motion would be warned based upon the indication. ACC signal is used for inferring different movement variations.

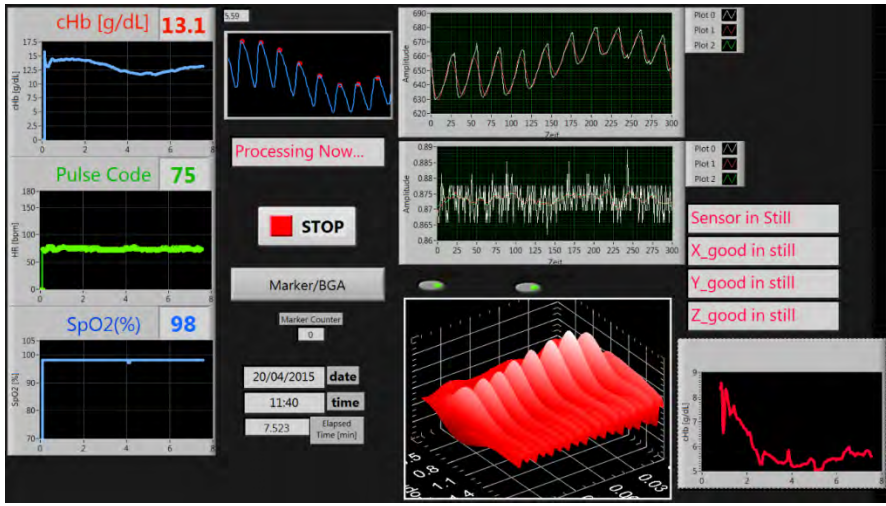


Figure 4.20: ACC and motion detection interface

#### 4.4 Summary

This chapter has described the optical-sensor system which includes the finger sensor probe and the main sensor board. The PPG and acceleration (ACC) signals are collected from the sensor device and made available for signal processing and human vitals monitoring. LabVIEW is used to compute the various optical absorption parameters, accelerometer coefficients and the derived coefficients (e.g., (SpO<sub>2</sub>), Hb and HR). A study of the effects of motion of the probe on the PPG signal shows that the PPG signal is potentially corrupted/degraded by movement, and strongly affected by height variation in vertical direction.

# CHAPTER 5.

## ANALYSIS OF PPG SIGNALS IN THE CONTEXT OF EXTERNAL PHYSIOLOGICAL PARAMETERS

---

### 5.1 Introduction

A wide study (a total of 23 human subjects) of the effect of motion on the Photoplethysmographic signals is reported. The investigation includes testing of two separate groups of 5 and 18 subjects who were asked to undertake set exercises whilst simultaneously monitoring a wide range of physiological parameters including breathing rate, HR and localised BP using commercial clinical sensing systems. The unique finger mounted PPG probe equipped with miniature three axis accelerometers for undertaking this investigation was a purpose built in-house version which is designed to facilitate reproducible application to a wide range of human subjects and the study of motion and has been described in Chapter 4. The subjects were required to undertake several motion based exercises including standing, sitting and lying down and transitions between these states. They were also required to undertake set arm movements including arm-swinging and wrist rotation. A comprehensive set of experimental results corresponding to all motion inducing exercises have been recorded and analysed including the BL value (DC component) and the amplitude of the oscillation of the PPG. All physiological parameters were also recorded as a simultaneous time varying waveform. The effects of the motion and specifically the localised BP have been studied and related to possible influences of the ANS and hemodynamic pressure variations. It is envisaged that a comprehensive study of the

effect of motion and the localised pressure fluctuations will provide valuable information for the future minimisation of motion artefact effect on the PPG signals of this probe and allow the accurate assessment of total Hb which is the primary function of the probe.

The experimental data was initially recorded on five subjects with PPG signals, acceleration data and respiration monitored simultaneously. This was subsequently widened to a test on 18 independent subjects in order to confirm the efficacy of the initial results. Data therefore have been gathered for a total of 23 healthy adults (13 males and 10 females) between the age of 24 and 55 years (mean age  $27.5 \pm 7.5$  years) with PPG signals, acceleration data and respiration monitored simultaneously. The room temperature was maintained constant at about  $18^{\circ}\text{C}$ , and all subjects had no known cardiovascular diseases, nor recent consumption of caffeine and/or nicotine.

The study of baseline and pulse amplitude from the viewpoint of local BP variation is provided in Section 5.2. The potential factors affecting the PPG signals are studied in detail e.g., body position, breathing pattern, externally applied pressure and motion at the wrist is discussed in Section 5.3. In particular, the corruption and/or degradation of the PPG signal is investigated when affected by local BP variation induced from motion of the subject. Section 5.4 takes a further step for the measurements of PPG signals in the presence of more vigorous movement e.g., repeated swinging of the arm with long or short resting time intervals. The discussion and conclusions are presented in the last section.

## 5.2 BL and Local BP

### 5.2.1 The BL of the PPG Signal

Figures 5.1–5.3 depict typical time varying PPG signals at a wavelength of 810 nm and ACC signal the accelerometer signals (ACC) signal measurements with predominant acceleration applied in the  $X$ ,  $Y$ , and  $Z$  directions respectively, captured with a period of about 40–50 s and the wearer in a sitting position. The results of Figures 5.1–5.3 show that the design of the PPG probe in this investigation has been successful and there appears to be minimal effect accruing from motion on the PPG signals in the respective

directions ( $X$ ,  $Y$  and  $Z$ ) when the acceleration (force) applied in those directions is relatively small (typically less than  $\pm 1$  g). Figure 5.1 corresponds to the case of the motion applied in the  $X$ -axis direction, in which case accelerations applied in the  $Y$ -axis and  $Z$ -axis directions were controlled to be as small as possible. The resulting acceleration signals are shown in Figure 5.1a ( $X$ ) and Figures 5.1c, 1d ( $Y$  and  $Z$  respectively). The acceleration in the  $X$  direction,  $a_x$  is 0.963 g ( $\approx 9.45 \text{ m/s}^2$ ) whereas  $a_y$  ( $Y$  direction) and  $a_z$  ( $Z$  direction) are 0.398 g ( $\approx 3.90 \text{ m/s}^2$ ) and 0.296 g ( $\approx 2.90 \text{ m/s}^2$ ). The time varying PPG signal during this motion event is shown in Figure 5.1a and the variation in the signal predominant is a frequency component due mainly to respiration [132]. Nitzan and et al [64] have also stated “Photoplethysmography (PPG) provides a qualitative measure of the tissue blood volume increase during systole by measuring the light transmission through the tissue as a function of time.” The time period relating to our study is not fixed (Figures 5.1–5.3) but is generally in the range of multiples of 10’s of seconds (usually between 40 and 50 s). In order to introduce a quantitative measure of the PPG signal change (amplitude) and offset from the zero line (analogous to a DC or continuous wave component) during this phase the definition has been applied to each record for the duration that is captured. The peak value in the PPG waveform, defined in terms of BL [64], and AM mark in chart of a PPG signal, are also illustrated in Figure 5.1. Results of acceleration applied mainly along the  $Y$ -axis direction are illustrated in Figure 5.2. The acceleration  $a_y$  is 1.330 g ( $\approx 13.05 \text{ m/s}^2$ ) whereas  $a_x$  and  $a_z$  are 0.573 g ( $\approx 5.62 \text{ m/s}^2$ ) and 0.378 g ( $\approx 3.71 \text{ m/s}^2$ ). However, when acceleration in the vertical ( $Z$ ) direction is dominant, e.g., in Figure 5.3d with the acceleration  $a_z$  is 2.059 g ( $\approx 20.20 \text{ m/s}^2$ ) whereas  $a_x$  and  $a_y$  are 0.484 g ( $\approx 4.75 \text{ m/s}^2$ ) and 1.018 g ( $\approx 9.99 \text{ m/s}^2$ ) respectively. The PPG signal (Figure 5.3a) shows stronger fluctuations than the case in Figure 5.1a or Figure 5.2a. It therefore appears that PPG signals are more greatly influenced by acceleration applied in the  $Z$ -axis direction. It is acknowledged that the acceleration values in the case of Figure 5.3a are greater than either Figure 5.1a or Figure 5.2a, but the effect on the waveform of the  $z$  axis acceleration is visibly different in the case of Figure 5.3a than either Figure 5.1a or Figure 5.2a, the signal in the former case showing a stronger oscillatory characteristic which broadly correspond the appearance of acceleration pulses and are not as clear or

even present in Figures 5.1a and 5.2a for which the dominant applied acceleration is in the horizontal plane.

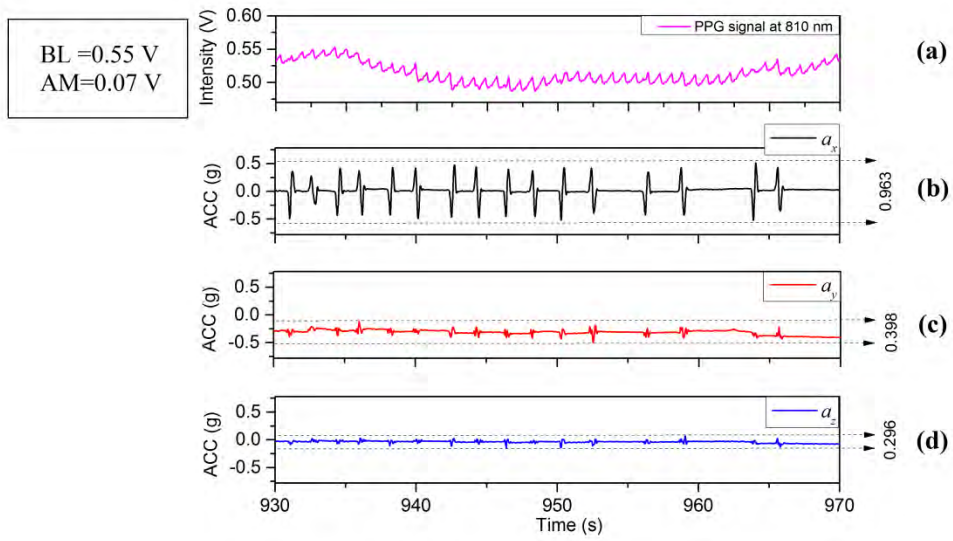


Figure 5.1: (a) PPG and (b-d) AAC signals measurement with main motion acceleration in x-axis

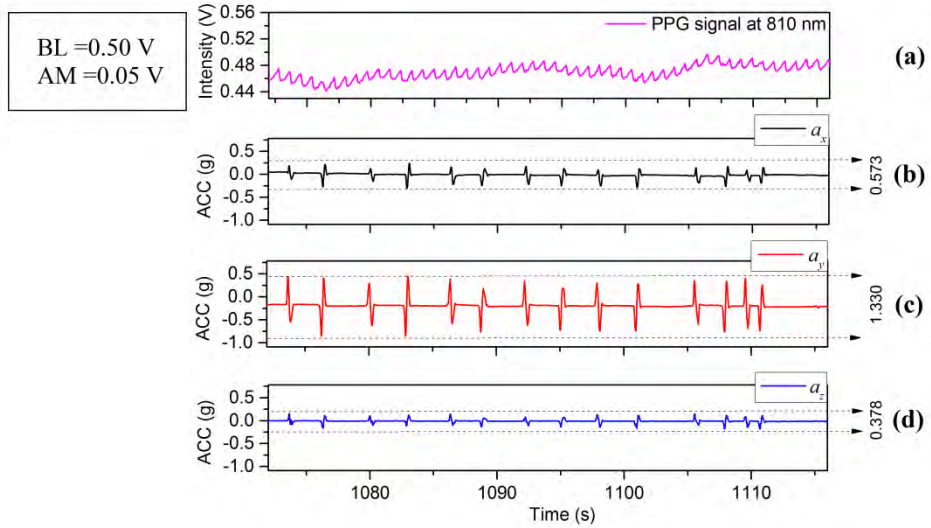


Figure 5.2: (a) PPG and (b-d) AAC signals measurement with main motion acceleration in y-axis

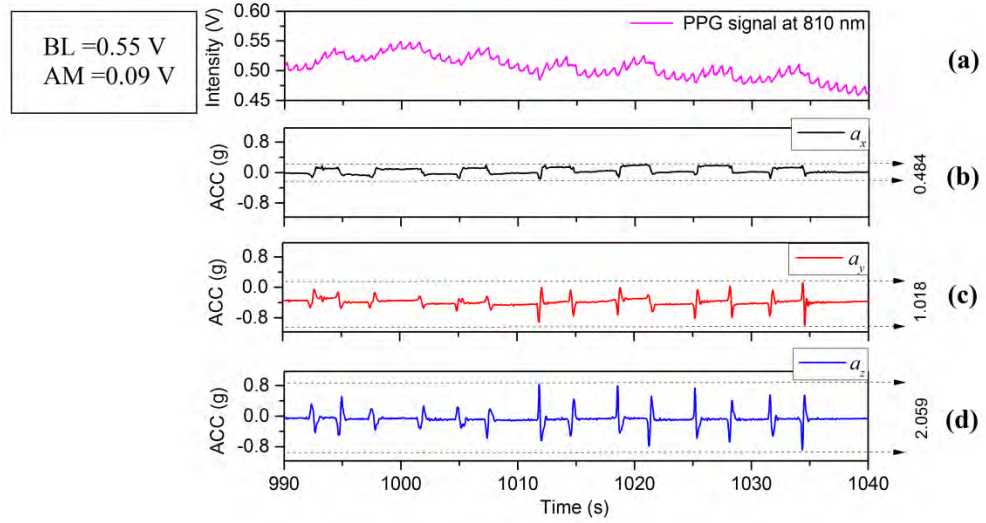


Figure 5.3: (a) PPG and (b–d) AAC signals measurement with main motion acceleration in z-axis

The PPG waveforms and ACC signals in the interval 990–1110 s in Figure 5.3 are shown in greater detail in Figure 5.4. Each acceleration event in the positive Z-axis direction, marked by regions of odd numerals (i, iii, and v) in Figure 5.4b, leads to an increase in BL, and meanwhile each acceleration in negative Z-axis direction, marked by regions of even numerals (ii, iv, and vi), represents a decrease in BL. The waveform is therefore most strongly influenced by movement in vertical Z-axis direction compared to motion in the horizontal x-y plane. The research in this investigation is aimed at the exploration and analysis of the properties of the PPG signal affected by physiological parameters associated with motion as described in the following sections.

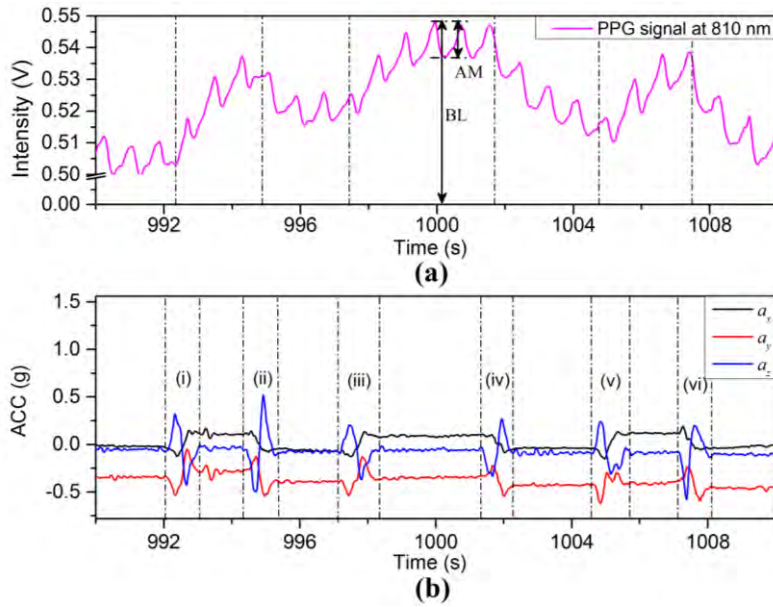


Figure 5.4: Enlarged portion of Figure 5.3 in the interval 990–1110 s

### 5.2.2 BP Response to VHD

Inflatable cuff blood pressure monitors are widely available for BP and HR monitoring. An inflatable cuff blood pressure monitor performs well when the monitored subject is in the resting position. The average values of systolic BP, diastolic BP and HR from one of the subjects were collected at different height levels (e.g., the height of the wrist, that the measurement cuff is on, relative to heart level) using the Sanitas SBC 27-wrist blood pressure monitor. The results corresponding to each of these parameters with differing height level are shown in Table 5.1. The instructions provided for the blood pressure monitor direct that measurements should be recorded with the cuff located at the same height as heart level in order to obtain optimum accurate readings, which means the first set of readings in Table 5.1 should be the most accurate. Although increasing VHD is not a recommended way to use the blood pressure monitor, these readings were recorded to provide an indication of variation in local BP variations. The results of Table 5.1 show that BP measurements tend to be influenced by VHD variations. In detail, the systolic BP decreases about 5 mmHg for every 5 cm increase in height above heart level, fall from 112 mmHg to 89 mmHg over the entire recording interval (35 cm). The diastolic BP readings show a similar decrease from 84 mmHg to 45 mmHg over the same height range. In the situation where VHD increases, HR readings remain relatively stable (a second reference for the HR reading was also available from the Oxygen

Saturation Monitor PULSOX-8, Minolta, Osaka, Japan). These results demonstrate that change of VHD affects the local BP due to blood volume change at the measuring site. It is well known [133, 134] that a variation in BP of 2 mmHg for every 25 mm can occur above or below the heart level and therefore for every 50 mm it can be extrapolated that a BP variation of 4 mmHg would occur, which is in good agreement with the results of this investigation. The variation recorded in references [133, 134] is well known and established, and therefore provides efficacy of the results recorded for these parameters in this investigation.

Table 5.1: Systolic, Diastolic And HR at Different Height Level

Count	Above heart level(cm)	Systolic(mmHg)	Diastolic(mmHg)	HR/min)
1	0	112	84	74
2	5	112	79	74
3	10	107	74	74
4	15	103	68	75
5	20	98	65	75
6	25	93	57	75
7	30	91	53	76
8	35	89	45	75

### 5.3 Factors which can Affect PPG Signals

The PPG signal is a qualitative measure related to blood volume changes at the point of measurement site, the fingertip being the most widely adopted measurement site due to the wide distributed peripheral blood circulation. The PPG signal includes a higher frequency component (circa 1–1.5 Hz under normal light physiological stress conditions) which synchronizes with the cardiac system attributed to each heartbeat as well as various other lower frequency components e.g., variations due to respiration. The PPG signal is easily affected by various factors resembling that of affecting the blood volume in the measurement area [69]. These factors could be summarized as variation of local BP induced from the change of blood flow in the measurement site and are described below.

#### 5.3.1 VHD Variation

Results were recorded initially for five subjects being in the sitting, standing and lying positions in order to study the effect on the PPG signals of VHD variation. In each measuring position, the height of the finger sensor probe was set at three different

levels, 25 cm above heart level, at heart level, and at 25 cm below heart level with support for 2 minutes in each position. The PPG sensor probe was maintained in the normal position on the finger at all times. The PPG signals from the five subjects were captured at the three different vertical levels for which the subjects were in the sitting position, standing position, and lying position. Figures 5.5–5.7 illustrate the data of these tests for each case of body position respectively.

A further set of measurements were recorded for 18 additional subjects who were healthy adults (9 Males and 9 females). Data were recorded for each of the body positions referred to above, but due to limitations of available space the data set is represented for only the sitting position. The results from each of these tests are captured in Table 5.2.

Table 5.2: Mean BLs and AMs at Different VHD Values for 18 individual subjects were in the sitting position and the finger sensor probe set at three different vertical levels

Subject	Mean Baseline ( $\pm$ SD) (V)			Mean AM ( $\pm$ SD) $\times 10^{-3}$ (V)		
	25 cm above Heart Level	Heart Level	25 cm below Heart Level	25 cm above Heart Level	Heart Level	25 cm below Heart Level
1	0.728 ( $\pm$ 0.032)	0.705 ( $\pm$ 0.027)	0.688 ( $\pm$ 0.031)	6.61 ( $\pm$ 0.248)	5.21 ( $\pm$ 0.213)	5.53 ( $\pm$ 0.304)
2	0.378 ( $\pm$ 0.024)	0.350 ( $\pm$ 0.032)	0.331 ( $\pm$ 0.017)	23.64 ( $\pm$ 0.823)	13.85 ( $\pm$ 0.465)	14.24 ( $\pm$ 0.569)
3	0.426 ( $\pm$ 0.041)	0.403 ( $\pm$ 0.024)	0.378 ( $\pm$ 0.029)	22.67 ( $\pm$ 0.543)	32.04 ( $\pm$ 0.817)	16.87 ( $\pm$ 0.481)
4	0.409 ( $\pm$ 0.035)	0.352 ( $\pm$ 0.030)	0.336 ( $\pm$ 0.042)	26.64 ( $\pm$ 0.351)	17.01 ( $\pm$ 0.721)	16.52 ( $\pm$ 0.611)
5	0.543 ( $\pm$ 0.022)	0.442 ( $\pm$ 0.055)	0.421 ( $\pm$ 0.042)	12.30 ( $\pm$ 0.267)	22.44 ( $\pm$ 0.439)	19.32 ( $\pm$ 0.325)
6	0.619 ( $\pm$ 0.021)	0.589 ( $\pm$ 0.025)	0.550 ( $\pm$ 0.026)	6.42 ( $\pm$ 0.523)	8.07 ( $\pm$ 0.547)	8.44 ( $\pm$ 0.413)
7	0.173 ( $\pm$ 0.012)	0.165 ( $\pm$ 0.011)	0.149 ( $\pm$ 0.019)	8.04 ( $\pm$ 0.512)	4.44 ( $\pm$ 0.391)	5.61 ( $\pm$ 0.452)
8	0.426 ( $\pm$ 0.049)	0.403 ( $\pm$ 0.038)	0.363 ( $\pm$ 0.072)	12.57 ( $\pm$ 0.745)	13.89 ( $\pm$ 0.584)	18.17 ( $\pm$ 0.487)
9	0.812 ( $\pm$ 0.068)	0.794 ( $\pm$ 0.091)	0.765 ( $\pm$ 0.048)	8.89 ( $\pm$ 0.761)	9.11 ( $\pm$ 0.649)	9.66 ( $\pm$ 0.946)
10	0.602 ( $\pm$ 0.051)	0.684 ( $\pm$ 0.077)	0.640 ( $\pm$ 0.059)	7.08 ( $\pm$ 0.649)	10.57 ( $\pm$ 0.381)	10.95 ( $\pm$ 0.874)
11	0.962 ( $\pm$ 0.021)	0.663 ( $\pm$ 0.034)	0.639 ( $\pm$ 0.028)	25.25 ( $\pm$ 0.915)	23.63 ( $\pm$ 0.874)	33.91 ( $\pm$ 1.207)
12	0.507 ( $\pm$ 0.030)	0.485 ( $\pm$ 0.026)	0.448 ( $\pm$ 0.047)	9.85 ( $\pm$ 0.449)	6.85 ( $\pm$ 0.759)	5.09 ( $\pm$ 0.618)
13	0.713 ( $\pm$ 0.094)	0.652 ( $\pm$ 0.028)	0.553 ( $\pm$ 0.079)	16.89 ( $\pm$ 0.672)	19.58 ( $\pm$ 0.364)	15.36 ( $\pm$ 0.655)
14	0.478 ( $\pm$ 0.035)	0.470 ( $\pm$ 0.014)	0.436 ( $\pm$ 0.029)	5.75 ( $\pm$ 0.493)	9.54 ( $\pm$ 0.816)	7.61 ( $\pm$ 0.638)
15	0.356 ( $\pm$ 0.061)	0.322 ( $\pm$ 0.050)	0.277 ( $\pm$ 0.043)	17.94 ( $\pm$ 0.679)	18.66 ( $\pm$ 0.745)	12.08 ( $\pm$ 0.483)
16	0.831 ( $\pm$ 0.020)	0.812 ( $\pm$ 0.048)	0.762 ( $\pm$ 0.037)	7.33 ( $\pm$ 0.957)	9.04 ( $\pm$ 0.461)	6.95 ( $\pm$ 0.587)
17	0.647 ( $\pm$ 0.051)	0.623 ( $\pm$ 0.075)	0.604 ( $\pm$ 0.091)	5.39 ( $\pm$ 0.518)	6.81 ( $\pm$ 0.349)	5.32 ( $\pm$ 0.247)
18	0.431 ( $\pm$ 0.036)	0.412 ( $\pm$ 0.048)	0.401 ( $\pm$ 0.067)	10.15 ( $\pm$ 0.425)	12.29 ( $\pm$ 0.348)	11.58 ( $\pm$ 0.591)

The studies of PPG baseline amplitudes are shown as histograms with standard deviations in Figures 5.5–5.7, for which the subjects were in sitting, standing and lying positions, respectively. The Mean BL and AM values in Table 5.2 are the mean of the maximum and minimum BL and AM values across a single record and the  $\pm$ SD is the standard deviation in that value over the entire duration of the record (typically in the range 20 to 30 s) around the mean level. The standard deviation in this case represents

the variation of the signal in a single time frame as illustrated in Figure 5.4a. The results of Figures 5.5–5.7 clearly demonstrate a consistent decrease of BL in the PPG signal with the decrease of positive VHD deviation. These observations demonstrate that the PPG signals reflect blood volume changes (hydrostatic pressure changes) in tissue when the BP near the finger probe (at the wrist) is varied with respect to VHD. The PPG signals at the point of measurement are clearly affected by the VHD between the finger probe and heart level.

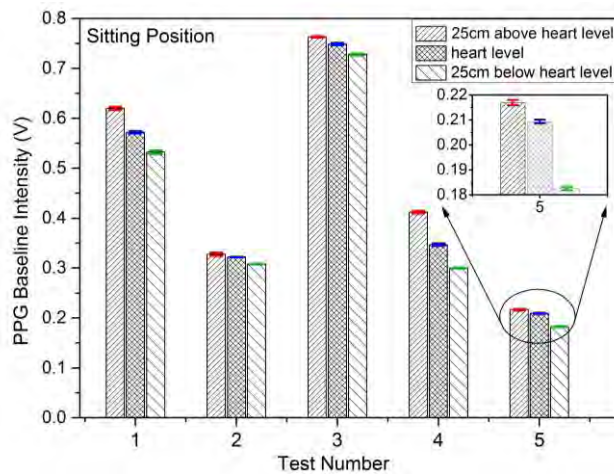


Figure 5.5: PPG baseline intensities and standard deviations when the subjects were in the sitting position and the finger sensor probe set at three different vertical levels

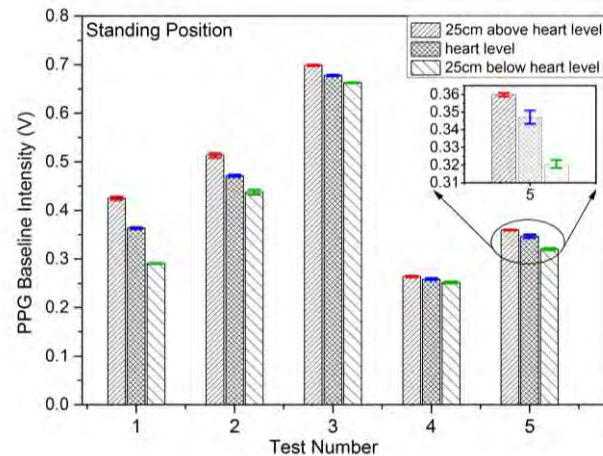


Figure 5.6: PPG baseline amplitudes and standard deviations when the subjects were in the standing position and the finger sensor probe set at three different vertical levels

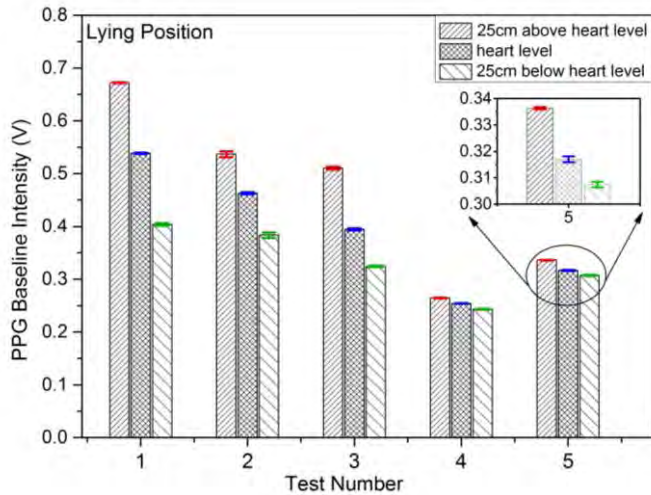


Figure 5.7: PPG baseline amplitudes and standard deviations when the subjects were in the lying position and the finger sensor probe set at three different vertical levels

The data sets, mean and median of BLs vs. VHD deviation are represented graphically in Figure 5.8. The BLs of the PPG signals increase with increasing positive VHD deviation from 0 cm at heart level to 25 cm above heart level and likewise decrease with increasing negative VHD deviation from 0 cm at heart level to 25 cm below heart level. This is true for all 18 cases measured with the exception of subject number 10 which includes a single anomalous result. Taken in conjunction with the results of Figure 5.5, this means that results from 22 out of 23 subjects have exhibited this consistent trend. It can therefore be deduced that the BP near the finger sensor probe consistently decreases with increasing positive VHD deviation and increases with the increasing negative VHD deviation. Furthermore, in the case of increasing VHD deviation, the BP at the point of measurement tends to decrease (Table 5.1) whilst the BL of the PPG signal tends to increase (Figure 5.5 and Figure 5.8); conversely for increasing negative VHD deviation, the BP near the finger sensor probe tends to increase while BL of PPG signal tends to decrease.

A preliminary statistical analysis involving calculation of the mean, median, the standard deviation and interquartile range of BL and AM from the 18 sets of PPG signals at Different VHD Deviation was undertaken on the results of Table 5.2. These are presented in summary form for BL and AM of the PPG signal in Tables 5.3 and 5.4.

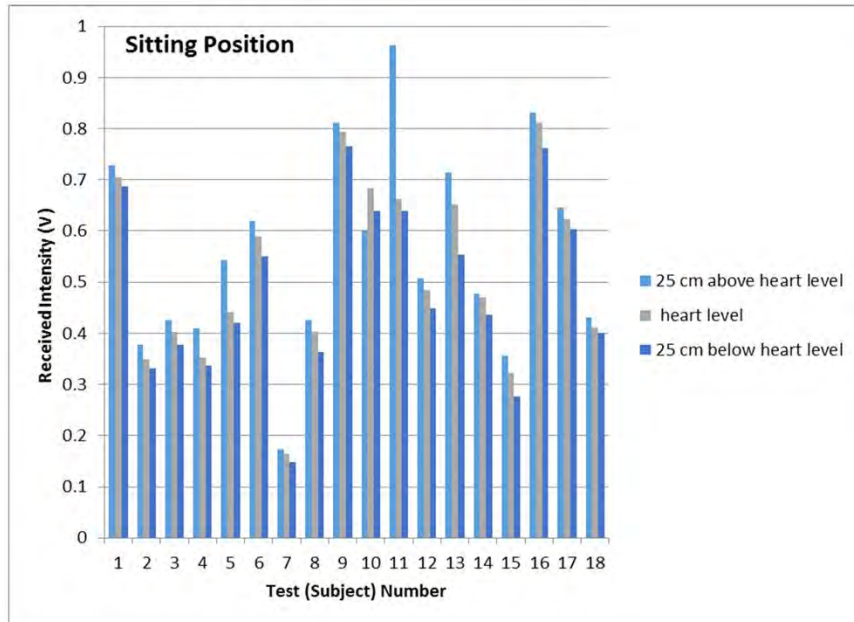


Figure 5.8: PPG baseline amplitudes for 18 subjects whilst in the sitting position and the finger sensor probe set at three different vertical levels

Table 5.3: Mean, Median, Standard Deviation, and Interquartile Range of Baseline from 18 sets of PPG signals at Different VHD Deviation

Statistical Analysis	Baseline of 18 Sets PPG Signal (V)		
	25 cm above Heart Level	Heart Level	25 cm below Heart Level
Mean	0.558	0.518	0.487
Median	0.525	0.478	0.442
Standard Deviation	0.199	0.179	0.173
Interquartile Range	0.271	0.257	0.264

Table 5.4: Mean, Median, Standard Deviation, and Interquartile Range of AM from 18 sets of PPG signal at Different VHD Deviation

Statistical Analysis	AM of 18 Sets PPG Signal (mV)		
	25 cm above Heart Level	Heart Level	25 cm below Heart Level
Mean	12.96722	12.97588	12.40056
Median	10	10.57	11.265
Standard Deviation	7.293668	7.711909	7.147762
interquartile range	10.535	8.94	9.115

### 5.3.2 Analysis of ANS Variation

The dynamic change of blood flow and arterial BP during postural change from sitting to standing has been discussed by Olufsen et al [135]. ANS stimulation induced from physiological events tends to vary the blood flow and BP, as well as the local BP near the sensor probe.

This section includes the results of an experiment in which the finger sensor probe was fixed at the same VHD whilst changing the body position. In one of the experiments the finger sensor probe was kept in front of chest at heart level whilst changing body positions between sitting, standing and lying positions. The subjects were requested to breathe evenly and smoothly without talking throughout the experiments. The recorded respiration data corresponding to the arbitrary analog output of the respiration monitor belt device is shown in Figure 5.9b. The period from the rising edge of PPG signal to the start of a stable region (no significant signal change) is defined as a PPG-fluctuation, e.g., the regions (I–III) in Figure 5.9c. Region (i) in Figure 5.9a indicates a sitting down process (from standing to sitting). The reason for the PPG-fluctuation in Figure 5.2c is believed to arise from ANS variations induced by the change in body position. Since there is no VHD, the observed values of BLs are almost the same before and after the PPG-fluctuation as was to be expected. Region (ii) represents the process of lying down for which the height of the finger sensor probe was unavoidably changed from heart level to a level about 6 cm above heart level since the finger sensor probe was kept in front of chest at all the times. The PPG fluctuation [region (II) in Figure 5.9c] is believed to be caused by an ANS variation accompanied with BP changes resulting from hydrostatic changes caused by the body position variation. Similarly, region (iii) corresponds to the postural change from lying to sitting, and another PPG-fluctuation [region (III) in Figure 5.9c] is associated with it. Rotating the wrist was also included in this experiment, indicated by region (ii) and (iii), in Figure 5.9a. The effect of wrist rotation on PPG signals is discussed in detail in Section 5.3.4 of this chapter.

Results were initially gathered from five separate randomly selected subjects for which body position varied from a standing position to a sitting position corresponding to the tests outlined above. These are characterised using the parameters outlined in Table 5.5. These parameters are defined as the period (of body variation process as)  $t_{\Delta ACC}$  (in seconds); the interval of the PPG fluctuation according to body position variation as  $t_{\Delta BL}$  (in seconds); respiration rate (RR) (in units of per min); and the difference between the peak value of BL in the fluctuation and average of BL before the fluctuation (a 60 s interval used in this case) as  $\Delta BL$  (in Volts). The demonstration shows that the PPG signals at the point of measurement are affected by the ANS variations induced by change in body position.

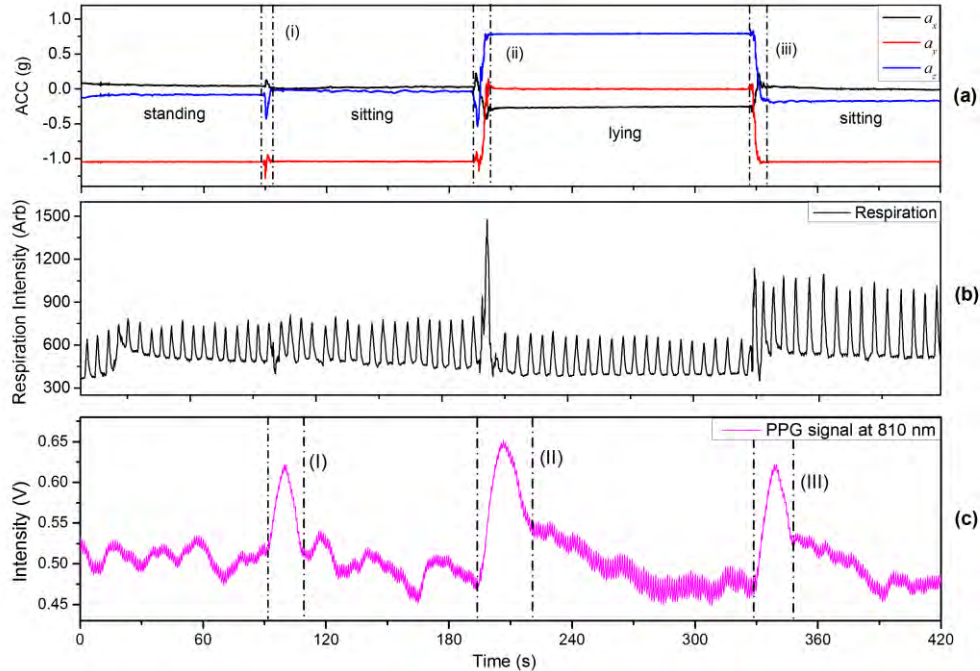


Figure 5.9: (a) ACC; (b) respiration and (c) PPG signals recorded from changing body positions

Further independent tests results were obtained from the other 18 subjects as referred to in Section 5.3.1. The body position was varied from a sitting position to a standing position and these are listed in Table 5.6, accompanied with a study of the preliminary statistical analysis including mean, median, standard deviation and interquartile range as shown in Table 5.7. These results captured for a large group of subjects confirm the efficacy of the earlier results (Table 5.5) and hence the validity of the measurement technique employed in this investigation.

Table 5.5: Main parameters of body variation from a standing position to a sitting position

Subject	t $\Delta$ ACC (s)	t $\Delta$ BL (s)	RR (min $^{-1}$ )	$\Delta$ BL (V)
1	7.23	16.00	20	0.0572
2	5.67	18.12	15	0.0868
3	4.43	17.43	12	0.1107
4	8.44	13.58	18	0.1387
5	5.65	17.16	20	0.1098

Table 5.6: Primary Parameters of Body Variation from Sitting Position to Standing Position

Subject	tΔACC (s)	tΔBL (s)	RR (min <sup>-1</sup> )	ΔBL (V)
1	11.36	20.60	18	0.0797
2	9.09	16.23	15	0.0321
3	10.91	16.46	21	0.0499
4	8.63	20.19	18	0.0276
5	11.10	18.52	18	0.0656
6	9.15	19.74	17	0.0434
7	12.06	22.10	23	0.0167
8	10.61	18.84	12	0.0673
9	8.63	19.97	19	0.1287
10	8.49	18.46	19	0.0754
11	10.78	17.26	17	0.0874
12	9.75	18.68	16	0.0756
13	6.88	15.91	22	0.0471
14	10.85	21.32	18	0.0817
15	9.74	19.98	18	0.0459
16	5.26	15.47	16	0.0715
17	8.19	20.62	22	0.0934
18	7.43	16.48	18	0.0692

Table 5.7: Mean, Median, Standard Deviation, and Interquartile Range of Primary Parameters of Body Variation from Sitting to Standing

Statistical Analysis	tΔACC (s)	tΔBL (s)	RR (min <sup>-1</sup> )	ΔBL (V)
Mean	9.383889	18.71278	18.16667	0.064344
Median	9.445	18.76	18	0.06825
Standard Deviation	1.762338	2.010536	2.684377	0.026935
Interquartile Range	2.3075	3.4625	2	0.032475

The experimental results of this section show the effect of body positional changes on the PPG signal. A position change involves a change in blood flow and BP, and homeostasis is recovered by means of the ANS. The PPG fluctuation is therefore most likely caused by hemodynamic changes and not solely by the ANS. Furthermore it is generally accepted that the parasympathetic system dominates whilst in the lying position, and therefore the effect of the ANS should be present throughout the duration of the lying position.

PPG and ACC time dependent signals are shown in Figure 5.10 for which the subjects were required to maintain the finger sensor probe at the same height above the floor and the VHD was varied by changing body position. The time period A<sub>1</sub> represents the subject standing still with the finger sensor probe at 25 cm below heart level. Region (i) represented by  $t_{1\_ACC} = 7.6$  s in Figure 5.10b shows the process of sitting down slowly

and the VHD changing from 25 cm below heart level to a level close to heart level, where the amplitudes of accelerations are low being about 0.05 g ( $0.49 \text{ ms}^{-2}$ ). Referring to Figure 5.10a, it can be seen that there is an increase of BL in the PPG signal during the time period defined by  $t_{1\_PPG} = 22.7 \text{ s}$ . The time duration difference between  $t_{1\_ACC}$  and  $t_{1\_PPG}$  is 15.1 s, however during  $t_{1\_PPG}$  the BL fluctuates significantly whereas the accelerometer on the finger sensor probe detects only limited acceleration due to motion. The time period  $B_1$  corresponds to signals recorded for which the subject was sitting with the finger sensor probe at heart level. Region (ii) which is defined by  $t_{2\_ACC} = 6.7 \text{ s}$  in Figure 5.10b shows the accelerometer signal while the subject was standing up and the VHD changes from heart level to 25 cm below heart level. During the interval (ii), the BL of the PPG signal decreases and the time interval for the PPG signal change is described by  $t_{2\_PPG} = 20.3 \text{ s}$ . There is a 13.6 s difference between  $t_{2\_ACC}$  and  $t_{2\_PPG}$ . The transition intervals (iii) and (iv) thereafter are similar to those of (i) and (ii), being 18.8 s and 18.0 s difference, respectively, between the accelerometer data settling and the PPG signal settling.

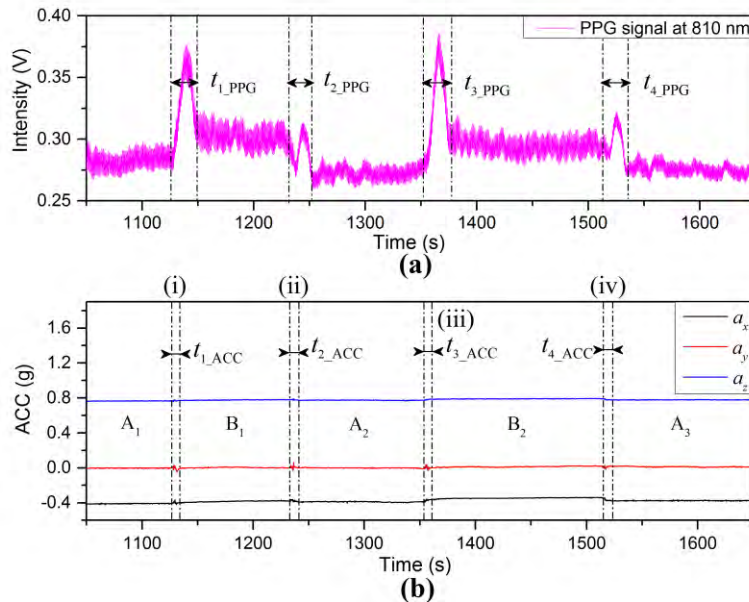


Figure 5.10: (a) PPG and (b) ACC signals for which the subject maintained the finger sensor probe at the same height above the floor and varied the VHD by changing body positions

The details of the PPG and the ACC signals in the interval 1110–1280 s in Figure 5.10 are represented in Figure 5.11. The PPG fluctuation in Region (A) is the period from the rising edge of PPG signal to the start of a stable region. This interval can be divided into

two regions for both signals:  $A_{1\_ACC}$  and  $A_{2\_ACC}$  for the ACC signals (Figure 5.11b; and these are transposed to  $A_{1\_PPG}$  and  $A_{2\_PPG}$  for the PPG signal in the case of Figure 5.11a. Region ( $A_{1\_ACC}$ ) defines the total interval during which the body position was changed from the standing to the sitting position. The decrease of VHD between the finger sensor probe and heart level is 25 cm due only to change of body position (while the finger sensor probe was kept still and stayed at the same height above the floor). The BP near the finger sensor probe decreases with decreasing negative (i.e., positive) VHD deviation according to the previous result in Section 5.2.2 and the increase of BL according to the previous result in Figure 5.8, as shown by the region  $A_{1\_PPG}$  in Figure 5.11a. Region  $A_{2\_ACC}$  (Figure 5.11b), is an interval where the accelerometer on the finger sensor probe detects only limited or no acceleration due to motion, while the BL of component  $A_{2\_PPG}$  initially increases (dominated by the sympathetic part of the ANS) and then decreases (dominated by the parasympathetic part) during which time the homeostasis process is recovered via the ANS [64, 136].

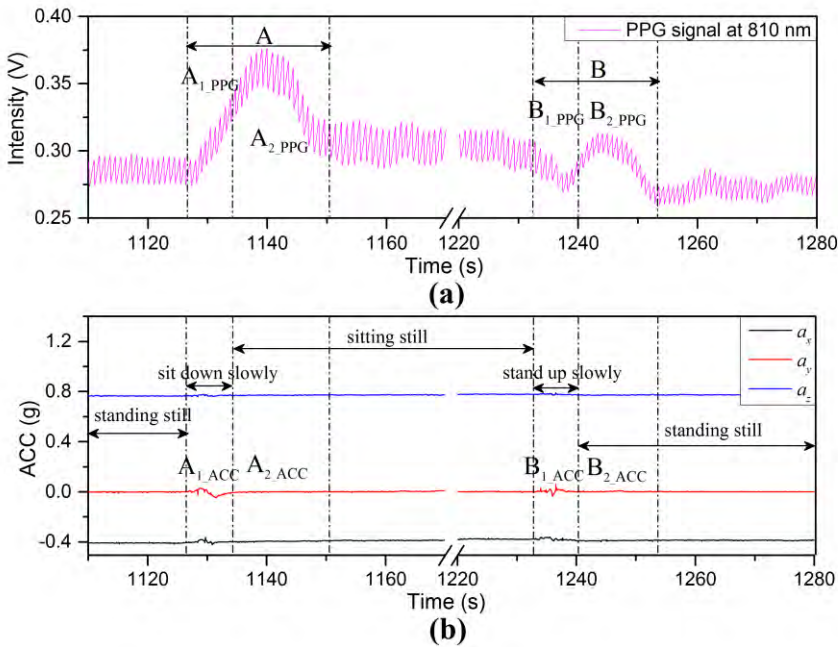


Figure 5.11: Enlarged portion of the PPG (a) and the ACC signals (b) in the interval 1110–1280 s in Figure 5.10

Region (B) in Figure 5.11 is the interval from the decreasing edge of the PPG signal to where it stabilizes again. This interval can be divided into two regions for both signals:  $B_{1\_ACC}$  and  $B_{2\_ACC}$  for the ACC signals;  $B_{1\_PPG}$  and  $B_{2\_PPG}$  for the PPG signal. Region

( $B_{1\_ACC}$ ) is the interval during which the body position was changed from a sitting to a standing position. The increase of VHD is 25 cm (while the finger sensor probe was kept still and stayed at the same height above the floor). The BP falls with the decrease of VHD (consistent with the data of Figure 5.8), leading to the decrease of BL, as shown by region ( $B_{1\_PPG}$ ). Region ( $B_{2\_ACC}$ ) defines the interval where the accelerometer on the finger sensor probe detects limited or no acceleration due to motion, while the BL of component  $B_{2\_PPG}$  firstly increases (dominated by sympathetic part of the ANS) and then decreases (dominated by parasympathetic part) during which time the homeostasis process is recovered via the ANS. The PPG fluctuation observed in region (B) is dominant by the body position variation (governed by BP changes from hydrostatic changes in the body position variation) over the increase of negative VHD deviation accompanied with blood volume changes and hydrostatic changes (increase of BP near the finger sensor probe induced by the VHD variation). Clearly, BL variations of components  $A_{2\_PPG}$  and  $B_{2\_PPG}$  are not induced by motion (because there is little or no motion in components  $A_{2\_PPG}$  and  $B_{2\_PPG}$ ) and therefore more likely to be caused by the increase of the BP at the point of measurement. It is conjectured that changing the body position leads to a physiological variation with hydrostatic pressure changes, resulting in an increase of BP, which stimulates a response of the ANS. This is also explained in references [10, 64].

PPG signals are sensitive to physiological variations; several examples are given in the literature [10], such as changes in the breathing pattern, coughing or yawning. Similar experiments were conducted for the current investigation and detailed results include the PPG waveforms resulting from these tests described in the following.

Many types of physiological influences can result in an increase, or decrease of the local BP at the measuring site, which affects the BL and the AM of the PPG signals. Figure 5.12 illustrates PPG and acceleration signals during a deep yawn event. As can be seen from the intensity of PPG signal in Figure 5.12a, the average value of BL is about 0.35 V before the deep yawn. The activity of a deep yawn started at the time of 835 s. The next 25 s shows a PPG-fluctuation triggered by the yawn event. Repeated experiments (40 times) show that: (1) the value of AM tends to be restricted and (2) the BL tends to continue without significant variation. A zoomed PPG signal in the time

period of 852–857 s is included as an inset on the top left of Figure 5.12a. The interval  $l$  is the instantaneous period of the PPG waveform, at a given point in time, and has been used to determine HR. Two examples of the AM of the diastolic peak are illustrated by  $x_1$  and  $x_2$ , whereas  $y_1$  and  $y_2$  are examples of the AM of the systolic peaks [137]. The mean ratio of diastolic peak to systolic peak during the period 810–830 s is 0.403 ( $\pm 0.023$ ) in Figure 5.12 prior to the yawning event. During the yawning event, the value of the ratio  $x_1/y_1$  (e.g., 0.83 at the peak point, A) is larger than that of  $x_2/y_2$  (e.g., 0.52 at the valley point, B), and the BL/AM ratio is also affected during the PPG fluctuation. Even though the PPG signal is highly affected by the yawn activity, the interval  $l$  can still be reliably used to calculate HR [115, 138].

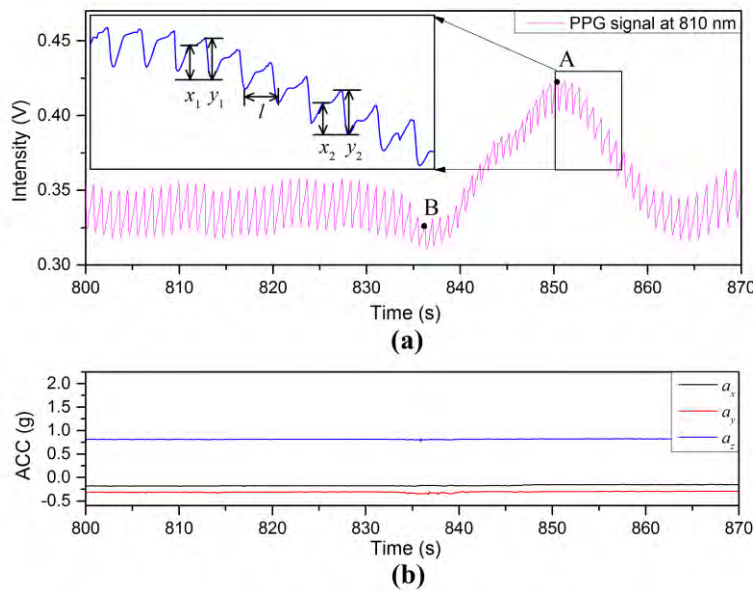


Figure 5.12: (a) PPG signal and (b) ACC signals with a deep yawn event

Another type of physiological variation from variation of breathing pattern, deep breathing ( $t_1$ ) and talking ( $T_1$ ) events, can also affect the PPG signals as observed in PPG-fluctuations [region (A) and (B)], shown in Figure 5.13.

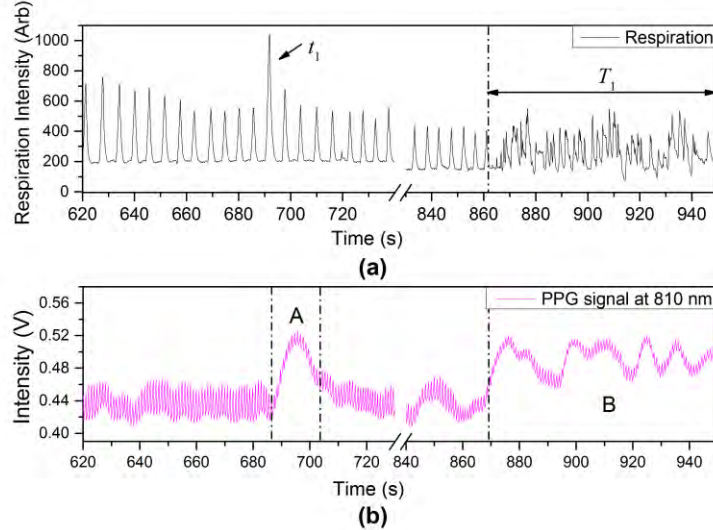


Figure 5.13: (a) Respiration including deep breathing and talking events and (b) PPG signal

### 5.3.3 External Pressure at the Measuring Site

Figure 5.14 shows other types of PPG-fluctuation caused by local BP variations at the point of measurement due to Figure 5.14a external pressure being applied to the finger sensor probe and Figure 5.14b external pressure applied to the wrist by inflating a cuff as used in blood pressure monitors. According to the manufacturer's/supplier's data sheet the blood pressure monitor was capable of applying continuous pressure on the wrist in the range of around 95–195 mmHg. The applied pressure from the cuff inflation tends to block perfusion, affecting the blood volume at the point of measurement, and after the release of pressure or cuff deflation, the amplitude of the PPG signal gradually returns to the pre-inflation level, which is also described in reference [69]. External pressure is therefore a third factor that can affect the PPG signal in addition to VHD and ANS.

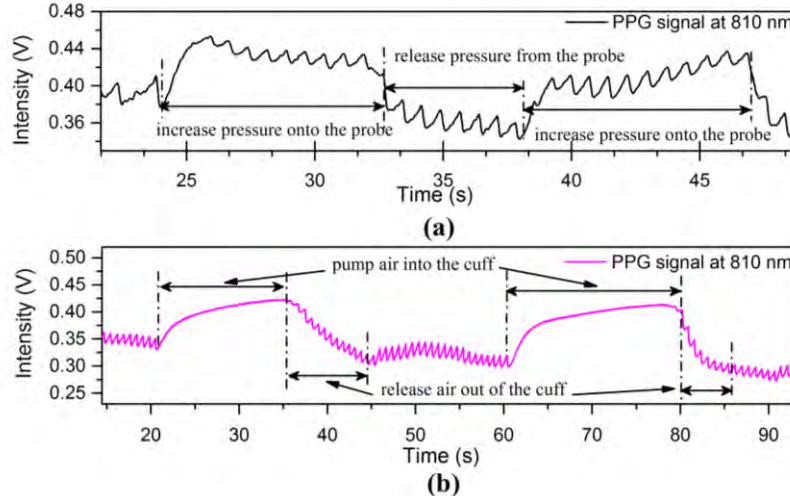


Figure 5.14: The PPG signal affected by local BP variations at the measuring site due to (a) external pressure applied on finger probe and (b) external pressure applied on wrist by processing the inflatable-cuff type blood pressure monitor

### 5.3.4 PPG Signal Response to Wrist Rotation

More experiments were performed to study the response of the PPG signal to wrist rotation. The sensor probe on the finger was initially placed at heart level. One experiment was conducted by slowly rotating the wrist through 90° anticlockwise or 90° clockwise rotation along the *X*-axis (the direction which the finger is pointing). The PPG signal together with the accelerometer signals when actuating this motion are shown in Figure 5.15b. Region (i) shows the PPG signal for a 90° anticlockwise rotation of the wrist. The enlarged PPG waveforms (left) in the interval 1150–1156 s are slightly disturbed by motion artefact, but the values of BLs and AMs are relatively stable compared with those without the wrist rotation regions. Region (ii) shows a 90° clockwise rotation of the wrist. The enlarged PPG waveforms (middle) in the interval 1172–1178 s are minimally affected by the rotation process. Region (iii) is a repeat process of region (i), which has its detail shown in top right in Figure 5.15a. This experiment indicates that wrist rotation does not significantly affect the PPG signals.

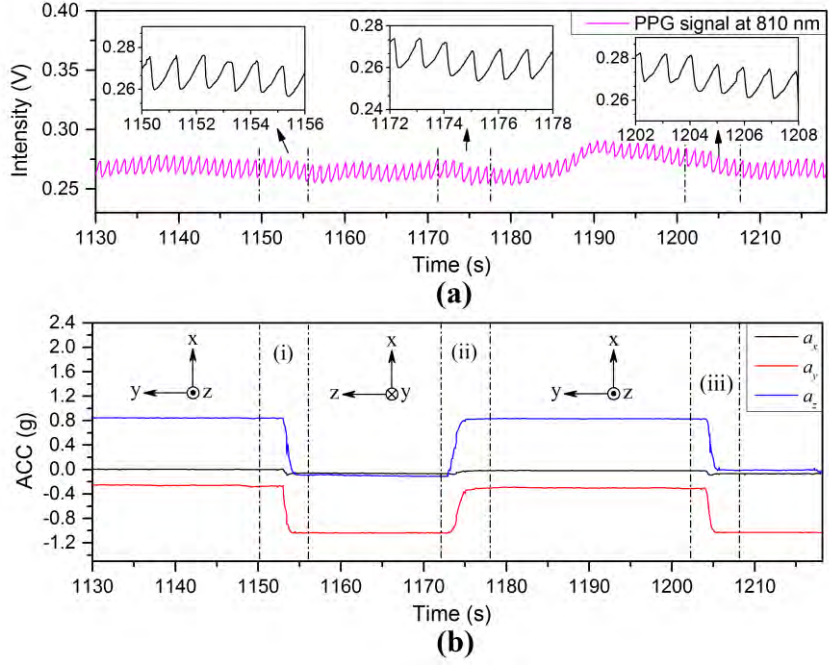


Figure 5.15: Illustration of (a) PPG and (b) ACC signals recorded from rotating wrist

#### 5.4 Severe Motion Tests

Two further experiments were conducted where the finger sensor probe was placed on the finger in line with the upper arm and forearm, and the subject's arm was fully outstretched and held straight.

Figures 5.16a and 5.16b show the PPG and  $X$ -axis acceleration signals in the process of swinging the arm up and down by rotation at the shoulder. The positions of the finger sensor probe are indicated by the  $a_x$  signals in Figure 5.16b, where dotted lines (i), (ii), and (iii) mark the sensor probe at 35 cm above heart level, heart level, and 35 cm below heart level, respectively. Dotted lines ( $a_i$ ) mark the probe rising from 35 cm below heart level to the heart level, dotted lines ( $b_i$ ) mark the start of the probe moving from heart level to 35 cm above heart level, dotted lines ( $c_i$ ) mark the probe being lowered from 35 cm above heart level to heart level, dotted lines ( $d_i$ ) mark the changes of the probe from heart level to 35 cm below heart, et al.

In the process of swinging the finger sensor probe up and down with long resting intervals (approximately 10 s), the values of the PPG intensity, in Figure 5.16a, vary in a manner similar to  $a_x$  in Figure 5.16b. Region (A) is the stationary stage following lifting

of the finger sensor probe to 35 cm above heart level. The BL of PPG signal shows a sharp increase and the AM is seriously degraded. The increase of positive VHD deviation results in significant attenuation of the pulsatile component. Region (B) shows the PPG signal with the finger sensor probe returning back down to heart level. The amplitude signal returns to its normal quality prior to initiating the motion after a short delay. When the finger sensor probe was set at 35 cm below heart level, indicated by Region (C), the AM of the PPG signal tends to be less than that at heart level. Region (D) delimits a period when the finger sensor probe was raised to heart level and the BL of the PPG increases with the increase of the  $a_x$  value. Region (E) represents a repeat of the movements in region (A) but with a higher acceleration. An observation from this experiment is that the VHD between the finger sensor probe and heart level can be inferred from the X-axis acceleration. The PPG signals show large time delay before they reach a constant value following all the movements.

Figure 5.17 shows the PPG and acceleration signals captured in the process of swinging the arm up and down repeatedly with short resting time intervals (less than 5 s). In Region (A) the finger sensor probe is subject to rapid up-and-down motions between a height of 35 cm above heart level and heart level. Region (B) corresponds to the finger sensor probe being quickly and repeatedly moved up and down between heart level and a height of 35 cm below heart level. Results show that the values of BL in Figure 5.17a vary in a manner similar to the values of X-axis acceleration in Figure 5.17b and PPG signals tends to be highly affected by the VHD variation.

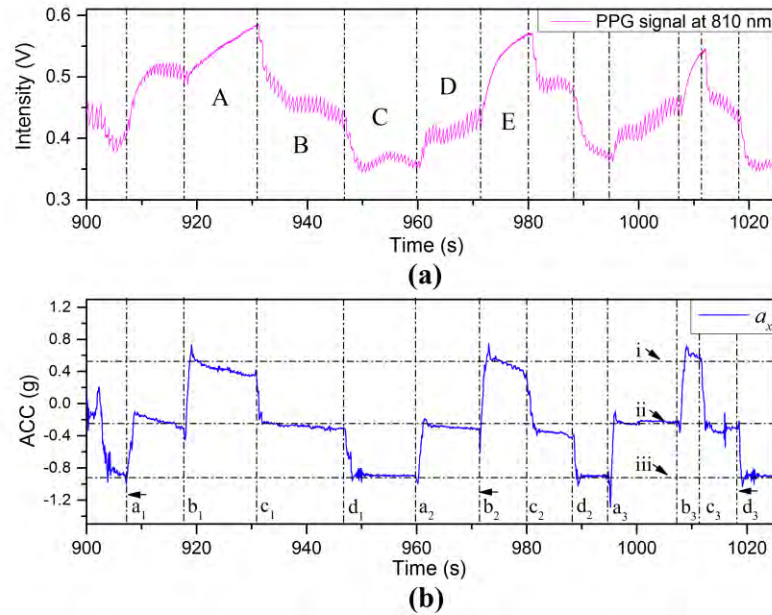


Figure 5.16: (a) PPG and (b) X-axis ACC signals captured in the process of swinging the arm up and down with long resting time intervals

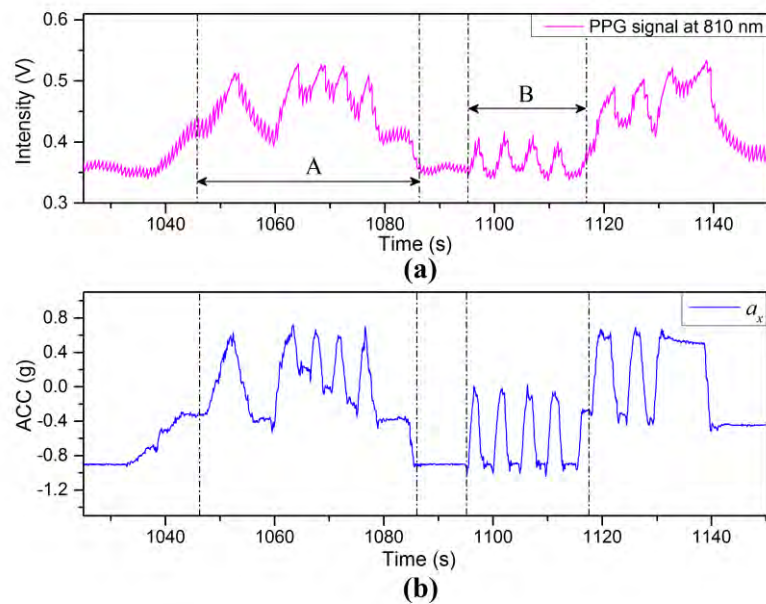


Figure 5.17: (a) PPG and (b) ACC signals captured in the process of swinging the arm up and down with short resting time intervals

## 5.5 Summary

The values of BL and AM from PPG signals can vary from one person to another due to the finger sensor probe's size, its placement, effects of body position, individual differences and even differences between the two arms. A PPG signal involves a relatively high frequency component (typically in the range 1–2 Hz) which synchronizes with the heartbeat as well as various lower frequency components relating to ANS (including respiration, e.g., talking, deep breathing events, and physiological events, e.g., body position variation), BP control (local BP variation near sensor probe arising from VHD and thermoregulation).

A variation in BP corresponding to changing the arm position was measured using a commercial wrist worn BP monitor and was accompanied by a variation in the PPG signal. A drop of approximately 4 mmHg was measured for each 5 cm rise in VHD, which is in good agreement with the values previously measured in the literature [133, 134] which in turn provides efficacy of the results recorded for these parameters in this investigation. However, the purpose of this investigation has been to bring local BP variations into consideration when attempting to remove motion artefact in PPG signals. In summary, factors that may affect the PPG signal during motion have been identified and these are illustrated in Figure 5.18. External pressure on/near the measuring point, the ANS, and the VHD between the measurement site and heart level in the vertical direction, all influence the local BP at the point of measurement. In particular, the induced ANS variations can be as a result of physiological events, including: body position changes (Figure 5.10), yawn events (Figure 5.12) and talking events (Figure 5.13). Also the experimental results indicated that wrist rotation does not significantly affect the PPG signal (Figure 5.15).

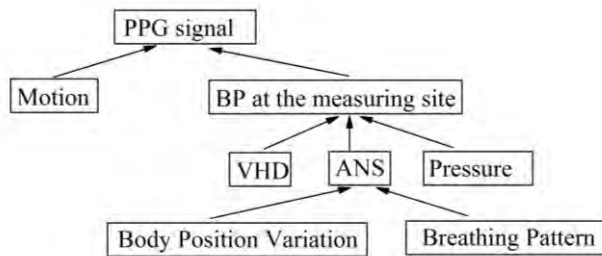


Figure 5.18: Factors which can affect PPG signals

For the PPG signal, it has the properties that the BL of a PPG signal increases with the increase of positive VHD deviation and decreases with the increase of negative VHD deviation. For the case of decreasing of positive and negative VHD deviation, the PPG signal tends to decrease and increase, respectively. The mean and median BLs are derived from the data of Table 5.2 and Figure 5.8 and shown in Tables 5 and 6. The slope of a linear analysis arising from the positive and negative VHD deviation are  $0.629 \times 10^{-3}$  cm/V and  $0.769 \times 10^{-3}$  cm/V, respectively. Curve fitting for the variation of VHD deviation and BL of PPG would be necessary due to non-linearity but this could be accommodated in the memory of the processing electronics. Therefore, in reverse, the BL of PPG from the finger sensor probe could be used to locate the position of the finger, but only in very controlled circumstances and this is beyond the scope of this investigation.

The ACC data can be used to infer the finger sensor probe's direction and acceleration for the analysis of PPG based devices. The PPG finger sensor position can be inferred, from the BL of the PPG signal based on BP variation. PPG-fluctuations can also be used to infer some indication of: (1) a body position change with variation of the finger sensor probe's position if BL of PPG varies after motion; (2) a body position change without variation of finger sensor probe's position if BLs of PPG before and after motion are the same; and (3) other physiological variations (e.g., yawn event and deep breathing event). In the context of the existing literature, the results presented in the work of the current investigation are unique and their capture has only been possible due to the high degree of integration of the optical PPG signal detection electronics and accelerometers in one compact unit. Previous work on multi-wavelength PPG signal detection has been performed including some of the authors of this investigation [72], as well as motion artefact reduction (primarily through application of software based post processing [12-14]. However, to the best of the knowledge of the authors the *in situ* accelerometer signals combined with relatively simple algorithms applied to the PPG signals as presented in this article provides a unique opportunity for the possible correction of motion artefact signals in real time.

It has been demonstrated experimentally that the captured PPG signal exhibits sensitivity in its response to the subject's muscular tension level and limb motion.

Devices such as an accelerometer, a respiration monitor belt and a blood pressure monitor, have been deployed in conjunction with the custom designed PPG sensor system for investigation of the effects of external physiological parameters on the PPG signals in the context of ANS and local BP. The results have shown that the BL of PPG signal is affected by acceleration particularly in the vertical direction as opposed to acceleration in the horizontal plane for the system under test (Figures 5.1–5.3 in Section 5.2.1). Experimental results from a total of 23 subjects demonstrated that PPG signals during motion events are influenced by the variation of local BP at the point of measurement which is in turn induced from: (1) the VHD between the measuring site and the reference level (Section 5.3.1); and (2) the ANS (Section 5.3.2). The results of a statistical analysis conducted on 18 subjects (9 male and 9 female) have shown that the dependency of the Baseline (BL) and Amplitude (AM) values of the PPG signal are only weakly dependent on the VHD. It is envisaged that the results of this investigation can be used as a basis for optimizing measurements of PPG based sensors in terms of potential removal of motion artefact.

# CHAPTER 6.

## ANS EFFECT ON HUMAN VITALS

---

### 6.1 Introduction

The collection of PPG signals from optical based sensor probe has been used extensively for the monitoring of HR, respiration rate and SpO<sub>2</sub>. Prior research by the Optical Fibre Sensor Research Group has extended the information provided by PPG based devices from monitoring HR and SpO<sub>2</sub> to include Hb. Research presented here demonstrates that PPG signals are severely influenced by the ANS variations induced by physiological events, such as yawning and coughing, which also has been reported by Allen [10] and Nitzan [64] due to physiological variation resulting from movement of the body and the sensor probe. In general, sympathetic nervous system speeds up heart and respiration rates, boosts BP; parasympathetic nervous system, in contrast, counters the sympathetic one by mediating the body's relaxing functions, slowing down HR and breathing speed, releasing BP [59-61]. ANS variations induced by physiological events include changes in the breathing pattern, e.g., yawning, coughing, gasping, and activities such as exercise and eating. ANS activity can affect BP and breathing rate and reduce the quality of PPG signals. Using a finger sensor probe with an embedded accelerometer, further investigation demonstrates that PPG based measurements including HR, SpO<sub>2</sub> and Hb are strongly degraded by ANS both during a) movement of body position and b) physiological variation. The amplitude of a PPG signal is directly proportional to the vascular dispensability; this leads to that the PPG signal tends to be influenced by ANS. Large pulse amplitude will be introduced with the presence of high arterial BP. This chapter mainly focuses on the effects of ANS on the quality of non-invasive blood diagnosis by PPG-based sensor system. Therefore, the development of PPG based devices for monitoring human vitals, e.g., BP, respiration, and SpO<sub>2</sub>, should bring effect of ANS activity into consideration.

## 6.2 SpO<sub>2</sub>, HR and Hb Affected by ANS

### 6.2.1 SpO<sub>2</sub> Analysis

The effects of ANS on the quality of PPG based measurements, including HR, SpO<sub>2</sub> and Hb, are discussed in this section. A SpO<sub>2</sub> signal is illustrated in Figure 6.1b while multiple wavelengths PPG signals and 3-axis accelerometer signals are displayed in Figures 6.1a and 6.1c, respectively. The measuring of the SpO<sub>2</sub> coefficient is based on the different optical absorbance properties of deoxyhaemoglobin and oxyhaemoglobin [72, 139].

Movements of body position can stimulate the ANS to influence the PPG signal, e.g., standing up, as shown by the dotted lines a<sub>1</sub>. In Figure 6.1c, time  $t_{a\_ACC}$  indicates the start of a change in body position from a sitting position to a standing position while probe is kept at heart level. There is a PPG-fluctuation after this event as illustrated in Figure 6.1a. At time  $t_{a\_PPG}$ , the BL of the PPG-fluctuation reach its maximum. In Figure 6.1b, the values of the SpO<sub>2</sub> vary in a manner similar to the manner in which the BL of the PPG-fluctuation varies, which is expected as the SpO<sub>2</sub> is calculated from the PPG signals. Time  $t_{a\_SpO_2}$  marks the maximum SpO<sub>2</sub> value resulting from the event. A 8.6s time delay results from the signal processing necessary to compute the various optical absorption parameters, accelerometer coefficients and the derived coefficients (e.g., SpO<sub>2</sub>, Hb, HR), and this time delay is highlighted using the dotted line a<sub>2</sub>.

Physiological transition events can also stimulate the ANS resulting in variations in PPG signal, e.g. a deep yawn or a cough. The events of a deep yawn and a cough are illustrated by  $t_{b\_ACC}$  and  $t_{c\_ACC}$  in Figure 6.1c. Even the accelerometer on the finger clip probe detects limited or no motion depicted in Figure 6.1c, PPG-fluctuations occur due to physiological events, as can be seen in Figure 6.1a. The times  $t_{b\_PPG}$  and  $t_{c\_PPG}$  mark the peak values in the PPG-fluctuations for a deep yawn and a cough. In Figure 6.1b, the values of the SpO<sub>2</sub> as again vary due to variations caused by PPG-fluctuations, while  $t_{b\_SpO_2}$  and  $t_{c\_SpO_2}$  present the maximum respective signal variation. Again, there are time delays between PPG-fluctuations and the SpO<sub>2</sub> fluctuation as illustrated by the dotted lines b<sub>2</sub> and c<sub>2</sub>. In general, it would appear that ANS variation tends to increase

$\text{SpO}_2$  readings. Since effect of hand rotation has been excluded from the effect of PPG signals (Section 5.3.4), the  $\text{SpO}_2$  readings are relatively stable, as shown in Figure 6.1b for the time period from 1050 s to 1120 s. Once again prove that the  $\text{SpO}_2$  readings tends not be affected by hand rotation.

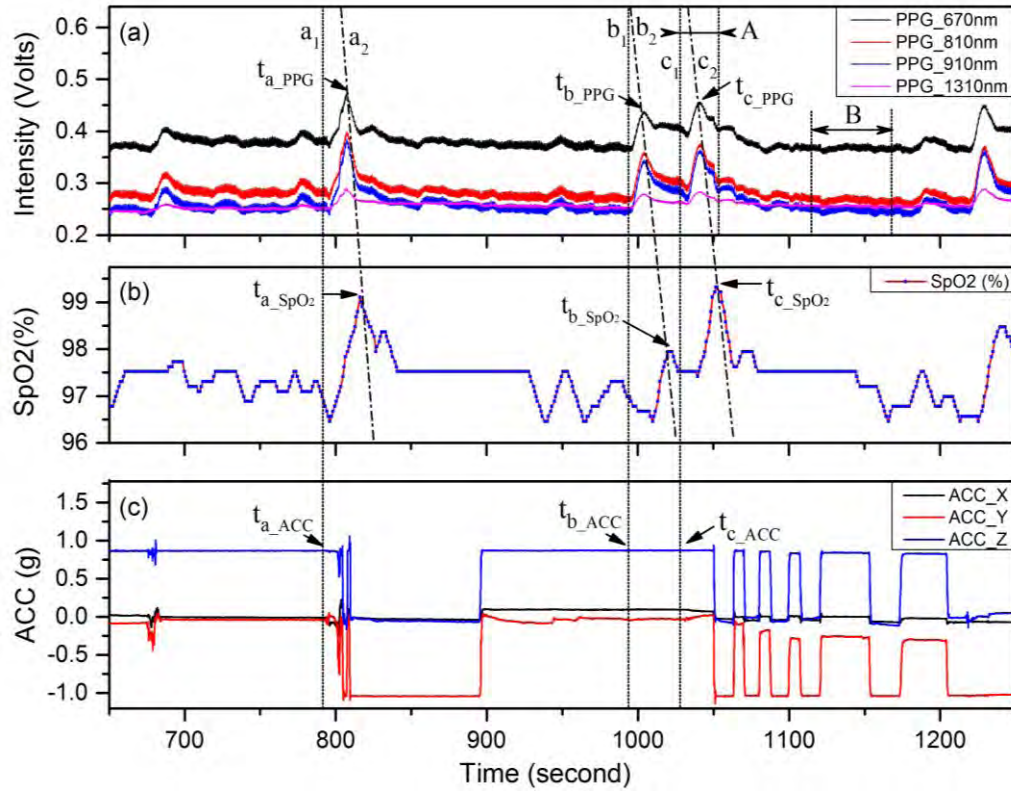


Figure 6.1: (a) PPG intensity, (b)  $\text{SpO}_2$  and (c) ACC signals. Dotted line a1 indicates the wearer standing up; dotted lines b1 and c1 indicates a deep yawn and a cough, respectively

### 6.2.2 HR and Hb Analysis

Furthermore, HR and Hb readings are presented in Figure 6.2a and in Figure 6.2b. HR is calculated based on the peak-to-peak interval method. In Figure 6.2a, the blue dots mark the instantaneous HR values, and the black solid line shows the trend of the HR values. Period of 7 is used in the moving average method for the trend line estimation. The HR values tend to increase during ANS variations induced by movement of body position (standing up) and physiological events (a yawn and a cough) in Figure 6.1c.

The measurement of Hb is based on the fact that there is a substantial absorptions difference of light in the red and near infrared regions between deoxyhaemoglobin, oxyhaemoglobin and blood plasma which optical properties are similar to water [72,

104]. Hb readings are illustrated in Figure 6.2b, where the blue dots mark instantaneous Hb values and the black solid line shows the trend of the Hb values. Period of 5 is used in the moving average method for the trend line estimation. The values of Hb moving average vary in a manner similar to the manner in which the values of BLs vary in Figure 6.1a. Specially, The Hb calibration curve taken over instantaneous Hb values are represented by the thick brown line. In general, Hb values tend to increase as a result of ANS responses to body movement and physiological variations.

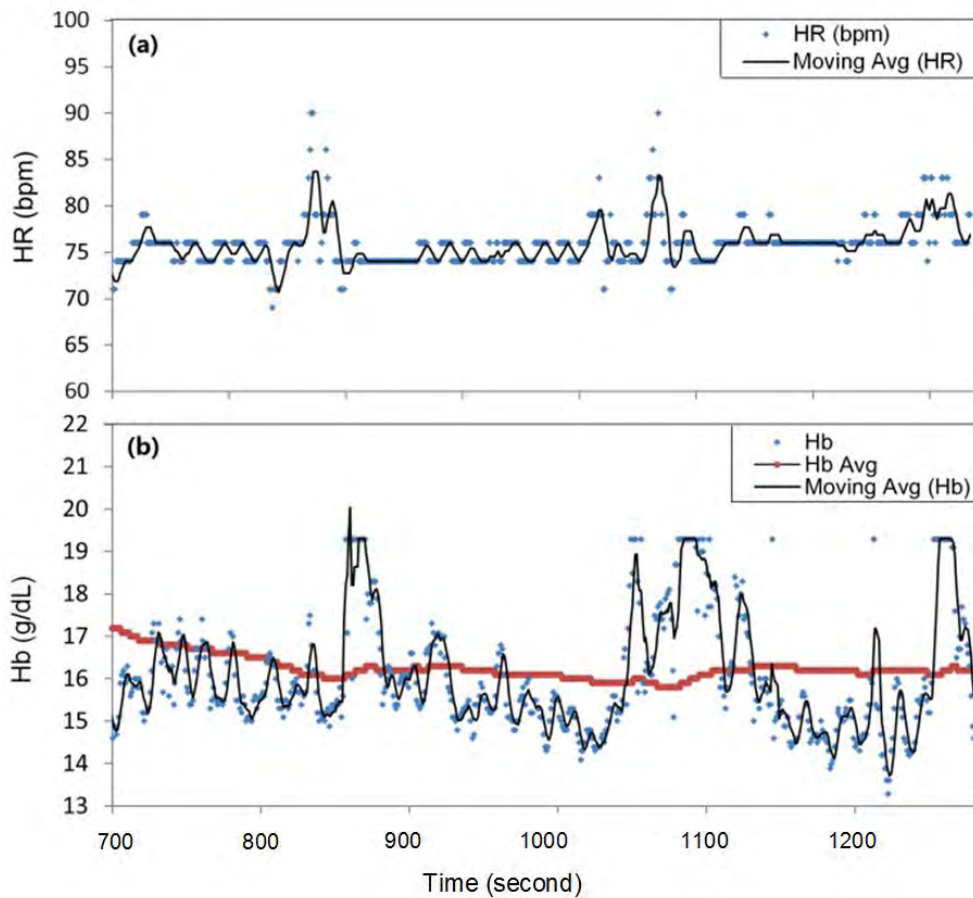


Figure 6.2: (a) HR and (b) Hb readings

### 6.3 Summary

In this chapter, research relating to the effects of ANS on the quality of PPG signals has been described. Results show that baseline values are strongly affected by ANS variation induced from physiological events, such as yawning, coughing, and so on. The SpO<sub>2</sub>, HR and total Hb values tend to increase as a result of ANS events, arising from either movement of the body position or certain physiological events, and this should be

considered in the application of PPG based sensor devices. Moreover, recognizing the role of ANS in modulating PPG based signals and combining this knowledge with accelerometer data, helps to gain a deeper insight into the interpretation of PPG based parameters.



# CHAPTER 7.

## MOTION ARTEFACT REMOVAL IN Hb MONITORING

---

Normally, in clinical environments, for the collection of clean physiological signals, the subject is required to remain static in sitting or lying position. It has been reported, in many, almost any motion events will strongly corrupt various physiological signals in current remote sensor systems, e.g., pulse oximetry, and greatly diminish/limit the system's ability to extract a reliable measurements [11, 15]. Accurate estimation of Hb coefficient is difficult to achieve when the original PPG from which it is derived is contaminated from noise components in the low frequency ranges (0–1 Hz) induced from any activities relating to hemodynamic pressure variation near the PPG sensor, such as respiration pattern variation, and movement of the subject (e.g., walking and swinging arm) accompanied with the measurement apparatus as demonstrated in Chapter 5 of this thesis. The situation is further complicated when non-pulsatile noise can become pulsatile during movement or/and respiratory events, whose frequency ranges overlap those of the original PPG signals and both amplitudes are comparable to each other [140].

### 7.1 Filtering Methods Used on PPG Data

#### 7.1.1 Low Pass/High Pass Filtering on Raw PPG Signal

PPG signals are sensitive to physiological variations; several examples are given in the literature [10, 141]. A low pass/high pass filter applied on a raw PPG signal is necessary to reduce the dominance of the lower frequency components without significantly distorting the PPG pulse shape. Generally, the lower cutoff frequency is chosen to be

around 0.5 Hz and the higher cutoff frequency is near 3.5 Hz for smoothing the baseline of a PPG signal [142]. An experiment was implemented for which the finger sensor probe was kept in front of chest at heart level on a stable support. The subjects were requested to breathe evenly and smoothly without talking for 4 mins previous the experiments.

An example of respiration data as recorded by a commercial respiration monitor belt (Neulog Respiration Monitor Belt logger NUL-236) measured in arbitrary analog unit (Arb) is shown in Figure 7.1a. The time periods of deep breathing and the talking events are indicated by the point ( $t_1$ ) and region ( $T_2$ ). Normally, deep breathing tends to induce a sharp increase in the amplitude of respiration intensity, and a talking event tends to severely distort the distribution of the respiration peaks, as can be seen in Figure 7.1a. The corresponding raw PPG signal at 810 nm is plotted in Figure 7.1b. The period from the rising edge of a dramatically changing baseline of the PPG signal to the start of a stable region (no significant signal change) is defined as a PPG-fluctuation, e.g., the region ( $T_1$ ) in Figure 7.1b. The quality of PPG signal during talking events (marked by region ( $T_2$ ) in Figure 7.1b) is also strongly degraded. Particularly, the amplitude of each PPG waveform tends to decrease significantly compared to that before the talking events. The FFT of the PPG signals recorded in the time intervals from 620 s to 730 s and from 870s to 950 s are shown in Figure 7.1c and 7.1d, respectively. The signal in the frequency domain indicates that the raw PPG signal is contaminated by low frequency components, especially in the lower frequency range (below 0.5 Hz). The heartbeat frequency corresponds to a dominant peak at about 1.02 Hz and the HR value can be indicated as approximately 61 beats per minute (BPM).

As a PPG signal involves a higher frequency component which synchronizes with the cardiac system attributed to each heartbeat as well as various lower frequency components relating to ANS, the hemodynamic pressure variation near the PPG sensor, motion artefact, as has been established in Chapter 5 of this thesis. When the raw PPG signal is filtered using an extensive low/high pass filter (lower cutoff frequency at 0.5 Hz and higher cutoff frequency at 3.5 Hz), and the low pass and the high pass filtered PPG signals are shown in Figure 7.1e. The slowly varying low pass filtered PPG signal is defined as the ‘DC’ component of PPG signal which shows no sign of cardiac

oscillation (changes in the blood volume with each heartbeat) and is mainly attributable to motion, ANS, and hemodynamic pressure variation in a lower frequency domain. Meanwhile, the high pass filtered PPG signal is defined as the AC component of PPG signal related to cardiac oscillation.

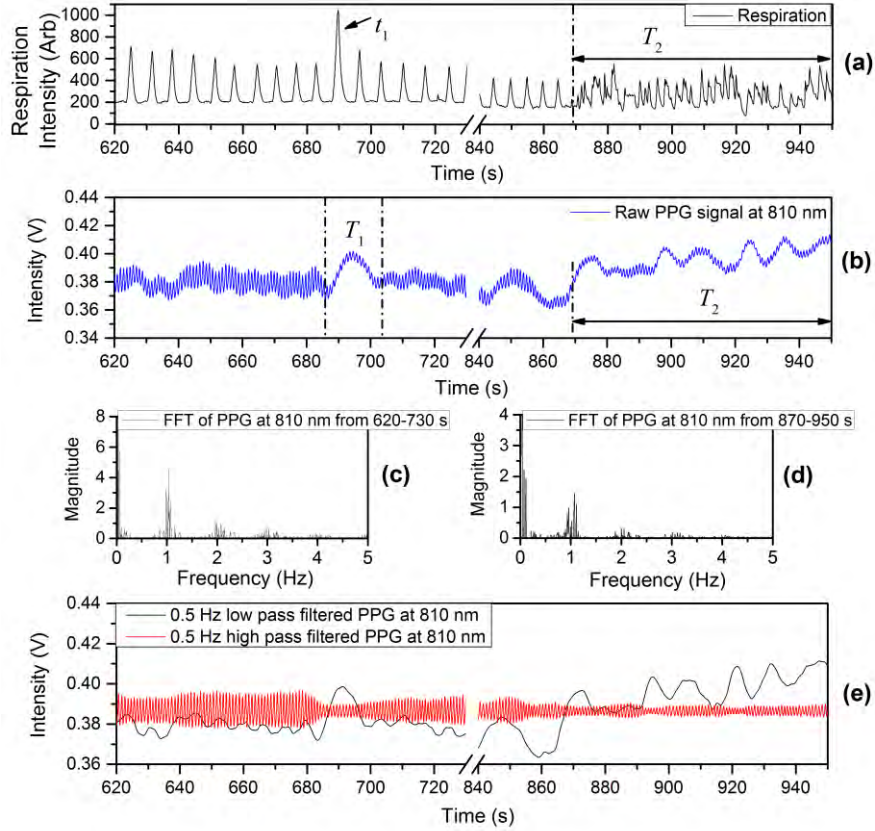


Figure 7.1: (a) Respiration; (b) raw PPG signal at 810 nm; (c) FFT of PPG at 810 nm during 620–730 s; (d) FFT of PPG at 810 nm during 870–950 s and (e) low/high pass filtered PPG at 810 nm (cutoff frequency at 0.5 Hz)

### 7.1.2 Empirical Mode Decomposition Method

Figures 7.2a–7.7a show the effect of using the EMD method on raw PPG signal. The raw PPG signal was recorded with a series of distortions, e.g., deep breathing, change of body position, swing the arm up and down by rotation at the shoulder, on the purpose of showing the EMD method can be widely applied on a PPG signal under different situations. According to section 3.2.2, the raw PPG signal can be decomposed into six IMF components  $c_i$  ( $i = 1, 2, 3, 4, 5, 6$ ) and one monotonic function (constant 0) in this case. The FFT of each IMF component is shown in Figures 7.2b–7.7b. The first IMF

component contains mainly the cardiac oscillation information correlated with raw PPG signals (frequency range is 0.5–3.5 Hz) [142]. The second and third IMF components (blue lines in Figures 7.3a and 7.4a) are associated with respiratory rate (0.14 to 0.75 Hz) [143, 144]. The last three low-frequency signals (blue lines in Figures 7.5a – 7.7a) may consist of unknown physiological significance [145].

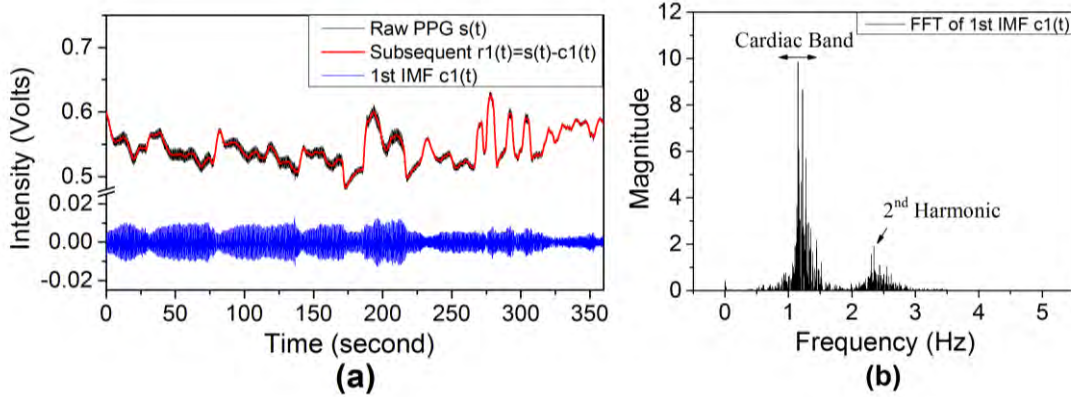


Figure 7.2: (a) Raw PPG signal, subsequent and 1<sup>st</sup> IMF, and (b) FFT of 1<sup>st</sup> IMF component

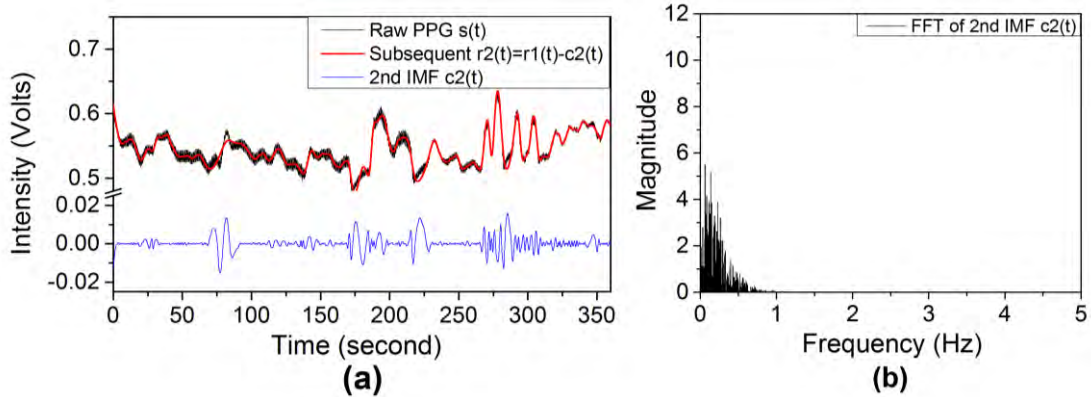


Figure 7.3: (a) Raw PPG signal, subsequent and 2<sup>nd</sup> IMF, and (b) FFT of 2<sup>nd</sup> IMF component

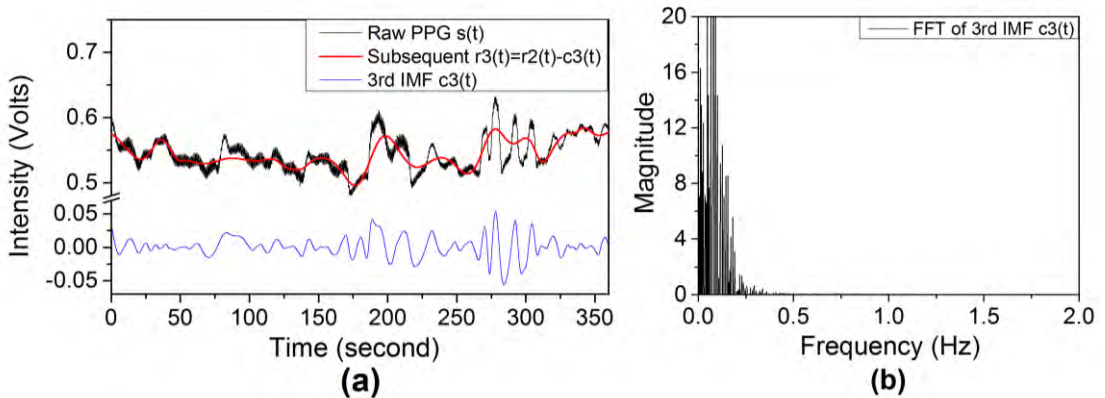


Figure 7.4: (a) Raw PPG signal, subsequent and 3<sup>rd</sup> IMF, and (b) FFT of 3<sup>rd</sup> IMF component

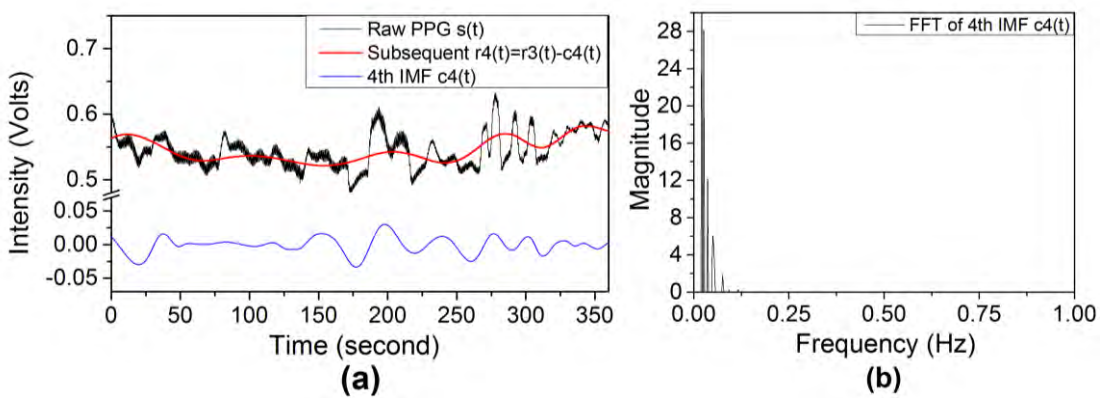


Figure 7.5: (a) Raw PPG signal, subsequent and 4th IMF, and (b) FFT of 4<sup>th</sup> IMF component

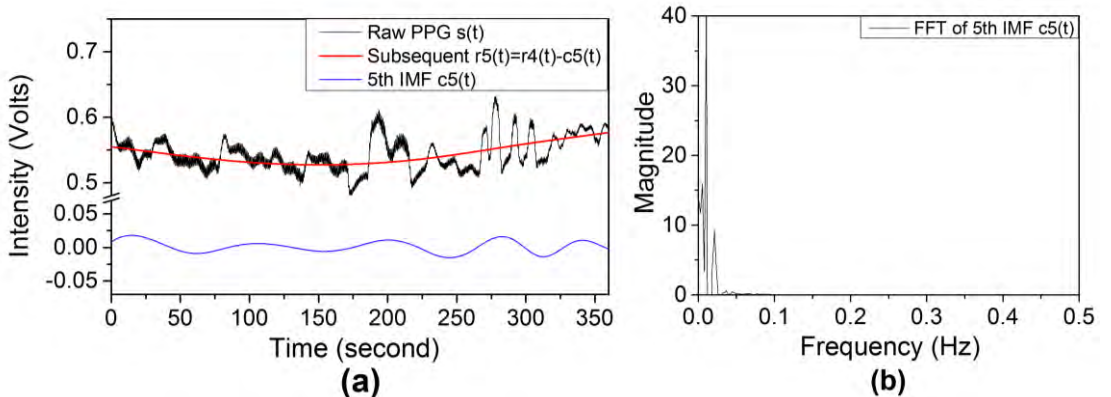


Figure 7.6: (a) Raw PPG signal, subsequent and 5th IMF, and (b) FFT of 5<sup>th</sup> IMF component

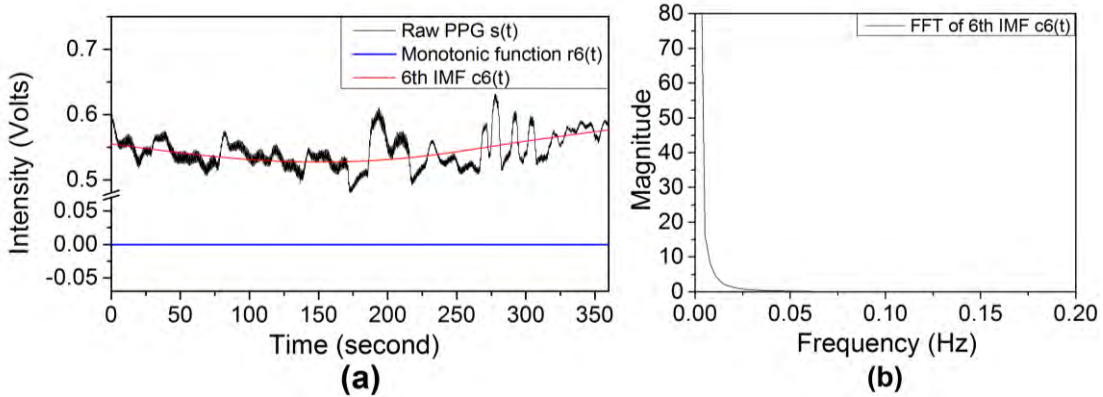


Figure 7.7: (a) Raw PPG signal, subsequent and 6<sup>th</sup> IMF, and (b) FFT of 6<sup>th</sup> IMF component

### 7.1.3 The Proposed Method Based on an Envelope Algorithm

The identical respiration and PPG signals as those in Figure 7.1a and 7.1b are shown in Figure 7.8a and 7.8b. The raw PPG signal with its upper (purple curve) and lower (blue curve) envelopes extracted are shown in Figure 7.8b using the proposed method (different from bandpass and EMD methods). The marked numerals (i, ii, iii, iv, v, and vi) in Figure 7.8a and 7.8b indicate that the upper/lower envelope of the PPG has the potential for estimation of the respiration rate, which in reverse sustains as an evidence that the raw PPG signal is affected/contaminated from breathing. This was established experimentally in Chapter 5 of this thesis.

The envelope filtered PPG signal by the proposed method is shown in Figure 7.8c. The frequency domain of PPG signal captured in the time interval 620–950 s is shown in Figure 7.8d for which low frequency (below 0.5 Hz) in the PPG signal has been filtered by the proposed envelope algorithm based filtering method. The details (time zoomed) of raw (Figure 7.8b) and envelope filtered (Figure 7.8c) PPG signals are represented in Figure 7.8f (in the intervals 680–710 s and 900–930 s). The clear advantage of the PPG optimized using equations (3.10) and (3.11) lies in that it optimizes the cardiac oscillation signal without significantly distorting pulse shape features. The envelope filtering method shows considerable improvement of the PPG signal quality (more smooth and stable) in terms of both BL and AM compared with the raw PPG signal.

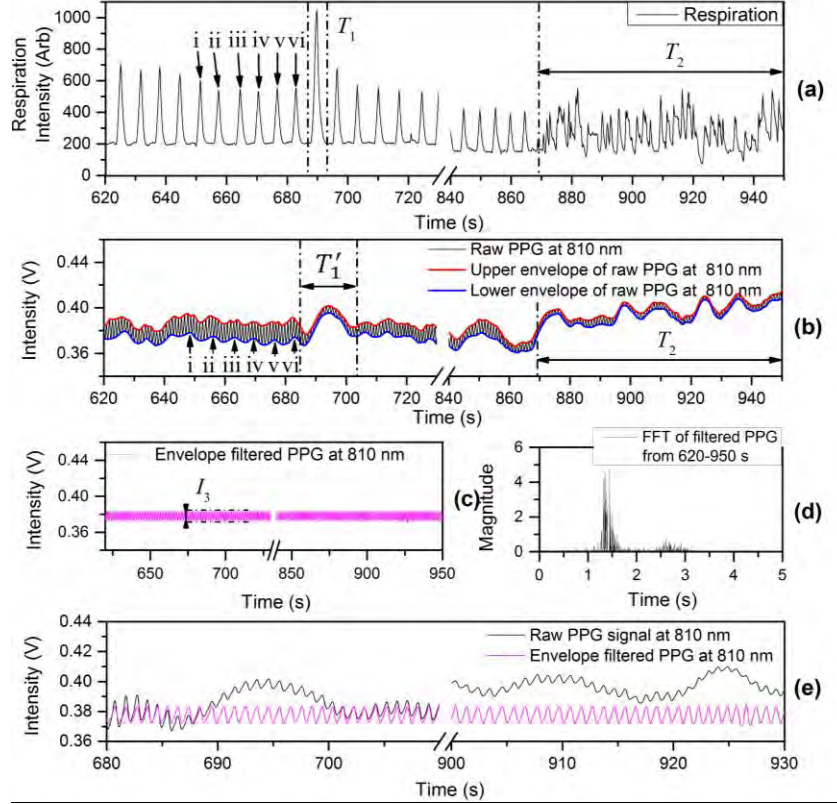


Figure 7.8: (a) Respiration; (b) raw PPG signal at 810 nm with both upper and lower envelopes; (c) envelope filtered PPG at 810 nm by the proposed method; (d) FFT of PPG at 810 nm during 620–950 s and (e) enlarged portion of raw and envelope filtered PPG signals (in the intervals 680–710 s and 900–930 s)

#### 7.1.4 Comparison of Filtering Methods

In the discussion of the filtering method in sections 7.1.1–7.1.3, the raw PPG signal, 0.7–3 Hz bandpass filtered PPG, EMD filtered PPG (1<sup>st</sup> IMF component  $c_1(t)$ ), and AC part of proposed method filtered PPG are shown on one chart (Figure 7.9) for comparison. All the three filtering methods possess efficiency of removal low frequency components in the raw PPG signal without significantly distorting the pulse shape. As the property of the PPG signals in the context of external physiological parameters has been discussed in chapter 5, a PPG signal tends to be distorted in both BL and AM of the PPG signal during a motion or ANS induced PPG-fluctuation. The amplitudes during the PPG-fluctuation of the four PPG signals are marked by  $a_1$ ,  $b_1$ ,  $c_1$  and  $d_1$ ; and the amplitudes after the PPG-fluctuation are marked by  $a_2$ ,  $b_2$ ,  $c_2$  and  $d_2$ . The proposed envelope algorithm based filtering method filtered PPG signal (purple line) shows a significant improvement in the PPG signal quality (more smooth and stable) in terms of

amplitude compared with the raw and other two methods filtered PPG signals (bandpass filtering marked by red line and EMD filtering by blue line).

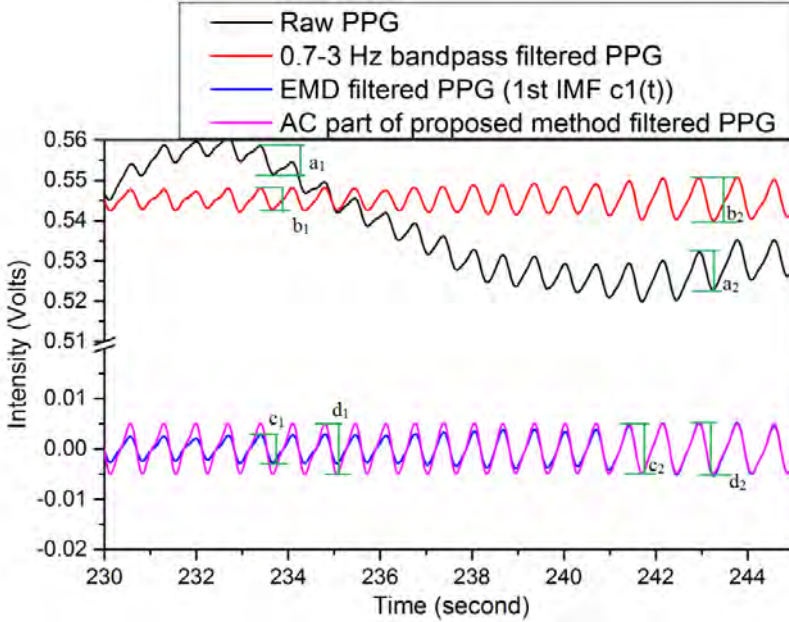


Figure 7.9: Raw PPG signal, 0.7–3 Hz bandpass filtered PPG, EMD filtered PPG ( $1^{\text{st}}$  IMF component  $c_1(t)$ ), and AC part of proposed method filtered PPG

## 7.2 Hb coefficients in Stationary and Non-Stationary States

Section 7.1 has been concerned with the analysis of the suitability of three different candidate methods for the removal of motion artefact and other noise contributes from the PPG signal. For the study of portable Hb monitoring, a series of potentially distorting motion based exercises have been deployed in the following experiments (which can be divided into stationary and non-stationary scenarios) with PPG signals, acceleration and respiration data monitored simultaneously. Initial tests on five randomly selected healthy subjects were carried out for non-invasive calculation of Hb coefficients from raw, band pass filtered, EMD filtered, and proposed envelope filtered PPG signals.

### 7.2.1 Hb Coefficient Development in a Stationary State

Firstly, experiments were conducted when the five participants were in a stationary scenario for which they were in a sitting position, breathing normally with the finger sensor probe kept in front of the chest at heart level on a stable support. A variety of

respiration pattern variations involving deep breathing, talking, and cough events were performed and the signals recorded.

One of the experimental results are shown in Figure 7.10: including (a) acceleration; (b) corresponding respiration; (c, e, g) PPG signals at 810 nm and 1300 nm, and (d, f, h) corresponding to Hb coefficients. In Figure 7.10a, limited or no acceleration was indicated in the time interval 100–1000 s. The corresponding respiration chart (Figure 7.10b) was recorded with two deep breathing events which occurred at 238 s and 332 s, talking events in the period 417–601 s, and one cough at 702 s. Raw PPG signals at 810 and 1300 nm captured from the sensor probe are shown in Figure 7.10c with no filtering applied (raw PPG). PPG-fluctuations, induced from hemodynamic pressure variations near the finger sensor position, occurred corresponding to each respiration pattern variation (Figure 7.10b) for both wavelengths. The 0.8–3.9 Hz band-pass filtered PPG signals (Figure 7.10e) and proposed envelope method filtered PPG signals (in Figure 7.10g) show the expected suppression of low-frequency noises compared to raw PPG signals without filtering (Figure 7.10c). Comparing between these two filtering methods on the PPG signal, e.g. at the wavelength 810 nm, the mean amplitude value ( $33.0 \pm 0.6$  mV) of the band-pass filtered PPG signal is larger than that ( $17.0 \pm 0.2$  mV) of the proposed envelope method filtered PPG signal. The limitation of the proposed method is that distortion of the PPG signal may occur, such as observed during the relatively short interval of 246–251 s (Figure 7.10g). In practice such short term events can be identified and noted as potentially unreliable data if they occur infrequently over the entire duration of a signal capture cycle. The corresponding calculation of the Hb coefficients (from PPG signals in Figures 7.10c, 7.10e, and 7.10g) are illustrated in Figures 7.10d (raw), 7.10f (band pass), and 7.10h (envelope), respectively. The Hb coefficients are equally affected by respiration pattern variations of Figure 7.10b and the least fluctuation takes place in Figure 7.10h. The mean and standard deviation (shown in brackets) of the Hb coefficient data for each of the data sets of Figures 7.10d, 7.10f, and 7.10h were also calculated for the entire duration of each record (Hb coefficients). The results of this calculation were  $3.08 (\pm 0.15)$ ,  $3.06 (\pm 0.21)$  and  $2.81 (\pm 0.15)$ , for Figure 7.10d, 7.10f and 7.10h respectively. There is clearly an improvement in the deviation of the signal obtained for Figure 7.10h in comparison with Figure 7.10f. The reason of the mean Hb coefficient 2.81 calculated by the proposed filtering method being

less than the mean of raw Hb coefficient 3.08 and the band pass filtered PPG calculated Hb coefficient 3.06 is due to that the filtered PPG signal by the proposed filtering method has a smaller value of DC part (related with BL) of the PPG signal.

The band pass filtered Hb coefficients is supposed to be better than raw Hb coefficients, but experimental results of raw and band pass filtered Hb coefficients reading are 3.08 ( $\pm 0.15$ ), 3.06 ( $\pm 0.21$ ). The author has explained how a raw signal is process by a high/low pass filtering in section 7.1.1. The direct advantage of bandpass filtered PPG signal is a constant value BL obtained, but the AM of the PPG signal is still severely disturbed. It could be argued that the exist of noises including motion artifact stands as proof that the traditional high pass or bandpass filtering is not efficient in removing noises.

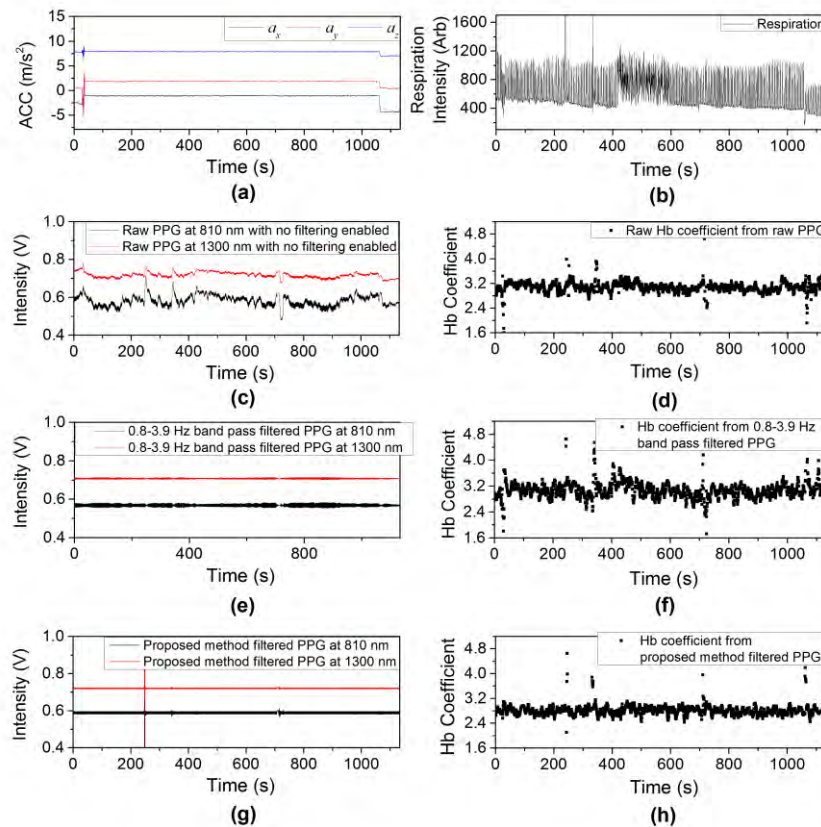


Figure 7.10: (a) Acceleration; (b) respiration; (c) raw PPG at 810 nm and 1300 nm with no filtering enabled; (d) Hb coefficient from raw PPG; (e) 0.8–3.9 Hz band pass filtered PPG signals at 810 nm and 1300 nm; (f) Hb coefficient during 0.8–3.9 Hz band pass filtered PPG; (g) proposed method filtered PPG signals at 810 nm and 1300 nm; and (h) Hb coefficient from proposed method filtered PPG

The same experiment was processed by EMD filtering method, as shown in Figure 7.11. As has been described in section 7.1.2, the first IMF component contains mainly the cardiac oscillation information correlated with raw PPG signals and the amplitude of the first IMF component is defined as  $X_{AC,EMD}$ . The DC part (baseline) of EMD filtered PPG signal can be deduced from the low pass filtered components ( $X_{DC,low}$ ) and then the EMD filtered PPG signal can be expressed as  $X_{AC,EMD} + X_{DC,low}$  (as shown in 7.11a). The derivation of DC part (baseline) of EMD filtered PPG signal can also be a constant value  $X_{DC,constant}$  using equation 3.11, and then the EMD filtered PPG signal can be expressed as  $X_{AC,EMD} + X_{DC,constant}$  (as shown in 7.11b). The Hb coefficients derived from 810 nm and 1300 nm EMD filtered PPG signals are shown in Figure 7.11c and 7.11d, respectively. The mean and standard deviation (shown in brackets) of the Hb coefficient data for each of the data sets of Figures 7.11c and 7.11d were also calculated for the entire duration of each record (Hb coefficients). The results of this calculation were 2.93 ( $\pm 0.16$ ) and 2.92 ( $\pm 0.14$ ) for Figure 7.11c and 7.11d. The comparison of Hb coefficients derived by the four methods proves that the EMD filtering method is effective in the process of Hb coefficients. Results of four calculation methods of Hb coefficients in the stationary state show that cough and deep breathing events tend to disturb the Hb monitoring which could be hardly recovered.

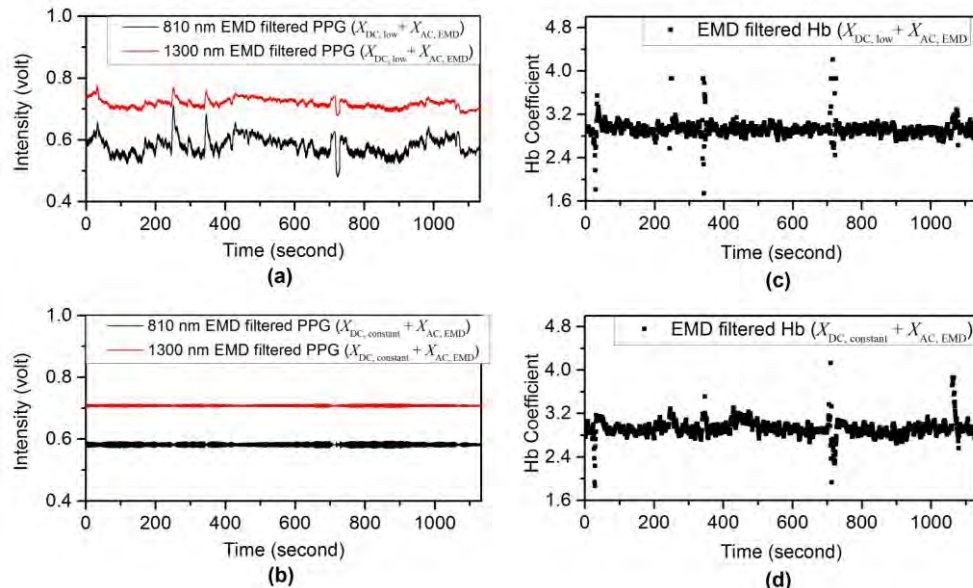


Figure 7.11: (a) EMD filtered PPG ( $X_{DC,low} + X_{AC,EMD}$ ); (b) EMD filtered PPG ( $X_{DC,constant} + X_{AC,EMD}$ ); (c) EMD filtered Hb ( $X_{DC,low} + X_{AC,EMD}$ ); (d) EMD filtered Hb ( $X_{DC,constant} + X_{AC,EMD}$ )

## 7.2.2 Hb Coefficient Development in Non-Stationary States

The experiments on the five participants in a non-stationary state were conducted for which they were requested to (1) swing the arms on which the finger sensor probe is connected between 25 cm above heart level and 25 cm below heart level for several times while in a standing posture, and (2) walk with the finger sensor on in front of chest at heart level. A normal position is defined as a straight standing position for which the finger with the sensor probe on in front of chest at heart level. During the event of arm swing, the finger sensor probe was placed on the finger in line with the upper arm and forearm, and the arm was fully outstretched and held straight.

One of the experimental results corresponding to this motion pattern are shown in Figure 7.12: including (a) acceleration; (b) respiration; (c, e, g) PPG signals at 810 nm and 1300 nm, and (d, f, h) corresponding Hb coefficients. In Figure 7.12a, the subject was initially in a normal rest position from 57 s to 329 s. The time interval 364–420 s indicates swinging the arm up and down by rotation at the shoulder with short resting intervals (peak-to-peak time interval approximately 5.5 s). This was followed by a process of walking which occurred in the interval 755–1120 s after the candidate was in a normal rest position from 493 s to 755 s. The end of the non-stationary scenario tests was accompanied by another normal rest position from 1120 s to 1492 s. The raw, the band-pass filtered, and the proposed envelope method filtered PPG signals at 810 nm and 1300 nm are shown in Figures 7.12c, 7.12e, and 7.12g, respectively. The corresponding calculations of Hb coefficients from these PPG signals are shown in Figures 7.12d, 7.12f, and 7.12h. The mean and standard deviation of Hb coefficient data for each in Figures 7.12d, 7.12f, and 7.12h were calculated as in Section 2.6 above (Hb coefficients). The envelope method (Figure 7.12h) has almost completely removed the Hb coefficient signal artefact due to the arm waving action.

A similar mean and SD analysis conducted over the confined period of 364–420 s which included the swinging arm results but not the walking yielded the following results. The mean and  $\pm$ SD values for swinging the arm events only, were calculated as 3.26 and  $\pm$ 0.38 for the raw Hb coefficients, 3.48 and  $\pm$ 0.33 for the Hb coefficients from band pass filtered PPG signals, and 2.89 and  $\pm$ 0.20 for the Hb coefficients from the proposed

envelope method filtered PPG signals. This is also clearer if each waveform is viewed purely from a visual point of view as the extent of the worst case scenario of signal corruption occurs during the walking phase and this is most prominent in Figures 7.11d and 7.11f. The mean ( $\pm$ SD) of walking events was calculated as 3.20 ( $\pm$ 0.40) for the raw Hb coefficients, 3.11 ( $\pm$ 0.36) for the Hb coefficients from band pass filtered PPG signals, and 2.89 ( $\pm$ 0.31) for the Hb coefficients from the proposed envelope method filtered PPG signals. The Hb coefficients from the proposed envelope method filtered PPG (Figure 7.12h) exhibit a relatively superior performance in terms of stability compared with the raw Hb coefficient readings (Figure 7.12d) and Hb coefficients from the band-pass filtered PPG (Figure 7.12f).

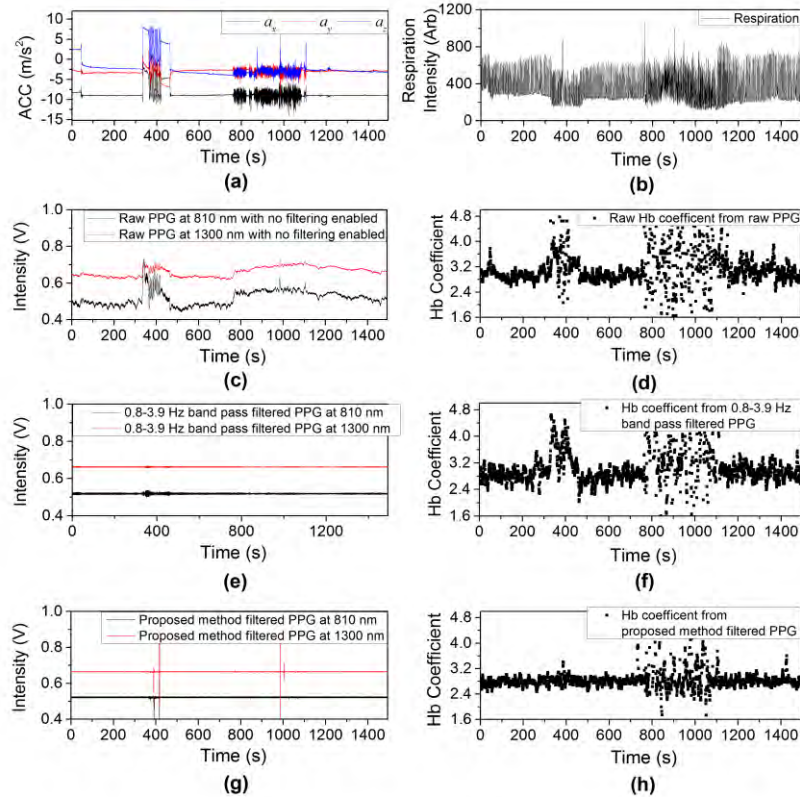


Figure 7.12: **(a)** Acceleration; **(b)** respiration; **(c)** raw PPG at 810 nm and 1300 nm with no filtering enabled; **(d)** Hb coefficient from raw PPG; **(e)** 0.8–3.9 Hz band pass filtered PPG signals at 810 nm and 1300 nm; **(f)** Hb coefficient during 0.8–3.9 Hz band pass filtered PPG; **(g)** proposed method filtered PPG signals at 810 nm and 1300 nm; and **(h)** Hb coefficient from proposed method filtered PPG

The same experiment in non-stationary scenarios was also processed by EMD filtering method, as shown in Figure 7.13. The EMD method can be expressed by the same

$X_{AC,EMD}$  but with different DC parts: (a) in Figure 7.13a,  $X_{DC,low}$  indicates the low pass filtered components (as baseline of the EMD filtered PPG signal); (b) in Figure 7.13b,  $X_{DC,constant}$  stands for a constant value of baseline as the DC part of the EMD filtered PPG signal. The Hb coefficients derived from 810 nm and 1300 nm EMD filtered PPG signals are shown in Figure 7.13c and 7.13d. The mean and standard deviation (shown in brackets) for swinging the arm events only in each of the data sets of Figures 7.13c and 7.13d were 3.57 ( $\pm 1.05$ ) and 3.60 ( $\pm 0.40$ ). The mean ( $\pm SD$ ) of walking events was calculated as 3.23 ( $\pm 0.83$ ) and 3.55 ( $\pm 0.77$ ) for Figure 7.13c and 7.13d. The comparison of Hb coefficients derived by the EMD and the proposed envelope filtering method indicates that the latter is more effective in the process of both swinging the arm and walking events than the EMD filtered method.

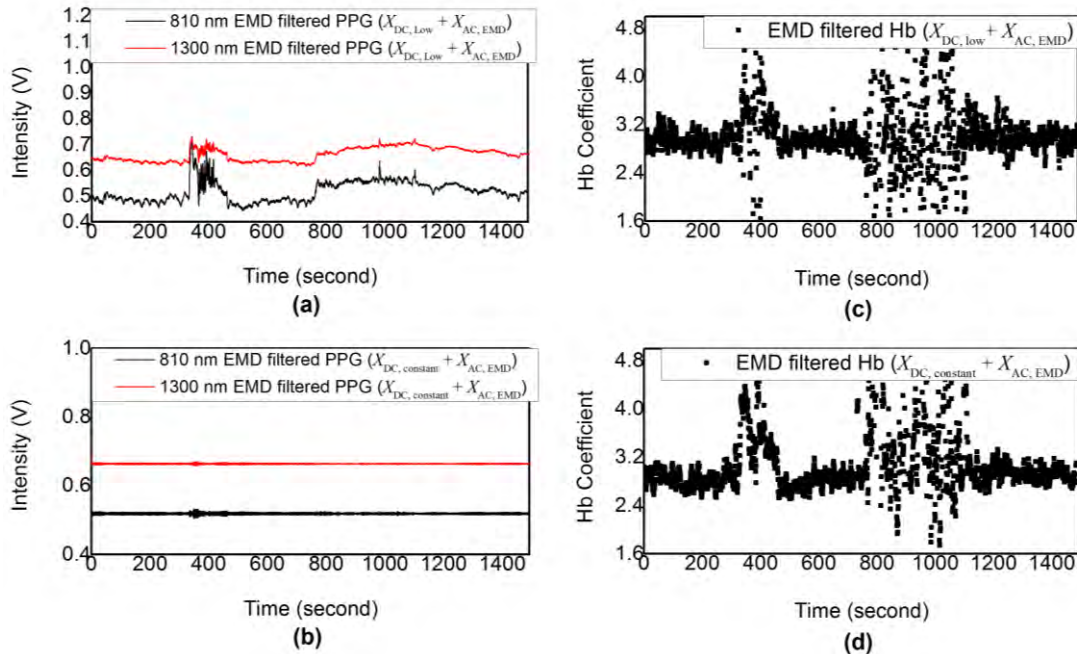


Figure 7.13: (a) EMD filtered PPG ( $X_{DC,low} + X_{AC,EMD}$ ); (b) EMD filtered PPG ( $X_{DC,constant} + X_{AC,EMD}$ ); (c) EMD filtered Hb ( $X_{DC,low} + X_{AC,EMD}$ ); (d) EMD filtered Hb ( $X_{DC,constant} + X_{AC,EMD}$ )

### 7.3 Hb Coefficient with Respect to VHD Variation

In section 7.2, VHD variations were introduced through swinging arm events. The tests of the VHD variation were conducted and observed in non-stationary states. The effect of VHD on the PPG signal has been discussed in detail in references [135, 141, 146]. As hemodynamic pressure variation near the sensor probe in the lower frequency domain is

induced from VHD between the finger sensor probe and the heart level, it is worth studying this effect in the stationary state. In detail, measurements were recorded for which the sensor's position with the finger sensor probe on was placed/set in three different locations and maintained stationary for at least 60 s: 25 cm above heart level, heart level and 25 cm below heart level; while the subjects were in sitting position.

A typical experimental result for the study of the PPG signal and Hb coefficient with respect to VHD variation is shown in Figure 7.14. The acceleration and respiration signals are shown in Figure 7.14a and 7.14b. The height of the finger sensor probe was set at three different locations, 25 cm above heart level (region (A)), heart level (region (B)), and 25 cm below heart level (region (C)), as shown in Figure 7.14a. Raw and proposed method filtered PPG signals at 810 nm/1300 nm during these period are shown in Figure 7.14c/7.14d. The baseline of the raw PPG signal tends to decrease with the decline of the sensor probe's height (the moment of decline can be observed in the acceleration signals (Figure 7.14a)). Compared with the filtered PPG signal, the raw PPG signals are highly influenced by VHD between the finger sensor probe and the heart level, especially during the moment of changing the finger sensor probe's height (accompanied with PPG-fluctuations). The advantage of the proposed method filtered PPG signals is the suppression of the affect from VHD without significantly distorting the pulse shape and PPG signals in accordance with cardiac oscillation (changes in the blood volume with each heartbeat) and these have been successfully recovered from VHD events.

The raw Hb coefficients (black square dots) and the Hb coefficients from the proposed method filtered PPG (red circle dots) are shown in Figure 7.14e. Compared with the filtered Hb coefficient readings, the raw Hb coefficient readings are more affected by VHD. The raw Hb coefficient readings vary in a manner similar to the baseline of the raw PPG signal varies whereas the filtered Hb coefficients show a relatively stable reading during the VHD recording period.

Results of the mean (with standard deviation, typically in 25 s) of Hb coefficients from the raw and proposed method filtered PPG signals were recorded for all the five randomly selected subjects are captured in Table 7.1 according to VHD variation (the

finger sensor probe set at 25 cm above heart level, heart level, and 25 cm below heart level). The studies of the raw Hb coefficients (no filtering) as well as those using the proposed method filtered PPG signals are shown as histograms with standard deviations in Figures 7.15a and 7.15b, for which the five subjects were in the sitting position and their hands with the finger sensor probe on were set at three different vertical levels. The histograms in Figure 7.15a show the consistency that raw Hb coefficients from the five subjects are correlated with VHD. Specifically, the raw Hb coefficients tend to decrease with the decline of the vertical height of the sensor probe with respect to the heart level. The values of the Hb coefficients from the band pass filtered PPG (Figure 7.15b) and proposed method filtered PPG (Figure 7.15c) exhibit less disturbance from VHD variation in comparison to the Hb coefficients from the raw PPG signals.

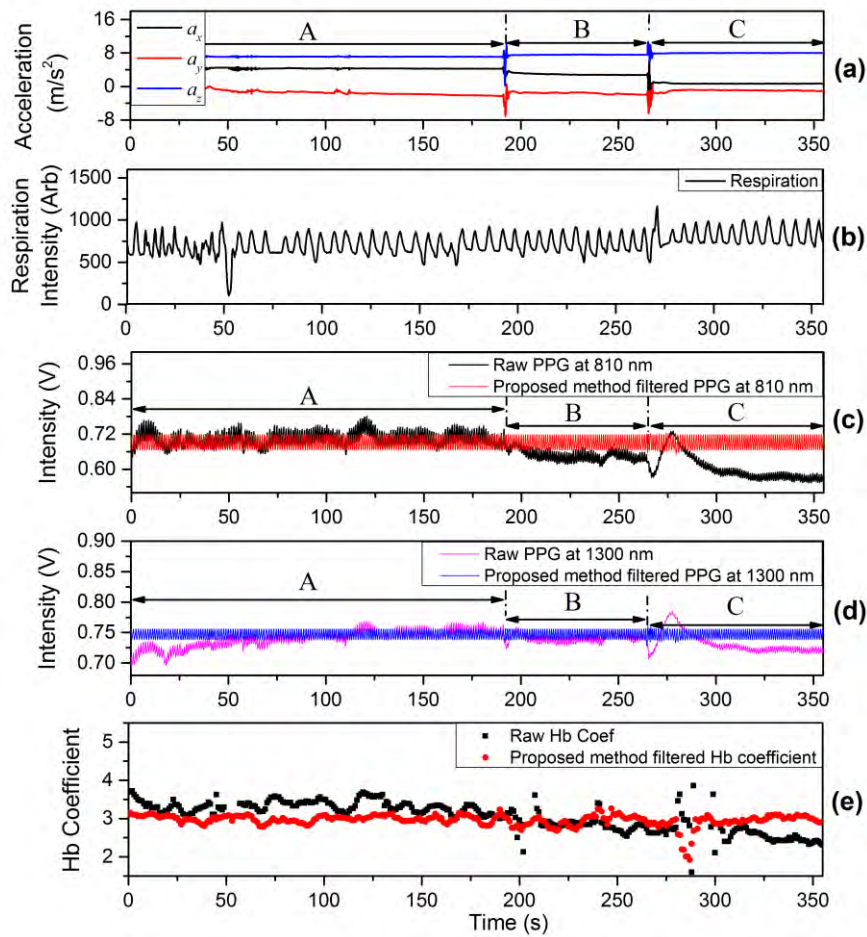


Figure 7.14: (a) Acceleration; (b) respiration; (c) raw and proposed method filtered PPG signals at 810 nm; (d) raw and proposed method filtered PPG signals at 1300 nm; and (e) raw Hb coefficient (black square point) and proposed method filtered Hb coefficient (red circle point)

Table 7.1: Hb coefficients deduced from raw and proposed method filtered PPG signals for which the five individual subjects were in the sitting position and the finger sensor probe set at three different vertical levels

Subject	Hb coefficients by raw PPG data ( $\pm$ SD)			Hb coefficients by proposed method ( $\pm$ SD)		
	25 cm above Heart Level	Heart Level	25 cm below Heart Level	25 cm above Heart Level	Heart Level	25 cm below Heart Level
1	3.43( $\pm$ 0.16)	2.96 ( $\pm$ 0.09)	2.50 ( $\pm$ 0.47)	3.46 ( $\pm$ 0.23)	3.20 ( $\pm$ 0.18)	3.23 ( $\pm$ 0.17)
2	3.68 ( $\pm$ 0.16)	3.38 ( $\pm$ 0.62)	2.90 ( $\pm$ 0.53)	3.65 ( $\pm$ 0.07)	3.56 ( $\pm$ 0.15)	3.91 ( $\pm$ 0.24)
3	3.34 ( $\pm$ 0.14)	2.72 ( $\pm$ 0.09)	2.43 ( $\pm$ 0.14)	3.00 ( $\pm$ 0.07)	3.02 ( $\pm$ 0.10)	3.04 ( $\pm$ 0.05)
4	3.11 ( $\pm$ 0.11)	2.68 ( $\pm$ 0.11)	1.83 ( $\pm$ 0.11)	2.69 ( $\pm$ 0.15)	2.65 ( $\pm$ 0.08)	2.69 ( $\pm$ 0.03)
5	3.74 ( $\pm$ 0.20)	3.49 ( $\pm$ 0.41)	3.22 ( $\pm$ 0.35)	3.36 ( $\pm$ 0.14)	3.21 ( $\pm$ 0.41)	3.49 ( $\pm$ 0.35)

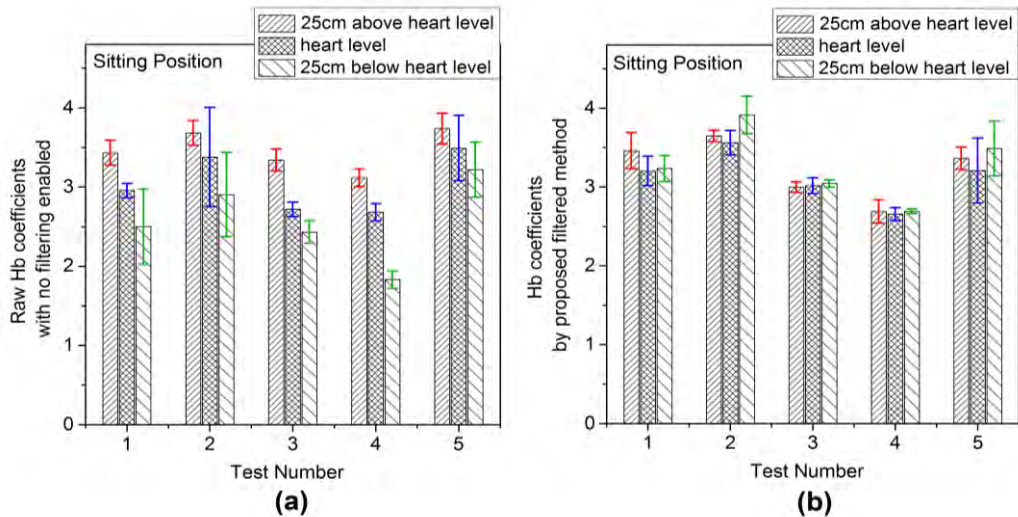


Figure 7.15: Histograms of (a) raw Hb coefficients (standard deviations) with no filtering enabled and (b) Hb coefficients by proposed filtered method (standard deviations) for which the subjects were in the sitting position and the hands with the sensor probe on were set at three different vertical levels

#### 7.4 The Test of Proposed Method in a Series of Distortions

The ruggedness of the proposed method was tested by deployment of a series of distortions which were applied continuously for the study of Hb coefficients under

different events. The experiments prototype include (i) ANS respiration (deep breathing and cough events) for which the hand positions with the finger sensor probe on was kept in front of chest at heart level on a stable support, (ii) VHD of the hand positions with the finger sensor probe on (e.g., change of the sensor's position from 25 cm below heart level to 25 cm above heart level while the subject in a sitting position), (iii) change of body position from a sitting to a standing posture for which the hand position with the finger sensor probe on was kept in front of chest, (iv) swinging of arm with finger sensor probe on between 25 cm above heart level and 25 cm below heart level for several times while the subject in a standing posture, and (v) walking with the finger sensor on in front of chest at heart level.

The experimental results of raw Hb coefficients (black square points) and filtered Hb coefficients (red circle points), raw PPG and envelope filtered PPG signals by the proposed method, ACC signals, and respiration intensity are shown in Figures 7.16a–7.16d, respectively. Region (A<sub>1</sub>) and Region (A<sub>2</sub>) in Figure 7.16d mark the deep breathing and cough events, and accordingly PPG-fluctuations occurred with the ANS variation in Figure 7.16b. Region (B) in Figure 7.16b indicates the VHD of the finger sensor position, and the raw PPG signal was affected from the local BP variation near the finger sensor position. Region (C) in Figure 7.16c shows the movement of body position with no variation of VHD between the finger sensor probe and the heart level. A PPG-fluctuation in Figure 7.16b indicates that change of body position can stimulate ANS variation to influence the raw PPG signal as well as raw Hb coefficients readings in Figure 7.16a. Region (D) in Figure 7.16c indicates the swinging of the arm with the finger sensor probe attached between 25 cm above heart level and 25 cm below heart level. The intensities of raw PPG signal vary in a manner similar to the manner in which the readings of the ACC signals vary. A zoomed raw PPG and the filtered PPG signals in the time period of 350–362 s can be found on the top right of Figure 7.16b. The baseline of the raw PPG is highly affected by the VHD whereas that of the filtered PPG has been optimized by the equation (3.11) without significantly distorting pulse shape features. Region (E) in Figure 7.16b shows the raw PPG signal during a walking event while the subject tried to breath at an even speed (Figure 7.16d). The measurements of raw Hb coefficients and filtered Hb coefficients are illustrated in Figure 7.16a. The walking event disturbs the raw Hb coefficient readings in a more observable manner

than other events in the series of the distortions test. The filtered Hb coefficient readings therefore exhibit better performance in stability compared with the raw Hb coefficient readings. The mean and standard deviation (shown in brackets) for the test in a series of distortions was calculated as 3.22 ( $\pm 0.50$ ) for the raw Hb coefficients and 2.88 ( $\pm 0.25$ ) for the Hb coefficients from the proposed envelope method filtered PPG signals.

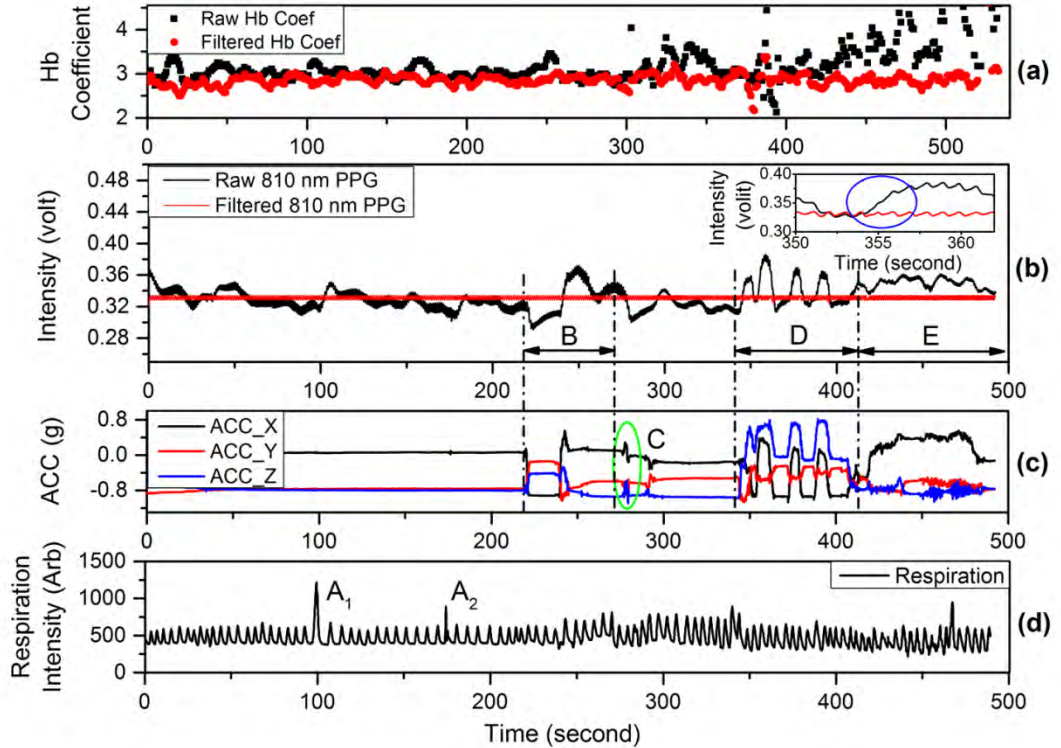


Figure 7.16: **(a)** Raw Hb coefficients (black square points) and filtered Hb coefficients (red circle points), **(b)** raw PPG and envelope filtered PPG signals by the proposed method, **(c)** ACC signals, and **(d)** respiration intensity

## 7.5 Summary

Devices including an accelerometer and a respiration monitor belt have been deployed in conjunction with the custom designed PPG sensor system for investigation of the Hb coefficients from PPG signals in the context of both static and non-static states. Initial tests on five randomly selected healthy subjects include acts of talking, swinging arm and walking events whilst the sensor probe was worn. Results demonstrate that Hb coefficient derived from proposed envelope method filtered PPG shows a better performance on minimisation of motion artefact than that from standard band pass filtered PPG data. As hemodynamic pressure variation near the sensor probe in the

lower frequency domain is induced from VHD between the finger sensor probe and the heart level, studies show that Hb coefficients from the proposed method filtered PPG signals have better performance on minimisation of motion artefact than those from raw PPG signals.

The results for the stationary state and non-stationary states have been tested on five subjects. The values by the proposed filtered Hb coefficients indicate more accurate readings than those from the raw and BP filtered PPG signals. The reason of why 2.81 (2.89 or 2.89) is smaller than 3.08 and 3.06 (or others) is due to that the filtered PPG signal by the proposed filtering method has a smaller value of DC part (related with BL) of the PPG signal. The proposed Hb reading varies in a smaller range (more stable) than the other methods used in the thesis. The further calibration of the Hb estimation by non-invasive method with invasive Hb reference will be different, but this will be out of the scope of this thesis.

## CHAPTER 8.

# CONCLUSIONS AND FUTURE WORK

---

This effective and proven optical Hb sensing platform presents a great opportunity for applications in a number of domains, not least within clinical care scenarios (MRI, CT, Cardiac and Neonatal ICUs), as well as within first responder kits. These targeted application domains require the on-going adaptation of the platform to meet the constraints and requirements presented by each. PPG technique is detecting blood volume changes in tissue obtained by an optical method from optical based sensor probes. PPG signals has been used extensively for the monitoring of HR, respiration rate and oxygen saturation. One of the drawbacks of PPG based measurement is that the signal is strongly degraded by motion artefact. Much research has been undertaken relating to the removal of motion artefact noise resulting from the wearer's movement. In particular, the motion of the patient can adversely affect the sensors measurements and must therefore be taken into account by the platform.

PPG and acceleration signals are collected from the sensor device and later analysed for human vitals monitoring. LabVIEW is used to compute the various optical absorption parameters, accelerometer coefficients and the derived coefficients (e.g., SpO<sub>2</sub>, Hb, HR). A study of the effects of motion of the probe on the PPG signal shows that the PPG signal is corrupted/degraded by movement event, and also strongly affected by height variation in vertical direction. A blood pressure monitor is used to measure the local BP in close proximity to the measuring site when the wearer's hand is moved to the various locations described. Results presented here illustrate that a reference no-movement baseline in PPG signal is more highly affected by acceleration in vertical direction as opposed to acceleration in the horizontal level. This thesis reports on the research relating to the effects of motion on the quality of a PPG signal, with a

particular emphasis on the effect of the local BP at the measuring site and also considers the influence of ANS.

Using commercially available accelerometers, a respiration monitor belt and a blood pressure monitor, PPG and acceleration signals were collected from the sensor device and later analysed for human vitals monitoring. A comprehensive study of the effect of a wide range of controlled human subject motion on PPG signals is reported. The investigation includes testing of two separate groups of 5 and 18 subjects who were asked to undertake set exercises whilst simultaneously monitoring a wide range of physiological parameters including breathing rate, HR and localised BP using commercial clinical sensing systems. The unique finger mounted PPG probe equipped with miniature three axis accelerometers for undertaking this investigation was a purpose built in-house version which is designed to facilitate reproducible application to a wide range of human subjects and the study of motion. The subjects were required to undertake several motions based exercises, including standing, sitting and lying down and transitions between these states. They were also required to undertake set arm movements, including arm-swinging and wrist rotation. A comprehensive set of experimental results corresponding to all motion inducing exercises has been recorded and analysed to include the baseline value and the amplitude of the oscillation of the PPG. All physiological parameters were also recorded as a simultaneous time varying waveform. The effects of the motion and specifically the localised BP have been studied and related to possible influences of the ANS and hemodynamic pressure variations.

Research presented here shows that the baseline of PPG signal is highly affected by acceleration in vertical direction as opposed to acceleration in the horizontal level for the system under test. Experimental results from a total of 23 subjects demonstrated that PPG signals during motion events are influenced by the variation of local BP at the point of measurement which is in turn induced from: (1) the VHD between the measuring site and the reference level (the heart level); and (2) the ANS. The results of a statistical analysis conducted on 18 subjects (9 male and 9 female) have shown that the dependency of the BL and AM values of the PPG signal are only weakly dependent on the VHD.

Experimental studies on the effect of the local BP variation on PPG signals have been reported in this thesis. It is expected to be an easier task to predict future application of these properties to PPG and ACC based sensor device given that Hb and SpO<sub>2</sub> coefficients. It is highly important to modify the evaluation function for Hb and SpO<sub>2</sub> monitoring, so that the ACC signal could be used for statue monitoring with less weight, low-pass filtering, and non-invasive real time monitoring of human vitals during motion events, tracking for the elder or exercise sports. Note, however, that the presence of mean average method for Hb monitoring is the main limitation for further application, and on the other hand a highly dependent of LEDs package is needed with great intensities, especially the 1300 nm LED (sufficiently strong optical feedback is required to), and a wide range sensitive photodiode ranged from 500 nm to 1500 nm to provide good quality of received PPG signals from reflective or transmitted light, so on and on. In summary, additional optimization is necessary for accurate prediction of PPG based sensor measuring readings.

Hence, in the procedure of removing such noises (e.g., ANS and VHD) from disturbing the correct estimation of interested original PPG signals, normal digital filtering methods, e.g., bandpass, Butterworth, FIR and et al, will be carefully selected to extract original PPG from raw PPG signals. In this thesis, a simple but effective envelope filtering method is developed to remove such frequency noises from original PPG signals which are used for diagnosis of non-invasive Hb monitoring in addition to spectral analysis. Initial tests on five randomly selected healthy subjects include respiration pattern variations, swinging arm and walking events with the sensor probe on their right hands index fingers. Results demonstrate that Hb coefficient derived from proposed envelope method filtered PPG has a better performance on minimisation of motion artefact than that from FFT of PPG data in both stationary and non-stationary states. Hb coefficient is more evident in VHD analysis when the proposed method is deployed.

The reason of band pass filtering method selected to be compared with proposed envelope filtering method is because both of these two filtered PPG signals can be divided into AC (amplitude) and DC (baseline value) components. The superiority of proposed envelope filtered PPG signals lies in possessing a smaller amplitude variations

comparing with those of band pass filtered PPG signals. However, the proposed envelope filtered PPG is not perfect for some situation/region with severe distortion from being recovered, which can be seen in Figures 7.10g and 7.12g.

It should be noted that the further work will concentrate on identification of whether a distortion occurs in a pulse from the proposed filtering method and improvement of signal quality. PPG signal could be applied first by band pass filter and then by the proposed filter (combination). The calculation of upper and lower envelope is based on cubic spline interpolation algorithm, and more algorithms, e.g., Hilbert-Huang transform and Akima interpolation algorithm, can also be adopted in the proposed envelope filtering method. Due to limitations of available space, the comparison between proposed filtering method and other popular filtering methods (e.g., Butterworth, Gaussian, empirical mode decomposition (EMD) and IIR filters) haven't been given into discussion in this thesis.

Finally, further test on a wider range of subjects with simultaneous collection of reference Hb (from HemoCue® Hb 201+) and our non-invasive sensor device under a variety of motion activity is very necessary but requires extensive clinical approval. In the present study, it focuses mainly on Hb coefficient calculation based on PPG signals at 810 nm and 1300 nm in stationary state, which makes providing more accurate assessment of Hb monitoring including calibration in non-stationary states our top priority in the next step of work. Some difficulty could be the lack of Hb reference in motion events since reading during motion could be different from invasive Hb readings (HemoCue® Hb 201+) and current commercial non-invasive Hb monitoring devices, e.g., radical-7 pulse co-oximeter from Masimo, in many, are limited to application in static states. It is envisaged that our proposed envelope filtering method could be extended on many other physiological signals including PPG signals. The research results in this thesis show that the proposed method and linear fitting calibration promise accurate assessment of non-invasive Hb reading. The direct advantage of the propose method in suppressing/removal motion artefact is that it broadens the application of remote bio sensor device, such as pulse oximeter, from being used in stationary state (normally set at heart level) to outdoor sport activities.

# Bibliography

- [1] S. Antoni, J. Ferlay, I. Soerjomataram, A. Znaor, A. Jemal, and F. Bray, "Bladder cancer incidence and mortality: a global overview and recent trends," *European urology*, vol. 71, pp. 96–108, 2017.
- [2] S. Rabin, P. Alexander, P. Anthoni, R. Henry, C. Huntingford, T. Pugh, M. Rounsevell, and A. Arneth, "Projecting optimal land-use and-management strategies under population growth and climate change using a coupled ecosystem & land use model framework," in *EGU General Assembly Conference Abstracts*, pp. 1158–1164, 2017.
- [3] O. Egen, K. Beatty, D. J. Blackley, K. Brown, and R. Wykoff, "Health and Social Conditions of the Poorest Versus Wealthiest Counties in the United States," *American journal of public health*, vol. 107, pp. 130–135, 2017.
- [4] A. Barford, D. Dorling, G. D. Smith, and M. Shaw, "Life expectancy: women now on top everywhere: during 2006, even in the poorest countries, women can expect to outlive men," *BMJ: British Medical Journal*, vol. 332, pp. 808–812, 2006.
- [5] V. Kontis, J. E. Bennett, C. D. Mathers, G. Li, K. Foreman, and M. Ezzati, "Future life expectancy in 35 industrialised countries: projections with a Bayesian model ensemble," *The Lancet*, vol. 389, pp. 1323–1335, 2017.
- [6] C. Murphy, P. Kearney, E. Shelley, T. Fahey, C. Dooley, and R. Kenny, "Hypertension prevalence, awareness, treatment and control in the over 50s in Ireland: evidence from The Irish Longitudinal Study on Ageing," *Journal of Public Health*, vol. 38, pp. 450–458, 2016.
- [7] M. Linden, and D. Ray, "Life expectancy effects of public and private health expenditures in OECD countries 1970–2012: Panel time series approach," *Economic Analysis and Policy*, vol. 56, pp. 101–113, 2017.
- [8] C. Devitt, A. Bobek, and G. Kingston, "Migrant workers in the Irish healthcare sector," vol. 3, pp. 145–168, 2015.
- [9] A. Grant, and L. Hoyle, "Print media representations of UK Accident and Emergency treatment targets: Winter 2014–2015," *Journal of clinical nursing*, vol. 45, pp. 235–241, 2017.
- [10] J. Allen, "Photoplethysmography and its application in clinical physiological measurement," *Physiological measurement*, vol. 28, pp. 61–75, 2007.
- [11] Y. Yan, C. C. Poon, and Y. Zhang, "Reduction of motion artifact in pulse oximetry by smoothed pseudo Wigner-Ville distribution," *Journal of NeuroEngineering and Rehabilitation*, vol. 2, pp. 3–9, 2005.
- [12] F. Peng, Z. Zhang, X. Gou, H. Liu, and W. Wang, "Motion artifact removal from photoplethysmographic signals by combining temporally constrained independent component analysis and adaptive filter," *Biomedical engineering online*, vol. 13, pp. 50–58, 2014.
- [13] H. Han, M. Kim, and J. Kim, "Development of real-time motion artifact reduction algorithm for a wearable photoplethysmography," in *Engineering in Medicine and Biology Society, 2007. EMBS 2007. 29th Annual International Conference of the IEEE*, pp. 1538–1541, 2007.

- [14] R. Yousefi, M. Nourani, S. Ostadabbas, and I. Panahi, "A motion-tolerant adaptive algorithm for wearable photoplethysmographic biosensors," *IEEE journal of biomedical and health informatics*, vol. 18, pp. 670–681, 2014.
- [15] R. Wijshoff, M. Mischi, P. Woerlee, and R. Aarts, "Improving pulse oximetry accuracy by removing motion artifacts from photoplethysmograms using relative sensor motion: A preliminary study," in *Oxygen Transport to Tissue XXXV*, Springer, 2013, pp. 411–417.
- [16] H. Lee, J. Lee, W. Jung, and G. Lee, "The periodic moving average filter for removing motion artifacts from PPG signals," *International journal of control automation and systems*, vol. 5, pp. 701–707, 2007.
- [17] M. R. Ram, K. V. Madhav, E. H. Krishna, K. N. Reddy, and K. A. Reddy, "Adaptive reduction of motion artifacts from PPG signals using a synthetic noise reference signal," in *Biomedical Engineering and Sciences (IECBES), 2010 IEEE EMBS Conference*, pp. 315–319, 2010.
- [18] S. D. Kreibig, "Autonomic nervous system activity in emotion: A review," *Biological psychology*, vol. 84, pp. 394–421, 2010.
- [19] D. McCane, R. L. Hanson, M.-A. Charles, L. T. Jacobsson, D. D. Pettitt, P. H. Bennett, and W. C. Knowler, "Comparison of tests for glycated haemoglobin and fasting and two hour plasma glucose concentrations as diagnostic methods for diabetes," *the British Medical Journal (BMJ)*, vol. 308, pp. 1323–1328, 1994.
- [20] C. Finch, P. Zimmet, and K. Alberti, "Determining diabetes prevalence: a rational basis for the use of fasting plasma glucose concentrations," *Diabetic Medicine*, vol. 7, pp. 603–610, 1990.
- [21] R. L. Hanson, R. G. Nelson, D. R. McCance, J. A. Beart, M. Charles, D. J. Pettitt, and W. C. Knowler, "Comparison of screening tests for non-insulin-dependent diabetes mellitus," *Archives of internal medicine*, vol. 153, pp. 2133–2140, 1993.
- [22] P. Millington, and R. Wilkinson, "Skin. Biological structure and function," *Cambridge University Press, Cambridge*, vol. 5, pp. 351–385, 1983.
- [23] A. Kamal, J. Harness, G. Irving, and A. Mearns, "Skin photoplethysmography—a review," *Computer methods and programs in biomedicine*, vol. 28, pp. 257–269, 1989.
- [24] E. H. Page., "Structure and Function of the Skin," *Skin Disorders, Biology of the Skin*, vol. <http://www.msdmanuals.com/home/skin-disorders/biology-of-the-skin/structure-and-function-of-the-skin> (accessed 07 September 2017).
- [25] T. Tumbar, G. Guasch, V. Greco, C. Blanpain, W. E. Lowry, M. Rendl, and E. Fuchs, "Defining the epithelial stem cell niche in skin," *Science*, vol. 303, pp. 359–363, 2004.
- [26] M. Stückler, A. Struk, P. Altmeyer, M. Herde, H. Baumgärtl, and D. W. Lübbbers, "The cutaneous uptake of atmospheric oxygen contributes significantly to the oxygen supply of human dermis and epidermis," *The Journal of physiology*, vol. 538, pp. 985–994, 2002.
- [27] D. A. Wrone, and N. J. Kwon, "Andrews' diseases of the skin: Clinical dermatology," *Archives of Dermatology*, vol. 137, pp. 518–518, 2001.
- [28] S. D. Puckett, "Select nanofabricated titanium materials for enhancing bone and skin growth of intraosseous transcutaneous amputation prostheses," ProQuest Dissertations And Theses, Brown University, 2009.

- [29] M. Delivoria-Papadopoulos, N. P. Roncevic, and F. A. Oski, "Postnatal changes in oxygen transport of term, premature, and sick infants: the role of red cell 2,3-diphosphoglycerate and adult hemoglobin," *Pediatric Research*, vol. 5, pp. 235–245, 1971.
- [30] M. J. Edwards, and D. A. Rigas, "Electrolyte-labile increase of oxygen affinity during in vivo aging of hemoglobin," *Journal of Clinical Investigation*, vol. 46, pp. 1579–1588, 1967.
- [31] A. Blumberg, and H. R. Marti, "Adaptation to anemia by decreased oxygen affinity of hemoglobin in patients on dialysis," *Kidney international*, vol. 1, pp. 263–270, 1972.
- [32] I. S. Saidi, S. L. Jacques, and F. K. Tittel, "Mie and Rayleigh modeling of visible-light scattering in neonatal skin," *Applied optics*, vol. 34, pp. 7410–7418, 1995.
- [33] A. Bashkatov, E. Genina, V. Kochubey, and V. Tuchin, "Optical properties of human skin, subcutaneous and mucous tissues in the wavelength range from 400 to 2000 nm," *Journal of Physics D: Applied Physics*, vol. 38, pp. 2543–2551, 2005.
- [34] R. R. Anderson, and J. A. Parrish, "The optics of human skin," *Journal of investigative dermatology*, vol. 77, pp. 13–19, 1981.
- [35] T. Lister, P. A. Wright, and P. H. Chappell, "Optical properties of human skin," *Journal of biomedical optics*, vol. 17, pp. 090901-1–0909011-5, 2012.
- [36] T. L. Troy, and S. N. Thennadil, "Optical properties of human skin in the near infrared wavelength range of 1000 to 2200 nm," *Journal of biomedical optics*, vol. 6, pp. 167–176, 2001.
- [37] M. Van Gemert, S. L. Jacques, H. Sterenborg, and W. Star, "Skin optics," *IEEE Transactions on biomedical engineering*, vol. 36, pp. 1146–1154, 1989.
- [38] A. R. Young, "Chromophores in human skin," *Physics in Medicine and Biology*, vol. 42, pp. 789–803, 1997.
- [39] H. Suzuki, N. Kobayashi, T. Nagaoka, K. Iwasaki, M. Umezawa, S. Takeda, and T. Togawa, "Noninvasive measurement of total hemoglobin and hemoglobin derivatives using multiwavelength pulse spectrophotometry-In vitro study with a mock circulatory system," in *Engineering in Medicine and Biology Society, 28th Annual International Conference*, pp. 799–802, 2006.
- [40] T. Harrison, "Structure of the Autonomic Nervous System," *Journal of anatomy*, vol. 125, pp. 205–206, 1978.
- [41] S. Julius, "Autonomic nervous system dysregulation in human hypertension," *The American journal of cardiology*, vol. 67, pp. B3–B7, 1991.
- [42] G. Mancia, and G. Grassi, "The autonomic nervous system and hypertension," *Circulation research*, vol. 114, pp. 1804–1814, 2014.
- [43] Y. Zhang, D. Agnoletti, J. Blacher, and M. E. Safar, "Blood pressure variability in relation to autonomic nervous system dysregulation: the X-CELLENT study," *Hypertension Research*, vol. 35, pp. 399–403, 2012.
- [44] D. Linz, F. Mahfoud, U. Schotten, C. Ukena, H. Neuberger, K. Wirth, and M. Böhm, "Renal Sympathetic Denervation Suppresses Postapneic Blood Pressure Rises and Atrial Fibrillation in a Model for Sleep ApneaNovelty and Significance," *Hypertension*, vol. 60, pp. 172–178, 2012.
- [45] C. Streeter, P. Gerbarg, R. Saper, D. Ciraulo, and R. Brown, "Effects of yoga on the autonomic nervous system, gamma-aminobutyric-acid, and allostasis in

- epilepsy, depression, and post-traumatic stress disorder," *Medical hypotheses*, vol. 78, pp. 571–579, 2012.
- [46] K. Muralikrishnan, B. Balakrishnan, K. Balasubramanian, and F. Visnagarawla, "Measurement of the effect of Isha Yoga on cardiac autonomic nervous system using short-term heart rate variability," *Journal of Ayurveda and Integrative medicine*, vol. 3, pp. 91–96, 2012.
- [47] D. S. Quintana, A. J. Guastella, T. Outhred, I. B. Hickie, and A. H. Kemp, "Heart rate variability is associated with emotion recognition: direct evidence for a relationship between the autonomic nervous system and social cognition," *International Journal of Psychophysiology*, vol. 86, pp. 168–172, 2012.
- [48] G. Tan, T. K. Dao, L. Farmer, R. J. Sutherland, and R. Gevirtz, "Heart rate variability (HRV) and posttraumatic stress disorder (PTSD): a pilot study," *Applied psychophysiology and biofeedback*, vol. 36, pp. 27–35, 2011.
- [49] K. Sasaki, and R. Maruyama, "Consciously controlled breathing decreases the high-frequency component of heart rate variability by inhibiting cardiac parasympathetic nerve activity," *The Tohoku journal of experimental medicine*, vol. 233, pp. 155–163, 2014.
- [50] A. L. Cervi, M. K. Lukewich, and A. E. Lomax, "Neural regulation of gastrointestinal inflammation: role of the sympathetic nervous system," *Autonomic Neuroscience*, vol. 182, pp. 83–88, 2014.
- [51] G. Brusselmans, H. N. Carvalho, E. De Schamphelaere, J. Devulder, and G. Crombez, "Skin temperature during cold pressor test in fibromyalgia: an evaluation of the autonomic nervous system," *Acta Anaesth. Belg*, vol. 66, pp. 19–27, 2015.
- [52] K. M. Alawi, A. A. Aubdool, L. Liang, E. Wilde, A. Vepa, M. Psefteli, S. D. Brain, and J. E. Keeble, "The sympathetic nervous system is controlled by transient receptor potential vanilloid 1 in the regulation of body temperature," *The FASEB Journal*, vol. 29, pp. 4285–4298, 2015.
- [53] M. Watanabe, O. Takano, C. Tomiyama, H. Matsumoto, N. Urahigashi, E. Kainuma, T. Madarame, M. Fukuda, and T. Abo, "The effects of application of an ancient type of acupuncture needle on body temperature, immune function and the autonomic nerve system," *Health*, vol. 4, pp. 775–780, 2012.
- [54] S. W. Porges, and S. A. Furman, "The early development of the autonomic nervous system provides a neural platform for social behaviour: A polyvagal perspective," *Infant and child development*, vol. 20, pp. 106–118, 2011.
- [55] A. Rezai, and M. Ansarinia, "Methods of treating medical conditions by neuromodulation of the sympathetic nervous system," in *US7877146 B2*, Google Patents, 2011.
- [56] G. Messina, V. De Luca, A. Viggiano, A. Ascione, T. Iannaccone, S. Chieffi, and M. Monda, "Autonomic nervous system in the control of energy balance and body weight: personal contributions," in *Neurology research international*, 2013.
- [57] R. W. Levenson, "The autonomic nervous system and emotion," *Emotion Review*, vol. 6, pp. 100–112, 2014.
- [58] A. Vinik, R. Maser, and D. Ziegler, "Autonomic imbalance: prophet of doom or scope for hope," *Diabetic Medicine*, vol. 28, pp. 643–651, 2011.
- [59] Y. Kano, M. Yoshizawa, N. Sugita, M. Abe, N. Homma, A. Tanaka, T. Yamauchi, H. Miura, Y. Shiraishi, and T. Yambe, "Discrimination ability and reproducibility of a new index reflecting autonomic nervous function based on

- pulsatile amplitude of photoplethysmography," in *Engineering in Medicine and Biology Society (EMBC), 36th Annual International Conference*, pp. 1794–1800, 2014.
- [60] Q. Liu, B. P. Yan, C. Yu, Y. Zhang, and C. C. Poon, "Attenuation of systolic blood pressure and pulse transit time hysteresis during exercise and recovery in cardiovascular patients," *IEEE Transactions on Biomedical Engineering*, vol. 61, pp. 346–352, 2014.
  - [61] S. Chen, and S. Chao, "Compressed sensing technology-based spectral estimation of heart rate variability using the integral pulse frequency modulation model," *IEEE journal of biomedical and health informatics*, vol. 18, pp. 1081–1090, 2014.
  - [62] G. Parati, and M. Esler, "The human sympathetic nervous system: its relevance in hypertension and heart failure," *European heart journal*, vol. 33, pp. 1058–1066, 2012.
  - [63] B. Pomeranz, R. Macaulay, M. A. Caudill, I. Kutz, D. Adam, D. Gordon, K. M. Kilborn, A. C. Barger, D. C. Shannon, and R. J. Cohen, "Assessment of autonomic function in humans by heart rate spectral analysis," *American Journal of Physiology-Heart and Circulatory Physiology*, vol. 248, pp. H151–H153, 1985.
  - [64] M. Nitzan, A. Babchenko, B. Khanokh, and D. Landau, "The variability of the photoplethysmographic signal—a potential method for the evaluation of the autonomic nervous system," *Physiological measurement*, vol. 19, pp. 93–102, 1998.
  - [65] B. Gal-on, I. Brown, and A. Nunn, "Monitoring and assessment of cardiovascular regulation in spinal cord injured patients," in *Engineering in Medicine and Biology Society*, pp. 6859–6862, 2006.
  - [66] N. Selvaraj, J. Santhosh, and S. Anand, "Feasibility of photoplethysmographic signal for assessment of autonomic response using heart rate variability analysis," in *3rd Kuala Lumpur International Conference on Biomedical Engineering*, pp. 391–395, 2007.
  - [67] M. Nitzan, A. Babchenko, D. Shemesh, and J. Alberton, "Influence of thoracic sympathectomy on cardiac induced oscillations in tissue blood volume," *Medical and Biological Engineering and Computing*, vol. 39, pp. 579–583, 2001.
  - [68] T. Tamura, Y. Maeda, M. Sekine, and M. Yoshida, "Wearable photoplethysmographic sensors—past and present," *Electronics*, vol. 3, pp. 282–302, 2014.
  - [69] I. Korhonen, and A. Ylihankala, "Photoplethysmography and nociception," *Acta Anaesthesiologica Scandinavica*, vol. 53, pp. 975–985, 2009.
  - [70] C. F. Bohren, and D. R. Huffman, "Absorption and scattering of light by small particles", *John Wiley & Sons, ISBN 9780471293408*, 2008.
  - [71] F. A. Jenkins, and H. E. White, "Fundamentals of optics", *Tata McGraw-Hill Education, ISBN 9789333183383*, 1957.
  - [72] U. Timm, E. Lewis, G. Leen, D. McGrath, J. Krahl, and H. Ewald, "Non-invasive continuous online hemoglobin monitoring system," in *Sensors Applications Symposium (SAS), 2010 IEEE*, pp. 131–134, 2010.

- [73] U. Timm, D. McGrath, E. Lewis, J. Kraitl, and H. Ewald, "Sensor system for non-invasive optical hemoglobin determination," in *Sensors*, pp. 1975–1978, 2009.
- [74] J. G. Webster, "Design of pulse oximeters", *CRC Press, ISBN 9780750304672*, 1997.
- [75] D. Sardar, and L. Levy, "Optical properties of whole blood," *Lasers in medical science*, vol. 13, pp. 106-111, 1998.
- [76] J. R. Lakowicz, K. W. Berndt, and M. L. Johnson, "Photon migration in scattering media and tissue," *Time-Resolved Laser Spectroscopy in Biochemistry II*, vol. 1204, pp. 468-480, 1990.
- [77] U. Timm, "Non-invasive haemoglobin monitoring by an LED based optical sensor system," Doctoral Thesis, University of Limerick, 2011.
- [78] A. M. Smith, M. C. Mancini, and S. Nie, "Second window for in vivo imaging," *Nature nanotechnology*, vol. 4, pp. 710–719, 2009.
- [79] A. Sangiovanni-Vincentelli, and M. Di Natale, "Embedded system design for automotive applications," *Computer*, vol. 40, 2007.
- [80] "MSP430F15x, MSP430F16x, MSP430F161x," Texas Instruments, <http://www.ti.com/lit/ds/symlink/msp430f1611.pdf> (accessed 07 September 2017).
- [81] "3-Axis,  $\pm 2$  g/ $\pm 4$  g/ $\pm 8$  g/ $\pm 16$  g Digital Accelerometer," Analog Devices, <http://www.analog.com/media/en/technical-documentation/data-sheets/ADXL345-EP.pdf> (accessed 07 September 2017).
- [82] R. E. Mayagoitia, A. V. Nene, and P. H. Veltink, "Accelerometer and rate gyroscope measurement of kinematics: an inexpensive alternative to optical motion analysis systems," *Journal of biomechanics*, vol. 35, pp. 537–542, 2002.
- [83] A. FornerCordero, M. MateuArce, I. FornerCordero, E. Alcántara, J. Moreno, and J. Pons, "Study of the motion artefacts of skin-mounted inertial sensors under different attachment conditions," *Physiological measurement*, vol. 29, pp. N21–N31, 2008.
- [84] V. Skelton, N. Wijayasinghe, S. Sharafudeen, A. Sange, N. Parry, and C. Junghans, "Evaluation of point-of-care haemoglobin measuring devices: a comparison of Radical-7™ pulse co-oximetry, HemoCue® and laboratory haemoglobin measurements in obstetric patients," *Anaesthesia*, vol. 68, pp. 40–45, 2013.
- [85] R. D. Miller, T. A. Ward, S. C. Shibuski, and N. H. Cohen, "A comparison of three methods of hemoglobin monitoring in patients undergoing spine surgery," *Anesthesia & Analgesia*, vol. 112, pp. 858–863, 2011.
- [86] M. W. Causey, S. Miller, A. Foster, A. Beekley, D. Zenger, and M. Martin, "Validation of noninvasive hemoglobin measurements using the Masimo Radical-7 SpHb Station," *The American journal of surgery*, vol. 201, pp. 592–598, 2011.
- [87] M. R. Macknet, M. Allard, R. L. Applegate, and J. Rook, "The accuracy of noninvasive and continuous total hemoglobin measurement by pulse CO-Oximetry in human subjects undergoing hemodilution," *Anesthesia & Analgesia*, vol. 111, pp. 1424–1426, 2010.
- [88] G. J. Kost, and N. K. Tran, "Continuous noninvasive hemoglobin monitoring: the standard of care and future impact," *Critical care medicine*, vol. 39, pp. 2369–2371, 2011.

- [89] M. J. Kim, Q. Park, M. H. Kim, J. W. Shin, and H. O. Kim, "Comparison of the accuracy of noninvasive hemoglobin sensor (NBM-200) and portable hemoglobinometer (HemoCue) with an automated hematology analyzer (LH500) in blood donor screening," *Annals of laboratory medicine*, vol. 33, pp. 261–267, 2013.
- [90] A. Belardinelli, M. Benni, P. Tazzari, and P. Pagliaro, "Noninvasive methods for haemoglobin screening in prospective blood donors," *Vox sanguinis*, vol. 105, pp. 116–120, 2013.
- [91] E. Hadar, O. Raban, T. Bouganim, K. TenenbaumGavish, and M. Hod, "Precision and accuracy of noninvasive hemoglobin measurements during pregnancy," *The Journal of Maternal-Fetal & Neonatal Medicine*, vol. 25, pp. 2503–2506, 2012.
- [92] A. A. Awad, M. A. M. Ghobashy, W. Ouda, R. G. Stout, D. G. Silverman, and K. H. Shelley, "Different responses of ear and finger pulse oximeter wave form to cold pressor test," *Anesthesia & Analgesia*, vol. 92, pp. 1483–1486, 2001.
- [93] J. Spigulis, R. Erts, V. Nikiforovs, and E. Kviesis-Kipge, "Wearable wireless photoplethysmography sensors," in *Proc. SPIE*, p. 69912O, 2008.
- [94] P. D. Mannheimer, "The Physio-optics of Pulse Oximetry: Numerical Modeling and Clinical Experience," Doctoral Thesis, University of Luebeck, 2003.
- [95] "Finapres NOVA," Finapres Medical Systems, Netherlands, <http://www.finapres.com/Products/Finapres-NOVA> (accessed 07 September 2017).
- [96] "Upper arm blood pressure monitor," Philips, Amsterdam, Netherlands, <https://www.usa.philips.com/c-m-hs/health-programs/upper-arm-blood-pressure-monitor> (accessed 07 September 2017).
- [97] E. Dewhirst, A. Naguib, P. Winch, J. Rice, M. Galantowicz, P. McConnell, and J. D. Tobias, "Accuracy of noninvasive and continuous hemoglobin measurement by pulse co-oximetry during preoperative phlebotomy," *Journal of intensive care medicine*, vol. 29, pp. 238–242, 2014.
- [98] S. Blumenthal, D. K. Kakaty, M. Marquardt, B. Beck-Schimmer, and A. Borgeat, "Clinical Validation of the Hemocue Plasma Low Hemoglobin Photometer-System," *Anesthesiology*, vol. 105, pp. A248–A252, 2006.
- [99] H. Gehring, C. Hornberger, L. Dibbelt, A. Roth-Isigkeit, K. Gerlach, J. Schumacher, and P. Schmucker, "Accuracy of point-of-care-testing (POCT) for determining hemoglobin concentrations," *Acta Anaesthesiologica Scandinavica*, vol. 46, pp. 980–986, 2002.
- [100] D. S. Prough, Y. E. Petrov, M. H. Klasing, M. Motamedi, and R. O. Esenaliev, "Continuous noninvasive optoacoustic monitoring of hemoglobin concentration: in vitro validation," *Anesthesiology*, vol. 95, pp. A555–A559, 2001.
- [101] W. Secomski, A. Nowicki, F. Guidi, P. Tortoli, and P. A. Lewin, "Noninvasive in vivo measurements of hematocrit," *Journal of ultrasound in medicine*, vol. 22, pp. 375–384, 2003.
- [102] U. Timm, G. Leen, E. Lewis, D. McGrath, J. Kraitl, and H. Ewald, "Non-invasive optical real-time measurement of total hemoglobin content," *Procedia Engineering*, vol. 5, pp. 488–491, 2010.
- [103] T. Matsumoto, T. Ushiroyama, and N. Tatsumi, "Lower peripheral circulation in eumenorrheic young women with premenstrual symptoms," *BioPsychoSocial medicine*, vol. 1, pp. 8–16, 2007.

- [104] U. Timm, E. Lewis, D. McGrath, J. Kraitl, and H. Ewald, "Sensor System Concept for Non-Invasive Blood Diagnosis," *Procedia Chemistry*, vol. 1, pp. 493–496, 2009.
- [105] W. B. Freire, "Strategies of the Pan American Health Organization World Health Organization for the Control of Iron Deficiency in Latin America," *Nutrition reviews*, vol. 55, pp. 183–188, 1997.
- [106] L. Lamhaut, R. Apriotesei, X. Combes, M. Lejay, P. Carli, and B. Vivien, "Comparison of the accuracy of noninvasive hemoglobin monitoring by spectrophotometry (SpHb) and HemoCue® with automated laboratory hemoglobin measurement," *The Journal of the American Society of Anesthesiologists*, vol. 115, pp. 548–554, 2011.
- [107] J. Kraitl, and H. Ewald, "Optical non-invasive methods for characterization of the human health status," in *1st International Conference on Sensing Technology*, pp. 466–470, 2005.
- [108] J. Kraitl, D. Klinger, D. Fricke, U. Timm, and H. Ewald, "Non-invasive measurement of blood components," in *Advancement in Sensing Technology*, Springer, 2013, pp. 237–262.
- [109] D. Meredith, D. Clifton, P. Charlton, J. Brooks, C. Pugh, and L. Tarassenko, "Photoplethysmographic derivation of respiratory rate: a review of relevant physiology," *Journal of medical engineering & technology*, vol. 36, pp. 1–7, 2012.
- [110] J. Nemes, and J. Eftis, "Several features of a viscoplastic study of plate-impact spallation with multidimensional strain," *Computers & Structures*, vol. 38, pp. 317–328, 1991.
- [111] E. Gayat, J. Aulagnier, E. Mattheiu, M. Boisson, and M. Fischler, "Non-invasive measurement of hemoglobin: assessment of two different point-of-care technologies," *PloS one*, vol. 7, pp. e30065–e30072, 2012.
- [112] Y. Park, J. Lee, H. Song, H. Byon, H. Kim, and J. Kim, "The accuracy of noninvasive hemoglobin monitoring using the radical-7 pulse CO-Oximeter in children undergoing neurosurgery," *Anesthesia & Analgesia*, vol. 115, pp. 1302–1307, 2012.
- [113] L. Berkow, S. Rotolo, and E. Mirski, "Continuous noninvasive hemoglobin monitoring during complex spine surgery," *Anesthesia & Analgesia*, vol. 113, pp. 1396–1402, 2011.
- [114] Y. Yan, C. C. Poon, and Y. Zhang, "Reduction of motion artifact in pulse oximetry by smoothed pseudo Wigner-Ville distribution," *Journal of NeuroEngineering and Rehabilitation*, vol. 2, pp. 3–11, 2005.
- [115] T. Fu, S. Liu, and K. Tang, "Heart rate extraction from photoplethysmogram waveform using wavelet multi-resolution analysis," *Journal of medical and biological engineering*, vol. 28, pp. 229–232, 2008.
- [116] M. T. Petterson, V. L. Begnoche, and J. M. Graybeal, "The effect of motion on pulse oximetry and its clinical significance," *Anesthesia & Analgesia*, vol. 105, pp. S78–S84, 2007.
- [117] N. V. Thakor, and Y. Zhu, "Applications of adaptive filtering to ECG analysis: noise cancellation and arrhythmia detection," *IEEE transactions on biomedical engineering*, vol. 38, pp. 785–794, 1991.

- [118] L. B. Wood, "Motion artifact reduction for wearable photoplethysmogram sensors using micro accelerometers and Laguerre series adaptive filters," Thesis, Massachusetts Institute of Technology, 2008.
- [119] Y. Yan, and Y. Zhang, "An efficient motion-resistant method for wearable pulse oximeter," *IEEE Transactions on information technology in biomedicine*, vol. 12, pp. 399–405, 2008.
- [120] Y. Chen, G. Zhang, S. Gan, and C. Zhang, "Enhancing seismic reflections using empirical mode decomposition in the flattened domain," *Journal of Applied Geophysics*, vol. 119, pp. 99–105, 2015.
- [121] Y. Chen, "Dip-separated structural filtering using seislet transform and adaptive empirical mode decomposition based dip filter," *Geophysical Journal International*, vol. 206, pp. 457–469, 2016.
- [122] N. E. Huang, Z. Shen, S. R. Long, M. C. Wu, H. H. Shih, Q. Zheng, N.-C. Yen, C. C. Tung, and H. H. Liu, "The empirical mode decomposition and the Hilbert spectrum for nonlinear and non-stationary time series analysis," in *Proceedings of the Royal Society of London A: Mathematical, Physical and Engineering Sciences*, pp. 903–995, 1998.
- [123] W. C. Chu, H. Chao, and S. J. Yang, "Intelligent Systems and Applications: Proceedings of the International Computer Symposium (ICS) ". Taichung, Taiwan, *IOS Press, ISBN 978-1-61499-483-1* 2015.
- [124] K. Lin, D. Chen, and S. Lee, "A robust vision-based heart rate evaluation," *Frontiers in Artificial Intelligence and Applications*, vol. 274, pp. 1052-1061, 2015.
- [125] S. Qin, and Y. M. Zhong, "A new envelope algorithm of Hilbert–Huang transform," *Mechanical Systems and Signal Processing*, vol. 20, pp. 1941–1952, 2006.
- [126] S. McKinley, and M. Levine, "Cubic spline interpolation," *College of the Redwoods*, vol. 45, pp. 1049–1060, 1998.
- [127] H. Akima, "A new method of interpolation and smooth curve fitting based on local procedures," *Journal of the ACM (JACM)*, vol. 17, pp. 589–602, 1970.
- [128] "Signal Processing, Algorithm (Envelope)," OriginLab, <http://www.originlab.com/doc/Origin-Help/Envelope-Algorithm> (accessed 07 September 2017).
- [129] X. Teng, and Y. Zhang, "The effect of contacting force on photoplethysmographic signals," *Physiological measurement*, vol. 25, pp. 1323–1329, 2004.
- [130] "FT232R USB UART IC Datasheet," FTFI Chip, [http://www.ftdichip.com/Support/Documents/DataSheets/ICs/DS\\_FT232R.pdf](http://www.ftdichip.com/Support/Documents/DataSheets/ICs/DS_FT232R.pdf) [http://www.ftdichip.com/Support/Documents/DataSheets/ICs/DS\\_FT232R.pdf](http://www.ftdichip.com/Support/Documents/DataSheets/ICs/DS_FT232R.pdf) (accessed 07 September 2017).
- [131] "ADP3338, Low Dropout Regulator," Analog Device, <http://www.analog.com/media/en/technical-documentation/data-sheets/ADP3338.pdf> (accessed 07 September 2017)
- [132] J. Allen, J. R. Frame, and A. Murray, "Microvascular blood flow and skin temperature changes in the fingers following a deep inspiratory gasp," *Physiological measurement*, vol. 23, pp. 365–371, 2002.
- [133] T. G. Pickering, J. E. Hall, L. J. Appel, B. E. Falkner, J. Graves, M. N. Hill, D. W. Jones, T. Kurtz, S. G. Sheps, and E. J. Roccella, "Recommendations for

- blood pressure measurement in humans and experimental animals," *Circulation*, vol. 111, pp. 697–716, 2005.
- [134] P. L. Mitchell, R. W. Parlin, and H. Blackburn, "Effect of vertical displacement of the arm on indirect blood-pressure measurement," *New England Journal of Medicine*, vol. 271, pp. 72–74, 1964.
- [135] H. T. Tran, "Blood pressure and blood flow variation during postural change from sitting to standing: model development and validation," in *Scientific Computing Nanjing*, pp. 58–63, 2005.
- [136] Y. Avnon, M. Nitzan, E. Sprecher, Z. Rogowski, and D. Yarnitsky, "Different patterns of parasympathetic activation in uni-and bilateral migraineurs," *Brain*, vol. 126, pp. 1660–1670, 2003.
- [137] M. Elgendi, "On the analysis of fingertip photoplethysmogram signals," *Current cardiology reviews*, vol. 8, pp. 14–25, 2012.
- [138] E. Gil, M. Orini, R. Bailón, J. Vergara, L. Mainardi, and P. Laguna, "Photoplethysmography pulse rate variability as a surrogate measurement of heart rate variability during non-stationary conditions," *Physiological measurement*, vol. 31, pp. 1271–1279, 2010.
- [139] S. Bagha, and L. Shaw, "A real time analysis of PPG signal for measurement of SpO<sub>2</sub> and pulse rate," *International journal of computer applications*, vol. 36, pp. 45–50, 2011.
- [140] P. Choudhari, M. Panse, R. Chopade, and S. Phad, "Removal of Baseline Wander from Physiological Signals Using Wavelet Transform," in *Emerging Research in Computing, Information, Communication and Applications*, Springer, 2016, pp. 225–234.
- [141] H. Yuan, S. Poeggel, T. Newe, E. Lewis, C. Viphavakit, and G. Leen, "An Experimental Study of the Effects of External Physiological Parameters on the Photoplethysmography Signals in the Context of Local Blood Pressure (Hydrostatic Pressure Changes)," *Sensors*, vol. 17, pp. 556–572, 2017.
- [142] Q. Wang, P. Yang, and Y. Zhang, "Artifact reduction based on Empirical Mode Decomposition (EMD) in photoplethysmography for pulse rate detection," in *2010 Annual International Conference of the IEEE Engineering in Medicine and Biology*, pp. 959–962, 2010.
- [143] K. V. Madhav, M. R. Ram, E. H. Krishna, N. R. Komalla, and K. A. Reddy, "Estimation of respiration rate from ECG, BP and PPG signals using empirical mode decomposition," in *Instrumentation and Measurement Technology Conference (I2MTC)*, pp. 1–4, 2011.
- [144] A. Garde, W. Karlen, P. Dehkordi, J. Ansermino, and G. Dumont, "Empirical mode decomposition for respiratory and heart rate estimation from the photoplethysmogram," in *Computing in Cardiology Conference (CinC)*, pp. 799–802, 2013.
- [145] Y. Lin, C. Liu, A. Liu, C. Yang, and H. Wu, "PPG Signal Processing with Ensemble Empirical Mode Decomposition for Small Animals," in *Proceedings of the Second APSIPA Annual Summit and Conference*, pp. 568–571, 2010.
- [146] P. Santos, V. Almeida, J. Cardoso, and C. Correia, "Photoplethysmographic logger with contact force and hydrostatic pressure monitoring," in *Bioengineering, 2013 IEEE 3rd Portuguese Meeting*, pp. 1–6, 2013.

# **Appendix A:**

## **Publications Arising from This Work**

H. Yuan, S. Poeggel, T. Newe, E. Lewis, C. Viphavakit, and G. Leen. An Experimental Study of the Effects of External Physiological Parameters on the Photoplethysmography Signals in the Context of Local Blood Pressure (Hydrostatic Pressure Changes). *Sensors*, 2017.

A comprehensive study of the effect of a wide range of controlled human subject motion on Photoplethysmography signals is reported. The investigation includes testing of two separate groups of 5 and 18 subjects who were requested to undertake set exercises whilst simultaneously monitoring a wide range of physiological parameters including Breathing Rate, Heart Rate and Localised Blood Pressure using commercial clinical sensing systems. Devices such as an accelerometer, a respiration monitor belt and a blood pressure monitor, have been deployed in conjunction with the custom designed PPG sensor system for investigation of the effects of external physiological parameters on the PPG signals in the context of autonomic nervous system and local blood pressure. The results have shown that the baseline of PPG signal is affected by acceleration particularly in the vertical direction as opposed to acceleration in the horizontal plane for the system under test. Experimental results demonstrated that PPG signals during motion events are influenced by the variation of local blood pressure at the point of measurement which is in turn induced from: (1) the VHD between the measuring site and the reference level(the heart level); and (2) the autonomic nervous system. The results of a statistical analysis conducted on 18 subjects (9 male and 9 female) have shown that the dependency of the Baseline (BL) and Amplitude (AM) values of the PPG signal are only weakly dependent on the VHD. It is envisaged that the results of this investigation can be used as a basis for optimizing measurements of PPG based sensors in terms of potential removal of motion artefact.

H. Yuan, S.F. Memon, T. Newe, E. Lewis, G. Leen. Motion Artefact Minimization from Photoplethysmography based Non-invasive Hemoglobin Sensor Based on an Envelope Filtering Algorithm. *Measurement*, 115 (2018) 288–298.

Devices including an accelerometer and a respiration monitor belt have been deployed in conjunction with the custom designed PPG sensor system for investigation of the Hb coefficients from PPG signals in the context of both static and non-static states. An envelope-filtered method of enhancement of non-invasive Hb monitoring is described. Five randomly selected healthy subjects were requested to undertake motion based exercises including talking, arm swinging and walking whilst wearing the PPG sensor probe. Results demonstrate that the Hb coefficient, based on the novel envelope method filtered PPG, has a superior performance on minimisation of the motion artefact than that from band-pass filtered PPG data in both stationary and non-stationary states. As a hemodynamic pressure variation near the sensor probe is induced from VHD between the finger sensor probe and the heart level, study results show that Hb coefficients from proposed method filtered PPG signals are also capable of minimisation VHD variation similar to traditional band pass filter method.

H. Yuan, G. Leen, and E. Lewis. Effects of autonomic nervous system on the quality of non-invasive blood diagnosis by PPG-based sensor system. *In Proceedings of the 2015 11th Conference on Ph.D. Research in Microelectronics and Electronics (PRIME)*, 2015.

The collection of photoplethysmography (PPG) signals from optical based sensor probe has been used extensively for the monitoring of heart rate (HR), respiration rate and Oxygen Saturation ( $\text{SpO}_2$ ). Prior research by the Optical Fibre Sensor Research Group has extended the information provided by PPG based devices from monitoring HR and  $\text{SpO}_2$  to include total Hb. In this paper research relating to the effects of ANS on the quality of PPG signals has been described. Results shows that baseline PPG values are severely affected by ANS variation induced from physiological events, such as yawning, coughing, and so on.  $\text{SpO}_2$ , HR and Hb are strongly affected by ANS events, arising from either movement of the body position or other physiological events.  $\text{SpO}_2$ , HR and Hb tend to increase as a result of ANS responses to body movement or physiological events and this should be considered in the application of PPG based sensor devices.

H. Yuan, D. Meere, G. Leen, and E. Lewis. A wireless, body-worn non-invasive device for measuring biometric parameters such as total haemoglobin concentration. *University Hospital Limerick (UHL) Research Symposium*, 2013.

The real-time evaluation of a patient's physiological condition is essential, not only during or after surgery, but also for on-going daily patient care. The current standard for haemoglobin (Hb) concentration determination requires invasive methods. Similar to non-invasive Oxygen Saturation ( $\text{SpO}_2$ ) monitoring, non-invasive Hb measuring is also an application of Photoplethysmography (PPG). PPG is based on the property that the spectral absorption of haemoglobin derivatives and  $\text{H}_2\text{O}$  are different in the visible and infrared wavelength ranges. Through the analysis of the level to which these wavelengths are absorbed whilst passing through a patient's tissue, the patient's diagnostic parameters, such as  $\text{SpO}_2$ , total Hb and pulse rate can be determined. This paper reports on research to help improve the accuracy of the Hb measurement when the patient is moving (e.g., movement artefact), through the use of accelerometers and research to implement the measurement probe using fibre optics, so that the measurement probe itself is immune to electromagnetic fields and therefore usable while the patient is having an MRI or CT scan. The developed Hb measurement device has undergone calibration testing to evaluate its effectiveness, and has shown good performance when compared with traditional invasive methods.

# Appendix B:

## MCU Code

```
//Title: 4 LED Control 13_01_2014

#include <msp430x16x.h>
#include <stdint.h>

#define ADXL_INT2    BIT3      // P2.3
#define ADXL_INT1    BIT5      // P2.5
#define ADXL_CS     BIT4      // P5.4
#define ADXL_CLK     BIT2      // P3.1
#define ADXL_MOSI    BIT3      // P4.3
#define ADXL_MISO    BIT0      // P5.0

/********************* Data type definition ********************/
#define UINT8     unsigned char
#define UINT16    unsigned int
#define INT16     signed int
#define uchar     unsigned char
#define uint      unsigned short
#define BOOL      unsigned char

#define TRUE      1
#define FALSE     0

/********************* ADXL345 Device register definition ********************/
#define DEVID     0x00          // Device ID
#define THRESH_TAP 0x1D          // Tap Threshold
#define OFSX_ADDR 0x1E          // X-axis offset
#define OFSY_ADDR 0x1F          // Y-axis offset
#define OFSZ_ADDR 0x20          // Z offset
#define DUR_ADDR   0x21          // percussion duration
#define LATENT_ADDR 0x22         // Tap delay
#define WINDOW_ADDR 0x23         // Tap on the window
#define THRESH_ACT_ADDR 0x24     // activity threshold
#define THRESH_INACT_ADDR 0x25   // Standstill threshold
#define TIME_INACT_ADDR 0x26     // Quiet time
#define ACT_INACT_CTL_ADDR 0x27  // Axis enable activity and inactivity detection
#define THRESH_FF_ADDR 0x28       // free fall threshold
#define TIME_FF_ADDR 0x29        // free fall time
#define TAP_AXES_ADDR 0x2A        // Click or double-click on the axis control
#define ACT_TAP_STATUS_ADDR 0x2B // Click or double-click the source
#define BW_RATE_ADDR 0x2C        // Data rate and power mode control
#define POWER_CTL_ADDR 0x2D      // Power saving feature control
```

```

#define INT_ENABLE_ADDR 0x2E      // Interrupt enable control
#define INT_MAP_ADDR 0x2F        // interrupt mapping control
#define INT_SOURCE_ADDR 0x30     // Interrupt source
#define DATA_FORMAT_ADDR 0x31    // Data format control
#define DATA_X0_ADDR 0x32        // X axis data 0
#define DATA_X1_ADDR 0x33        // X-axis data 1
#define DATA_Y0_ADDR 0x34        // Y-axis data 0
#define DATA_Y1_ADDR 0x35        // Y-axis data 1
#define DATA_Z0_ADDR 0x36        // Z-axis data 0
#define DATA_Z1_ADDR 0x37        // Z-axis data 1
#define FIFO_CTL_ADDR 0x38       // FIFO control
#define FIFO_STATUS_ADDR 0x39    // FIFO status

#include "ADXL_DEFS.H"

/********************* Function definition ********************/
void InitSimSPI(void);
void Init_ADXL345(void);
void udelay(UINT8 i);
void WriteADXL(UINT8 addr, UINT8 data);
UINT8 Single_ReadADXL(UINT8 addr);
void Multi_ReadADXL(UINT8 start_addr, UINT8 p[][6], int Cnt);
void ADXL345_ReadXYZ(int *XAx, int *YAx, int *ZAx);
int16_t ADXL345_GetAxis(UINT8 Address);

#define ADDRLENGTH 8
#define DATALENGTH 8
#define DeviceID 0xE5
#define SetADXL_TriggerMode()

void init_Clock(void);
void timera_init(void);
void timerb_init(void);
void mittel(void);
void init_DAC(void);
void init_SIO(void);
void init_ADC(void);

#define BUFFERSIZE 10
int BUFF_COUNTER = 0;
int16_t ADC_DATA;
unsigned short TimerAFlag = 0;
int16_t BUFF_X[BUFFERSIZE], BUFF_Y[BUFFERSIZE], BUFF_Z[BUFFERSIZE];

unsigned int val_DAC1 = 0X670; // for LED 1
unsigned int val_DAC3 = 0X870; // for LED 3
unsigned int val_DAC5 = 0X720; // for LED 5
unsigned int val_DAC7 = 0Xfff; // for LED 7

int16_t ADC_DATA;
volatile int ADC_val1 = 0; // for LED 1
volatile int ADC_val3 = 0; // for LED 3
volatile int ADC_val5 = 0; // for LED 5
volatile int ADC_val7 = 0; // for LED 7

long temp;
volatile int n_ta = 0; // Timer A overflow counter variable.

```

```

volatile char flag_adjust_DAC=0; // Flag to modify DAC in main.
volatile int n_tb = 0;
volatile int n_led = 0;
volatile char n_mw = 0;
volatile int off_br = 20;
volatile int NR_REF_LOW1 = 1900;
volatile long Sum;
volatile long Sum2;
volatile long Dark;
volatile long NR_UPDATE_DAC;
volatile char Digits[4];
volatile int *ptr_mw0;
volatile int *ptr_mw1;
volatile int *ptr_mw2;
volatile int *ptr_mw;
volatile int mw = 0;
volatile int mw0 = 0;
volatile int mw1 = 0;
volatile int mw2 = 0;
volatile long value;
volatile int n_send = 0;
#define NR_MEASUREMENTS 6 // NO READINGS
#define NR_REF_LOW 1900 // Low ref value 1.2 V(1920)
#define NR_REF_HIGH 2900 // High ref value 1.8 V(2900)

unsigned int Readings[NR_MEASUREMENTS]; //readings
unsigned int Readings2[ NR_MEASUREMENTS ];

volatile int adjust_DAC(volatile int average_ADC_val,unsigned int val_DAC)
{
    // Check whether Average_ADC_Val value is within range
    if ((average_ADC_val > 0)&& (average_ADC_val< 4096))
    {
        switch(n_led)
        {
            case 1:off_br = 1; break;
            case 3:off_br = 1; break;
            case 5:off_br = 1; break;
            case 7:off_br = 100; break;
        }
        switch(n_led)
        {
            default:NR_REF_LOW1=1900; break;
            case 7:NR_REF_LOW1=2400; break;
        }
        //If average_ADC_val is less than lower reference, then DAC
valued is increased by fixed value of off_br
        if (average_ADC_val < NR_REF_LOW )
        {
            if(average_ADC_val < 1000)
            { switch(n_led)
            {
                case 1:off_br = 50; break;
                case 3:off_br = 150; break;
                case 5:off_br = 150; break;
                case 7:off_br = 500; break;
            }

```

```

        if(average_ADC_val > 3050)
switch(n_led)
{
    case 1:off_br = 8; break;
    case 3:off_br = 20; break;
    case 5:off_br = 10; break;
    case 7:off_br = 500; break;
}

val_DAC = val_DAC + off_br ;

if (val_DAC >= 4095)
{
    val_DAC = 4095;
}
if (val_DAC <= 700)
{
    val_DAC = 650;
}
NR_UPDATE_DAC = 500;

}
else
{NR_UPDATE_DAC = 2000;}
//If average_ADC_val is greater than upper refference, then
DAC valued is decreased by fixed value of off_br
if(average_ADC_val > NR_REF_HIGH)
{
    val_DAC = val_DAC - off_br;
}
return(val_DAC);
}

void UART_transmit (unsigned char Transmit_Data) //UART0 Transmit
Subroutine
{
    while (!(IFG1 & UTXIFG0));                                //Wait for
ready U0TXBUF
    U0TXBUF = Transmit_Data;                                    //send data
}

void SendAccDataSerial(int16_t Axis_X, int16_t Axis_Y, int16_t Axis_Z)
{
    UART_transmit('0');
    UART_transmit(',');
    UART_transmit(Axis_X >> 8);
    UART_transmit(Axis_X);
    UART_transmit(',');
    UART_transmit(Axis_Y >> 8);
    UART_transmit(Axis_Y);
    UART_transmit(',');
    UART_transmit(Axis_Z >> 8);
}

```

```

        UART_transmit(Axis_Z);
        UART_transmit(',');
        UART_transmit('0');
        UART_transmit(',');
    }

void InitSimSPI()
{
    P2SEL &= ~(ADXL_INT2 + ADXL_INT1);
    P5SEL &= (ADXL_CS + ADXL_MISO);
    P3SEL &= ~ADXL_CLK;
    P4SEL &= ~ADXL_MOSI;

    P2DIR &= ~(ADXL_INT1 + ADXL_INT2);
    P5DIR |= ADXL_CS;
    P3DIR |= ADXL_CLK;
    P4DIR |= ADXL_MOSI;
    P5DIR &= ~ADXL_MISO;

    P2IES &= ~(ADXL_INT1 + ADXL_INT2);
    P2IE |= ADXL_INT1 + ADXL_INT2;
    P2IFG &= 0;
}

int main(void)
{
    WDTCTL=WDTPW+WDTHOLD;      // Stop watchdog timer
    ptr_mw = &mw;
    ptr_mw0 = &mw0;
    ptr_mw1 = &mw1;
    ptr_mw2 = &mw2;

    P1SEL = 0x00;              //Std.IO
    P1DIR = 0xFF;               //all outputs
    P1OUT = 0x00;               //at startup all outputs off

    P2SEL = 0x00;              //Std.IO
    P2DIR = 0xFF;

    P3SEL = 0x30;              // P3.4,5 = USART0 TXD/RXD
    P3DIR = 0xFF;

    P4SEL = 0x00;
    P4DIR = 0xFF;

    P5SEL = 0x00;              //Std.IO
    P5DIR = 0xFF;
    P5DIR |= BIT5;             //pin 5.5

    P6SEL = 0xFF;               //Peripheral Modul Function (ADC12)
    P6DIR = 0xC0;               //P6.3 OPA input, P6.5 Raw input,
                                //P6.6 DAC0 Opa ctrl output, P6.7

DAC1 LED output

    init_Clock();
    InitSimSPI();
}

```

```

timera_init();
timerb_init();
init_DAC();
init_ADC();
init_SIO();
Init_ADXL345();

NR_UPDATE_DAC=600;
ADC12IE = 0x0001;
IE1 &= ~UTXIE0;      //SIO0 TX-Int release

TACTL |= MC_1;           //Timer_A start: Timer A mode
control: 1 - Up to CCR0
TACCTL0 = CCIE | TACLR; //Timer A C/C Int Enable (for TACCR0): Enable
Capture/Compare Interrupt
TBCCTL0 = CCIE| TBCLR;
//Tiemr_B C/C Int Enable (for TBCCR0)
_BIS_SR(GIE);
//GIE = 1, globale Interrupt Enable: #define GIE      (0x0008u)

for(;;)      //Endless loop - waiting for interrupts
{
    // Waiting for DAC_Update Counter to overflow.
    if(flag_adjust_DAC == 1)
    {
flag_adjust_DAC = 0;
//Reset adjust flag
val_DAC1 = adjust_DAC(ADC_val1,val_DAC1);
// Adjustment for LED 1
val_DAC3 = adjust_DAC(ADC_val3,val_DAC3);
// Adjustment for LED 3
val_DAC5 = adjust_DAC(ADC_val5,val_DAC5);
// Adjustment for LED 5
val_DAC7 = adjust_DAC(ADC_val7,val_DAC7);
// Adjustment for LED 5
    }
}

void write_DAC0(unsigned int val_DAC)
{
    DAC12_0DAT = val_DAC;
}
void write_DAC1(unsigned int val_DAC2)
{
    DAC12_1DAT = val_DAC2;
}

void init_Clock( void )
{
    unsigned char i = 0;
    BCSCTL1 &= ~XTS;           // LF mode: Basic Clock System
Control 1* LFXTCLK 0:Low Freq.
    for (i = 0xFF; i > 0; i--); // Time for osc. to set

    BCSCTL1 &= ~XT2OFF;        // Turn on XT2 (8MHz)
do
{

```

```

        IFG1 &= ~OFIFG;
        for (i=0xFF;i>0;i--);
    }
    while ((IFG1 & OFIFG) != 0);

    DCOCTL = DCO0 + DCO1 + DCO2;
    BCSCTL1 = RSEL2 + DIVA_0;
    BCSCTL2 = SELS + DIVS_3 + SELM_2 + DIVM_0;
    // MCLK is 8 MHz (from XT2)
    // SMCLK is 8 MHz (from XT2)
    // ACLK is 32 kHz (from XT1)
}

#pragma vector=TIMER0_VECTOR
__interrupt void timer0_isr()
{
    n_ta++;

    if (n_ta > NR_UPDATE_DAC)
    {
        flag_adjust_DAC = 1;
        n_ta = 0 ;
    }

    if(n_led == 0)
    {
        write_DAC1(0);
        P5OUT &= ~BIT5;
    }
    if(n_led == 1)
    {
        P1OUT |= 0x80;           //P1.7 turn on 810 nm
        write_DAC0(1500);
        write_DAC1(val_DAC1);
        P5OUT |= BIT5;          //5.5 INSTEAD OF P6.7 FOR LED DRIVER CTRL
PIN
    }
    if(n_led == 2)
    {
        write_DAC1(0);
        P5OUT &= ~BIT5;
    }
    if(n_led == 3)
    {
        P1OUT |= 0x40;           //P1.6 turn on 670 nm
        write_DAC0(1500);
        write_DAC1(val_DAC3);
        P5OUT |= BIT5;          //5.5 INSTEAD OF P6.7 FOR LED DRIVER CTRL PIN
    }
    if(n_led == 4)
    {
        write_DAC1(0);
        P5OUT &= ~BIT5;
    }
    if(n_led == 5)
    {
        P1OUT |= 0x20;           //P1.5 turn on 905 nm
        write_DAC0(1500);
    }
}

```

```

        write_DAC1(val_DAC5);
P5OUT |= BIT5; //5.5 INSTEAD OF P6.7 FOR LED DRIVER CTRL PIN
}
if(n_led == 6)
{
    write_DAC1(0);
    P5OUT &= ~BIT5;
}
if(n_led == 7)
{
P2OUT |= 0x01;
write_DAC0(1500); //P2.0 turn on 1300 nm
    write_DAC1(val_DAC7);
    P5OUT |= BIT5; //5.5 INSTEAD OF P6.7 FOR LED DRIVER CTRL PIN
}

TBCCR0 = 0x20;
TBCTL |= MC_1;           //Timer_B erstmalig start: Timer A mode
control: 1 - Up to CCR0
n_mw = 0;
TBCCTL0 = CCIE;
}

void timera_init()
{
TACTL = TASSEL_1 | ID_0 | TACLR ; //SourceClock = 1MHz= SMCLK/ID_3
(8MHz/8):Timer A input divider: 0 - /1 */
    TACCR0 = 0x100; // TEST PMD NEU (55.4Hz each LED)
    TACTL |= MC_1;
}

#pragma vector=TIMERB0_VECTOR
__interrupt void timerb_isr()
{
    ADC12CTL0 |= ADC12SC; //SC = Start Conversion
}

void timerb_init()
{
    TBCTL = TBSSEL_1 | ID_0 ; //SourceClock = 1MHz= SMCLK/ID_3
(8MHz/8):Clock Source: ACLK1 (Input clock is passed directly to timer)
    TBCCR0 = 0x1C; // 5Khz slower
}

void init_DAC(void)
{
    DAC12_OCTL = DAC12IR + DAC12SREF_2 + DAC12AMP_5 + DAC12ENC;
// 1 reference voltage, medium speed
    DAC12_1CTL = DAC12IR + DAC12SREF_2 + DAC12AMP_5 + DAC12ENC;
// 1 reference voltage, medium speed
}

void to_ascii()
{
    unsigned char i;

    for(i=0; i<4; i++)

```

```

{
    Digits[i] = 0x30;
}

while(Sum > 999)      //1.000er Stelle abspalten
{
    Sum -= 1000;
    Digits[0]++;
}
while(Sum > 99)       //100er Stelle abspalten
{
    Sum -= 100;
    Digits[1]++;
}
while(Sum > 9)        //10er Stelle abspalten
{
    Sum -= 10;
    Digits[2]++;
}
while(Sum > 0)        //1er Stelle abspalten
{
    Sum -= 1;
    Digits[3]++;
}

void send0(void)
{
    U0TXBUF = '#';
}

void send1(void)
{
    U0TXBUF = '!';
}

void send2(void)
{
    U0TXBUF = '%';
}

void send3(void)
{
    U0TXBUF = '&';
}

void send4(void)
{
    U0TXBUF = '^';
}

void submit()    //submit
{
    unsigned char i = 0;
}

```

```

Sum = 0;
for(i=0; i<NR_MEASUREMENTS; i++)
{
    Sum += Readings[i];
}
Sum /= i;
i = 0;
}

#pragma vector=ADC12_VECTOR
__interrupt void adc_isr()
{
    // while ((ADC12IFG & BIT0)==0); // when ADC12IFG==1, end of
conversion
    while(ADC12CTL1 & ADC12BUSY);
    Readings[n_mw] = ADC12MEM0;

    if(n_tb == NR_MEASUREMENTS-1)
    {
        n_tb = 0;
        TBCCR0 = 0;           //Timer_B stop
        TBCCTL0 &= ~CCIE;
        P2OUT = 0x00;
P1OUT = 0x10; //0x10 v=-1 ; 0x18 v=-5 ; 0x08 v=-2
        write_DAC1(0x00); //DAC off
        P5OUT &= ~BIT5;
        if(n_led == 8)
        {
            n_led = 0;
        }
    }
    else
    {n_tb++;}
n_mw++;
if(n_mw == NR_MEASUREMENTS)
{
    n_mw = 0;
    switch(n_led)
    {
        case 0:submit();Dark = Sum;break;
        case 2:submit();Dark = Sum;break;
        case 4:submit();Dark = Sum;break;
        case 6:submit();Dark = Sum;break;
    }
    if(n_led == 0)
    {
        if(P2IN & ADXL_INT1)
    {
// ADC12CTL0 |= ADC12SC; //!!Start Single ADC Conversion
        if (BUFF_COUNTER >= BUFFERSIZE) { BUFF_COUNTER = 0; }
        ADXL345_ReadXYZ(&BUFF_X[BUFF_COUNTER], &BUFF_Y[BUFF_COUNTER],
&BUFF_Z[BUFF_COUNTER]);
        send4();
SendAccDataSerial(GetBUFFERAvg(BUFF_X), GetBUFFERAvg(BUFF_Y),
GetBUFFERAvg(BUFF_Z));
        // SendAccDataSerial(BUFF_X, BUFF_Y, BUFF_Z);
        BUFF_COUNTER++;
    }
}
}

```

```

        if(n_led == 1)
    {
        submit();
        ADC_val1=Sum;
        Sum = ADC_val1-Dark;
        to_ascii();
        send0();
    }
    if(n_led == 3)
    {
        submit();
        ADC_val3=Sum;
        Sum = ADC_val3-Dark;
        temp =Sum;
        to_ascii();
        send1();
    }
    if(n_led == 5)
    {
        submit();
        ADC_val5=Sum;
        Sum = ADC_val5-Dark;
        to_ascii();
        send2();
    }
    if(n_led == 7)
    {
        submit();
        ADC_val7=Sum;
        Sum = ADC_val7-Dark;
        to_ascii();
        send3();
    }
    n_led++;
}
ADC12IFG = 0x0000;
}

void init_ADC(void)
{
    ADC12CTL0 &= ~ENC ; //reset + REF2_5V + REFON
ADC12CTL0 = SHT0_14 + ADC12ON;
//Reference generator voltage. REFON must also be set: 0 set 1.5 V, or
1 set 2.5 V
ADC12CTL1 = CSTARTADD_0 + SHS_0 + SHP + ADC12DIV_1 + ADC12SSEL_2 +
CONSEQ_0;
ADC12MCTL0 = SREF_0 + INCH_5;
//VR+= AVCC and VR-= AVSS
    ADC12CTL0 |= ENC;      //ADC Enable
}

void SendBSerial(int16_t Data)
{
    UART_transmit('(');
    UART_transmit('.');
    UART_transmit(')');
}

```

```

    UART_transmit('.');
    UART_transmit(')');
}

int16_t GetBUFFERAvg(int16_t BUFFER[BUFFERSIZE])
{
    int16_t avg = 0;
    int i;
    for(i=0;i<BUFFERSIZE;i++)
    {
        avg += (float)BUFFER[i] / BUFFERSIZE;
    }
    return avg;
}

#pragma vector=USART0TX_VECTOR
__interrupt void sio0_isr(void)

{
    if(n_send < 4)
    {
        U0TXBUF = Digits[n_send];
        n_send++;
    }
    else
    {
        n_send = 0;
    }
}

void init_SIO(void)
{
    ME1 |= UTXEO;           //Transmitter enable
    U0CTL |= CHAR;          //8 data bits, 1 stop bit, no parity (8N1)
    U0TCTL |= SSEL1;
    UBR00=0x03; UBR10=0x00; UMCTL0=0xDF;
/* uart0 1000000Hz 256410bps */
    U0BR1 = 0x00;
    U0CTL &= ~SWRST;
}

/*****************
     ADX345 code
*****************/
static BOOL WriteSPI(UINT8 data,UINT8 length)
{
    for(UINT8 i=0; i < length; i++)
    {
        P3OUT &= ~ADXL_CLK; //CLK Falling edge
        udelay(1);
        if (data & 0x80)
            P4OUT |= ADXL_MOSI; // Read Mode for ADXL
        else
            P4OUT &= ~ADXL_MOSI; //Write mode to ADXL
        udelay(3);
        P3OUT |= ADXL_CLK; //CLK Rising edge
    }
}

```

```

        data <<=1;
        udelay(3);
    }
    return TRUE;
}

static UINT8 ReadSPI(UINT8 length)
{
    UINT8 data =0;
    for (UINT8 i=0;i<length;i++)
    {
        data <<= 1;
        P3OUT &= ~ADXL_CLK;
        udelay(1);
        if(P5IN & ADXL_MISO)
            data++;
        udelay(3);
        P3OUT |= ADXL_CLK;
        udelay(3);
    }
    return data;
}

void udelay(unsigned char i)
{
    unsigned char ii;
    for(ii = i; ii > 0; ii--)
    {
        _NOP();_NOP();_NOP();_NOP();
        _NOP();_NOP();_NOP();_NOP();
        _NOP();_NOP();_NOP();_NOP();
        _NOP();_NOP();_NOP();_NOP();
        _NOP();_NOP();_NOP();_NOP();
    }
}

void WriteADXL(UINT8 addr, UINT8 data)
{
    addr &= ~BIT7; // self test
    P5OUT &= ~ADXL_CS; // CHIP SELECT
    WriteSPI(addr,ADDRLENGTH);
    WriteSPI(data,DATALENGTH);
    P5OUT |= ADXL_CS; // CHIP SELECT
}

UINT8 Single_ReadADXL(UINT8 addr)
{
    UINT8 ii = 0;
    addr |= BIT7;
    //The address bit is added to the high-level read control bit
    P5OUT &= ~ADXL_CS; // CHIP SELECT
    WriteSPI(addr,ADDRLENGTH);//
    ii = ReadSPI(DATALENGTH);
    P5OUT |= ADXL_CS; // CHIP SELECT
    return ii;
}

```

```

void Multi_ReadADXL(UINT8 start_addr, UINT8 p[][6], int Cnt)
{
    UINT8    data = 0;
    UINT8    addr = start_addr;
    addr |= BIT7 + BIT6; // multi-read
    for(UINT8 ii = 0; ii < Cnt; ii++)
    {
        P5OUT &= ~ADXL_CS; // CHIP SELECT
        WriteSPI(addr, ADDRLENGTH);
        for(UINT8 j = 0; j < 6; j++)
        {
            data = 0;
            for (UINT8 i = 0; i < 8; i++)
            {
                data <<= 1;
                P3OUT &= ~ADXL_CLK;
                udelay(1);
                if(P5IN & ADXL_MISO)
                    data++;
                udelay(3);
                P3OUT |= ADXL_CLK;
                udelay(3);
            }
            p[ii][j] = data;
        }
        P5OUT |= ADXL_CS; // CHIP SELECT
        udelay(100);
    }
}

void Init_ADXL345()
{
    UINT8    i = 0;
    do{
        i = Single_ReadADXL(0x00);
        udelay(200);
    }
    while(i != DeviceID);

    WriteADXL(DATA_FORMAT_ADDR, 0x0B);
    //0000 1011b - Full Res +-16g, 10Bit
    WriteADXL(BW_RATE_ADDR, 0x0A);
    //0000 1010b - Low_Power = 0 - Datarate @ 100Hz
    WriteADXL(OFSX_ADDR, 0x00);
    //X Offset (All Two's Complement!!)
    WriteADXL(OFSY_ADDR, 0x00); //Y Offset
    WriteADXL(OFSZ_ADDR, 0x00); //Z Offset

    WriteADXL(THRESH_ACT_ADDR, 0x00);
    //Detect Activity Threshold (62.5mg/LSB)
    WriteADXL(ACT_INACT_CTL_ADDR, 0x00);
    //Activity Detection
    WriteADXL(INT_MAP_ADDR, 0x00);
    //ALL(!) Interrupts to IN1 Pin!
    WriteADXL(FIFO_CTL_ADDR, 0x94);
    //Stream Mode, Watermark Flag @ 20 Samples

    WriteADXL(POWER_CTL_ADDR, 0x08); //Measure Mode
}

```

```

void ADXL345_ReadXYZ(int *XAx, int *YAx, int *ZAx)
{
    int16_t Data;

    P5OUT &= ~ADXL_CS; // CHIP SELECT!

    WriteSPI((DATA_X0_ADDR | BIT7), ADDRLENGTH); //Read the 6 Data
Registers!
    Data = ReadSPI(DATALENGTH);
    WriteSPI((DATA_X1_ADDR | BIT7), ADDRLENGTH);
    Data |= ReadSPI(DATALENGTH) << 8;
    *XAx = Data;

    WriteSPI((DATA_Y0_ADDR | BIT7), ADDRLENGTH);
    Data = ReadSPI(DATALENGTH);
    WriteSPI((DATA_Y1_ADDR | BIT7), ADDRLENGTH);
    Data |= ReadSPI(DATALENGTH) << 8;
    *YAx = Data;

    WriteSPI((DATA_Z0_ADDR | BIT7), ADDRLENGTH);
    Data = ReadSPI(DATALENGTH);
    WriteSPI((DATA_Z1_ADDR | BIT7), ADDRLENGTH);
    Data |= ReadSPI(DATALENGTH) << 8;
    *ZAx = Data;

    P5OUT |= ADXL_CS; // CHIP SELECT!
}

int16_t ADXL345_GetAxis(UINT8 Address)
{
    int16_t AxisData;
    Address |= BIT7; // READ!
    P5OUT &= ~ADXL_CS; // CHIP SELECT!

    WriteSPI(Address, ADDRLENGTH);
    AxisData = ReadSPI(DATALENGTH);
    WriteSPI(Address+1, ADDRLENGTH);
    AxisData |= ReadSPI(DATALENGTH) << 8;
    P5OUT |= ADXL_CS; // CHIP SELECT!

    return AxisData;
}

```



# Appendix C:

## Parts List

Partlist for the PPG Sensor Device					
Part	Detail	Order Code	Value	Device	Package
C1		2070405	22pF	C-EUC0603	C0603
C2		1878005	10uF	CPOL-EU085CS-1AR	085CS_1AR
C3		2070497	100nF	C-EUC1206	C1206
C4		1828807	10uF	CPOL-EUCT3216	CT3216
C5		1650833	100nF	C-EUC0603	C0603
C7		2070497	100nF	C-EUC1206	C1206
C10		1650833	100nF	C-EUC0603	C0603
C11		1650833	100nF	C-EUC0603	C0603
C12		1878005	10uF	CPOL-EU085CS-1AR	085CS_1AR
C13		2070497	100nF	C-EUC1206	C1206
C14		1878005	10uF	CPOL-EU085CS-1AR	085CS_1AR
C16		2070405	22p	C-EUC0603	C0603
C17		1650833	100nF	C-EUC0603	C0603
C19		1828807	10 uF	CPOL-EUCT3216	CT3216
C20		1828807	10 uF	CPOL-EUCT3216	CT3216
C21		2070416	33pF	C-EUC0603	C0603
C22		2070416	33pF	C-EUC0603	C0603
C24		1650833	100nF	C-EUC0603	C0603
C25		1650833	100nF	C-EUC0603	C0603
IC1		2445067		MAX4105EUK	SOT23-5L
IC2		1663930RL	LTC6910	LTC6910	TSOT-23
IC3		1146032	FT232RL	FT232RL	SSOP-28
IC4		1389152	REF02HCSA	REF02HCSA	SO08
IC6		1651283RL		ADP3338(AKC-3.3)	SOT223
IC7		1470487	MSP430F161	1IPM MSP430F1611IPM	S-PQFP64-G64
LED1		1686066		LEDCHIPLED_0805	CHIPLED_0805
LED2		1686066		LEDCHIPLED_0805	CHIPLED_0805
LED4		1686066		LEDCHIPLED_0805	CHIPLED_0805
Q2		1666970		CRYTALHC49U-V	HC49U-V
R1 /810 nm	100 mA	2008363	22K	R-EU_R0603	R0603

Partlist for the PPG Sensor Device (Continued)					
Part	Detail	Order Code	Value	Device	Package
R2 /1300 nm	50 mA	1170927	25.5K	R-EU_R0603	R0603
R3 /905 nm	100 mA	2008363	22K	R-EU_R0603	R0603
R4		740-8842	0.22k	R-EU_R0603	R0603
R5		740-8868	0.47k	R-EU_R0603	R0603
R6		2008396	0k	R-EU_R1206	R1206
R7		2008365	47K	R-EU_R0603	R0603
R8 /670nm	20 mA	9330984	30K	R-EU_R0603	R0603
R9		740-8921	0.22K	R-EU_R0603	R0603
R10		740-8858	0.27k	R-EU_R0603	R0603
R11		2008396	0k	R-EU_R1206	R1206
U\$1 /905 nm	R2 (4)	1706560	AS1104	Instead of FAN5614	SC70-6L
U\$2 /810 nm	R1 (4)	1706560	AS1104	Instead of FAN5614	SC70-6L
U\$4 /1300 nm	R3 (2)	1706560	AS1104	Instead of FAN5614	SC70-6L
U\$5 /670 nm	R8 (1)	1706560	AS1104	Instead of FAN5614	SC70-6L
X2		3784678	MICROMATCH	MICROMATCH -14	MICROMATCH -14
X3	USB Link	666-1099	MINI-B	USB_MINI-B	MINI-B
ADXL 345	ACC	ADXL 345		ADXL345EB REV.1 by Intempco	
670 nm	LED	115161LXL			Custom designed LED package
805 nm	LED	12514XL			
910 nm	LED	13324XL-910			
1300 nm	LED	EOLC 1300-17-1			
EOLC -1300-17-1			0.6-1.7 μm	InGaAs Large Area PD	InGaAs Large Area PD